Modeling Stratosphere - Troposphere Exchange Using the UWNMS and START-08 Data

By

Elliot C. Shiben

A thesis submitted in partial fulfillment of the requirements for the degree of

Master of Science

(Atmospheric and Oceanic Sciences)

At the

University of Wisconsin - Madison

May 2017

Abstract

The NSF.NCAR Gulfstream V High-performance Instrumented Airborne Platform for Environmental Research (HIAPER) sampled the upper troposphere and lower stratosphere (UTLS) over North America from April to June 2008, as part of the Stratosphere-Troposphere Analyses of Regional Transport (START-08) campaign in order to provide analysis for stratosphere troposphere exchange (STE) events. Data from the flight campaign was compared to numerical data from the University of Wisconsin Non-Hydrostatic Model (UWNMS). By comparing flight data to model data over time we can study wind, temperature, potential vorticity, and atmospheric constituents.

Initially three different sets of flight data were analyzed using atmospheric constituents and other variables in order to create tracer-tracer plots. Next, the UWNMS was run for the same flight cases in order to study air masses in the surrounding regions in an effort to illustrate the different processes of STE that can take place. Findings include convections importance in STE events, and the importance of differential advection from air masses.

Acknowledgements

Table of Contents

Title: **Page:**

Figure List   Page

1. Introduction

This thesis aims to provide a better qualitative understanding of stratosphere troposphere exchange (STE) at both a synoptic and mesoscale. Through comparison of tracer-tracer plots from data collected from flights during the <u>S</u>tratosphere-<u>T</u>roposphere <u>A</u>nalysis of <u>R</u>egional <u>T</u>ransport (START-08) campaign, a contribution will be provided toward an understanding of mixing and transport processes in the upper troposphere and lower stratosphere (UTLS).

This flight data will be compared to simulations with the University of Wisconsin Non-hydrostatic Modelling System (UWNMS) in an effort to view synoptic scale phenomena during these flight missions. Results from analyzing particle trajectories in the UWNMS indicates that there are two primary mechanisms for mixing stratospheric and tropospheric air during baroclinic wave events. In the western portion of the upper level trough, sinking stratospheric lamina resembling an upper level trough undercuts air in the upper troposphere creating a stratospheric intrusion, despite minimal vertical motion. On the eastern portion of the trough convection dominates STE. Thunderstorm updrafts provide an injection of tropospheric air into the lower stratosphere, which is then carried poleward over air in the lower stratosphere, creating a tropospheric intrusion and double tropopause structure.

Jet cores are also analyzed in an effort to understand their contribution to mixing as well. Turbulent mixing around jet cores has been shown to provide some mixing within the jet cores themselves.

2. Background

STE is the transfer of air mass within the UTLS. The tropopause separates these two layers, and during exchange events in the mid-latitudes, may fold over on itself due to intrusions of stratospheric or tropospheric air. Tropopause folding events have been studied as early as 1955 by Reed using ozone to show rapid mixing of stratospheric and tropospheric air. More recently projects, funding, and technology have allowed the science to study the middle atmosphere with greater frequency. Stohl (2003) summarizes most of the findings in chemistry and theories behind dynamic tropopauses both in the tropics and extra tropics. Holton (1995) identifies tropopause folds as being the most common region for chemical mixing between the lower and middle atmosphere.

The goal of this thesis is to improve our understanding of STE using data from the START-08 airborne experiment and the UWNMS. Flight data from the START-08 experiment will be used to assess the accuracy of the UWNMS during these tropopause-folding events and periods mixing in and around the jet stream. VIS-5D will be used explore where the air masses originate and to assess their behavior during mixing events. The UWNMS will further be utilized to explore the evolution of synoptic-scale weather systems, which will provide context for understanding STE via tropopause folding events. A summation for STE and UTLS interactions will be presented using this research.

2.1. Chemistry of the Middle Atmosphere

In the lower atmosphere, temperature and water vapor content reduce as a function of altitude. This reduction is drastic in the upper Troposphere, where the cold ambient atmosphere

causes a 'freeze drying' effect. This occurs at the tropopause, which forms the transition layer between the troposphere and the stratosphere, where temperature begins increasing with height, characteristic of a stable layer (Hoinka 1997; Schnieder 2004). Water vapor is abundant in the troposphere, but scarce in the stratosphere (Forster and Shine 1997; Shepherd 2007). However water vapor has a source in the stratosphere: oxidation of methane (Ravishankara 2012). Findings have indicated that water vapor may have a cooling effect on the stratosphere which could exceed 1.0 K. Water vapor may contribute as much as 44% of the net temperature change on the surface of the Earth as well. Water vapor amounts have increased steadily since the 1970s and may contribute significant temperature change in the UTLS by oxidizing methane or variability of the tropical tropopause through human-induced climate change or natural variability which can play an impactful role to stratospheric change. (Forster and Shine 1999)

In the lower stratosphere, the atmosphere's chemical composition becomes increasingly complex and trace gases (such as ozone) become more prevalent. Ozone (O_3) is perhaps one of the most vital chemicals in the middle atmosphere, and exists as a very thin layer over the globe in the stratosphere where it absorbs ultraviolet radiation. Chapman (1930) first theorized the existence of an ozone layer and hypothesized that its presence is driven by the photolysis of oxygen (O_2) by solar radiation to form atomic oxygen (O), which can bond with diatomic oxygen in order to create ozone. Ozone has the unique ability to absorb ultraviolet radiation, thus protecting human life from harmful ultraviolet rays whilst also heating up the stratosphere. The work of Dobson (1973) showed that tropospheric intrusions appear as low ozone laminae in the stratosphere. Thus when observing the stratosphere, low ozone regions are a manifestation of tropospheric air reaching into the stratosphere.

2.2. Air Mass Pathways

STE provides a distribution of chemicals between the upper troposphere and lower stratosphere. Mixing will be assessed based on stratospheric water vapor and tropospheric ozone concentrations. An observed increase in water vapor (ozone) in the stratosphere (troposphere) would indicate that mixing is occurring. While not all mixing comes from STE, estimates suggest that it accounts for roughly 18% of tropospheric ozone, with high amounts of uncertainty (IPCC 4th assessment). By analyzing the mixed lamina in the UTLS this thesis will analyze tropospheric and stratospheric air masses during STE events.

The middle atmosphere includes the layers of the mesosphere and stratosphere. At the base of the stratosphere is the tropopause, which separates the upper troposphere and lower stratosphere. The tropopause is a dynamic structure that can be defined using potential vorticity (i.e. a 1.5 or 2.0 PV surface). The dynamic tropopause is located higher altitude in the tropics, relative to higher latitudes, but its pressure is low in the tropics and high in the high latitudes (Lackman 2011). Air flow from the tropics towards the poles or vice versa typically result in mixed air in the midlatitudes. Defining the tropopause as dynamic provides a few advantages, notably that jets are typically at differing pressure levels, but do reside near the dynamic tropopause. Tropopause pressure and potential temperature can be used to identify potential vorticity anomalies such as upper-level troughs and ridges as well. Because PV is a quasi-conserved variable, its distribution is controlled by advection. Of note around this dynamic tropopause is the idea of a tropopause fold, an area where stratospheric air can fold over on top of tropospheric air. The tropopause is also dynamically stable and stratified providing a constraint on flow. The thermal structure and stratification of the tropopause height is based on

fluxes of entropy and isentropic mass between the troposphere and stratosphere (Held 1982; Andrews, *et al.* 1987).

It has been shown that tropopause folds occur in association with Rossby wave breaking but not exclusively as a function Rossby waves (Hitchman and Postel, 2001; Hitchman and Huesmann, 2007). These folding events have since been understood to influence the troposphere in many ways. For example, folding events have demonstrable effects on weather patterns (Pan 2009), cyclogenesis (Uccellini 1985), significant precipitation events (Uccellini and Kocin 1987), and account for mass exchange between the lower and upper atmosphere due to chemical exchange (Lamarque and Hess 1994). The most efficient and effective way to view a tropopause fold is by using trace constituent gases. However there is still some debate about the relationship between tropopause folds and cyclogenesis, with some arguing that tropopause folding precedes cyclogenesis (Uccellini *et al*. 1985; Lackmann *et al*. 1997), however many more have found no real connection between the folding and cyclogenesis (Whitaker *et al*. 1988; Hines and Mechoso 1991; Bush and Peltier 1994; Reed and Sanders 1953; Reed 1955; Staley 1960; t 1970; Shapiro 1970). It has also been shown that the tropopause can fold even without cyclogenesis (Sanders *et al.* 1991).

Since Hoskins *et al. (1985),* PV has been a major diagnostic in case studies. PV can be used as a tracer for stratospheric air. Transport can only occur along lines of constant PV unless diabatic heating or turbulent mixing are occurring (Holton 2004). Stability at the boundary between the UTLS inhibits mixing. Focus has been applied to Davis' (1992; 1993) work on PV inversions to better understand upper and lower level features in the formation of cyclones which was built off of Emanuel and Davis (1991). Research was then tailored towards upper level trough evolution using PV in an effort to understand its effects on height fields (Hakim 1996;

Nielsen-Gammon and Lefevre 1996). A focus of this experiment will be PV's interactions during an upper level trough and a baroclinic wave's impacts on a tropopause fold's formation and intensification. It was shown that large PV gradients could also be used as an indication for studying upper level frontogenesis and cyclogenesis in the lower stratosphere which tilt isentropic surfaces vertically and drive horizontal gradients of vertical motion (Reed 1955; Sanders 1953).

Upper level frontogenesis is a longstanding theory of the presence of thermal frontal structures in the UTLS. The theory was first developed by Sanders (1953), Newton (1954), and Reed (1955) by observing radiosonde data which could be independent of surface frontal structures. The development of these structures occurs by tilting of upward and downward vertical motions. Subsidence on the warm side of the front is conducive to creating an upper level front, as the downward motion in that regions tilts isentropes into an even more vertical position the subsidence increases the horizontal temperature gradient creating a positive feedback loop. (Mudrick 1974) Likewise subsidence on the cold side of the front causes the isentropes to position themselves in a more horizontal direction resulting in a weakened horizontal temperature gradient. The subsidence on the warm side of the trough drives advection of higher PV valued air in the stratosphere down into the troposphere creating intrusions that are commonplace in upper front events. (Danielsen 1968)

Shapiro (1983) hypothesized that subsidence beneath jet cores (on the warm side of the upper level front) is influenced by cold air advection along the jet axis which promotes upper level frontogenesis. Warm air advection along the jet contrarily promotes upward vertical motion under the jet core which reduces the horizontal temperature gradient. Subsidence along the warm

side of the front creates an appearance of a thermally indirect circulation with warm air sinking and cold air rising as subsidence on the warm side of a baroclinic zone would imply.

Sawyer – Eliassen circulations (SE), derived by Sawyer (1956) and Eliassen (1962; 1990), can also be used to indicate upper level frontogenesis. In SE circulations cold air advection in cyclonic shear can induce subsidence which induces frontogenesis via vertical tilting. Transverse ageostrophic circulations diagnosed by the SE circulation equation can increase the horizontal temperature gradient further aiding in frontogenesis. This is indicated by thermal fronts that originate in the tropopause and can be located in the middle troposphere and are defined, on the warm side of the frontal zone, by the tilting term of a thermal cross front ageostrophic flow in the troposphere.

Subsidence conducive to upper – level frontogenesis can also be diagnosed by Sutcliffe's (1947) development theorem. Sutcliffe's development theorem can diagnose subsidence by identifying negative shear vorticity advection by thermal winds. Geostrophic cold air advection along jet axis promotes subsidence directly beneath the jet axis and on the warm side of the upper level front.

Wandishin *et al.* (2000) in a study of the effects of PV anomalies in the UTLS, considered a simple kinematic idea on the effect of tropopause structures, including horizontal differences in vertical motion and vertical differences in horizontal motion. Upon analysis of air parcel motion in high-resolution numerical simulations, it appears that folds can arise from simple differential advection of two air masses in the vertical. The tilting twisting term discussed earlier provides a mechanism for these stratospheric and tropospheric air masses to interact via sloping isentropes. These are long slightly angled trajectories with moderate changes in altitude and can provide another example of mixing. Figure 2 in Wandishin (2000) shows through high

resolution modeling that vertical and horizontal wind shears can actually provide a folding mechanism over the air. Rowe and Hitchman (2015; 2016) also indicated through numerical modeling that poleward displacement of air masses can act as stratospheric intrusions and have been indicated to have increased mixing around their boundaries. Poleward flow is then accelerated by inertial instability, which then provides an increase to positive zonal flow as well.

Davies and Rossa (1998) attempted to diagnose the upper-level frontogenesis using PV. Hoskins (1971, 1972) showed that tropopause genesis could evolve from initially weak baroclinicity. The necessary feature for PV isn't the presence of a strong gradient on a single isentropic surface but rather a gradient through a wide range of isentropic surfaces, which manifests itself into a vertically stretched dynamic tropopause. (Wandishin *et al.*, 2000). The development of said vertically stretched dynamic tropopause is possibly tied to stratospheric intrusions and exchange, which will be thoroughly investigated in this paper.

Finally, this thesis will also discuss the circulation and flow of stratospheric air around plumes of tropospheric air, notably from severe thunderstorms with strong updrafts. Previous work has indicated that stratospheric air wraps around the intruding tropospheric air as it's displaced (Hitchman et al. 2004; Pan et al. 2014). This creates a form akin to a mushroom cloud, in which the highest volume stratospheric air is pushed to the top of the mass, shape creating pockets of high volume stratospheric air around the cloud top which can resemble stratospheric intrusions around overshooting tops in mesoscale mixing events.

2.3. Overview of Flight Campaigns: START08 and HIPPO

START08 followed the START05 field campaign. START05 was designed to gather aerosols and examine large-scale transport in the atmosphere to better understand atmospheric chemistry (Bowman 2007). The START08 mission was charged with the gathering stratospheric and tropospheric air to observe middle atmosphere events such as Rossby Wave breaking and Stratospheric Tropospheric exchange. (Pan *et al*. 2004; Marcy *et al*. 2004; Pan *et al*. 2007). Pan and Konopka (2012) showed the importance of mixing as a physical exchange of chemicals in STE and indicated that mixing and STE must be accounted for in global models. Pan *et al*. (2009) also described the importance of understanding tracers and their impacts in the UTLS, which START-08 missions portrayed very accurately by observing chemical distribution, variations, and relationships during STE. Some variables, such as PV and theta, that were calculated using data from the Global Forecast System during the flight missions at their respective positions.

Homeyer *et al.* (2010) studied STE during the START-08 missions, specifically information on cyclonic rotation and its impacts on the tropopause transition layer. His focus was primarily on cyclone interaction during STE, particularly on a mesoscale and with thunderstorm activity. Wirth (2003) showed that the jump in static stability at the tropopause is much weaker in cyclonic flow and that the tropopause inversion layer is weaker in the presence of cyclonic flow in the upper troposphere. These observations would infer that mixing is more prominent during cyclonic activity.

Homeyer *et al.* (2010) is a recent study that showed tropospheric intrusions accompany Rossby wave breaking events. Homeyer *et al.* (2010) also used START-08 data, and was instrumental in finding that model data (GFS in their study) was accurate during the START-08

campaign sans a few instances where the model struggled to identify intrusion events. Their study highlighted the utility of back-trajectories in evaluating the primary sources of air during intrusion events; therefore a number of trajectory analyses will assist this present study in evaluating STE. Previous studies have by Hitchman *et al* (2005) have indicated that at high resolutions the UWNMS can accurately portray STE and provided accurate views of PV and winds. Ultimately, trajectory analyses such as in Homeyer *et al.* (2011) have added additional evidence supporting previous findings such as McIntyer and Palmer (1983), where Rossby wave breaking events and tropospheric intrusions often accompany one another.

2.4. Interpretation of Tracer-Tracer Plots

Tracer – tracer plots have a long history of usage in studies of the middle atmosphere. Though first used to determine linear relationships between the trace gases in the lower and middle atmosphere (Murphy *et al*. 1993; Weinheimer *et al*. 1993; Fahey *et al*. 1996; Keirn *et al*. 1997; Singh *et al*. 1997), these plots now see use in a variety of methodologies. In this thesis tracer-tracer plots will be used to identify mixed air in the upper troposphere and lower stratosphere.

Tracer-tracer plots depicting unmixed air can be described as a sharply angled, L-shaped transition from water vapor to lower ozone. This sharp angle marks the sudden change from the water vapor-rich upper troposphere to the lower, ozone-dense and dry stratosphere (Fischer 2000). Because this transition for unmixed air is so abrupt, any tendencies to stray from the typical troposphere – stratosphere L shaped transition can be inferred as mixing. This makes the tracer-tracer plot an effective tool for detecting mixing, as seen in Figure 1.
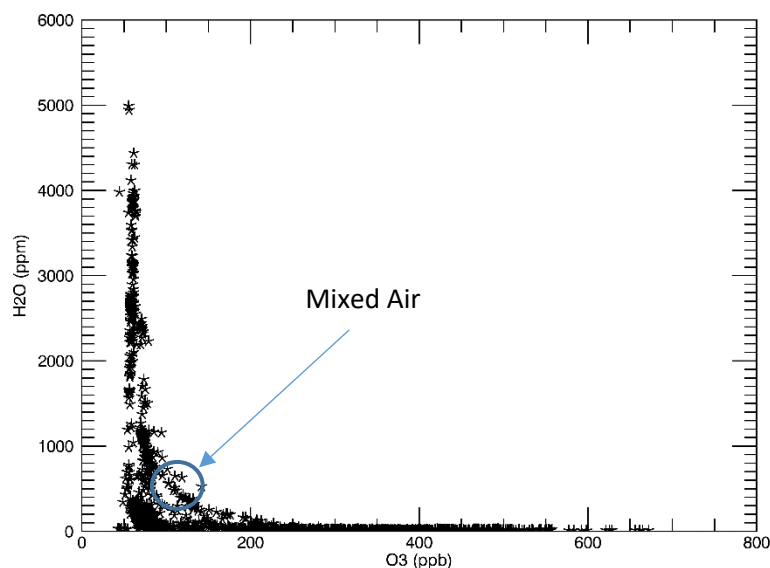
Figure 1: Tracer – tracer plot of water vapor (ordinate) and ozone (abcissa): note the 2 different bending structures in the plot (one at ~ 100 ppbv ozone and 500 ppmv H_2O and another at ~ 100 ppbv ozone and ~ 0 ppmv water vapor) the points with lower amounts of water vapor are the typical transition from the troposphere to the stratosphere, while the circled region shows a more mixed region due to higher water vapor amounts.

START-08 data will be used to identify mixing during the flights using tracer-tracer plots. Tracer-tracer plots can be used to indicate mixing between the UTLS, using PV. Each flight will be broken down into smaller segments and observed individually to view small-scale phenomena as well by comparing stratospheric constituents and tropospheric constituents in an effort to identify outliers (Plumb 2007). These "elbows" (or areas of exponential change in slope) in the data are then tagged and recorded. If the curve takes a second alternate path forming a second bend then mixing is implied. Essentially increased ozone activity occurring in the troposphere implies mixing (Pan *et al*. 2007). By isolating a period of time during which mixing

is present, specific periods during which the START-08 aircraft is recognizing mixing during the

flight can be determined. This allows other variables and relevant information in the flight to be

correlated with mixing events. Tropopause folding events, as given in this data, will be used to

verify the accuracy of the UWNMS.
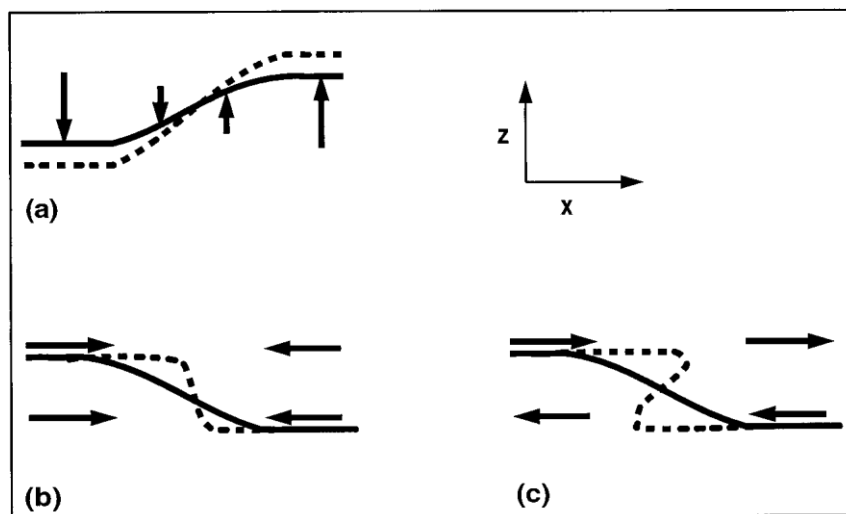
Figure 2: Adapted from Wandishin *et al*. (2000) a) indicates the tilting of the dynamic

tropopause, b) indicates baroclinic wave and horizontal winds steepening the tropopause, and c)

indicates the formation of a fold due to increased horizontal and vertical wind shear.

3. Equipment and Materials

3.1. START-08 Aircraft Data

The analysis in this thesis was primarily carried out using data from the START-08 mission, whose primary task was to study the transportation characteristics of the upper troposphere and lower stratosphere (UTLS) using the NFS/NCAR GV-HIAPER ((Gulfstream V High-performance Instrumented Airborne Platform for Environmental Research).

The GV-HIAPER is an aircraft specifically well suited for studying the middle atmosphere, measuring local atmospheric chemistry, climate, radiative fluxes, cloud physics, aerosols, turbulence, and mesoscale weather. It is a modified Gulfstream V aircraft that can reach altitudes of 15,500 meters, allowing the aircraft to take measurements in the lower stratosphere. The aircraft can carry up to 2540 kg of equipment and sensors aboard cabins located underneath its wings. Using air intakes, the aircraft can also gather samples that record temperatures and air quality in the upper portions of thunderstorms and hurricanes, making it ideal for studying thunderstorms.

The START-08 aircraft's temperature probe is calibrated by using radiosondes released by the aircraft. Several tests have been run in an effort to prove the accuracy of the temperature gauge (Haggerty 2010). Due to their proven accuracy, radiosondes are incredibly efficient at characterizing the temperature of Earth's atmosphere. The DADS (Data Archive and Distribution System)/ICATS (Integrated Corrective/Preventive Action Tracking System) had a slight warm temperature bias (roughly 0.8 Kelvin). Comparing the sensor to radiosonde data must account for pressure changes with altitude, pitch and roll changes, and areas with larger lapse rates (the sensor should not be calibrated in the troposphere as this causes higher lapse rates and less

accurate data.). After a field campaign flight, nearby radiosonde sites are located. Each site is then assessed for proximity of approach of the flight. Radiosondes are launched 12 and 24 hours before and after a scheduled flight campaign. In order to provide confidence in the recorded data, the variability recorded in temperature structures is assessed; if the recorded variability is high, the data is removed as an anomaly. Because radiosondes burst at approximately 30-35 km, lapse rates are estimated at this level (when necessary) in order to facilitate retrieval coefficient calculations.

The temperature probe contains 4 different sensors, each measuring temperatures from a different portion of the aircraft. One temperature is drawn from the Air Data Computer (ADC), another set of data is drawn from an unheated probe on the left side of the aircraft, while the last two are drawn from heated probes on the right side of the aircraft. During the START-08 mission data is gathered by the sensor on the left side of the aircraft at a 1 Hz frequency. When calibrating the sensor, pressure altitude becomes necessary to assess since temperature is pressure altitude dependent. The pressure altitude is sent through the ADC, which is computed from the corrected static pressure.

To calibrate the temperature four different techniques were used to measure the accuracy. The first was to compare the four recorded aircraft temperatures to radiosonde temperatures at their flight level. Data was analyzed from combined measurements of radiosondes released by the aircraft and ground based radiosonde measurements. The second calibration technique involves an in situ air temperature measurement outside the aircraft, which is then compared to that of the radiosondes as a function of a temperature threshold (if the value falls outside of this threshold it is removed and ignored). The third calibration technique involves the comparison of an in situ air temperature measurement and a radiosonde once again, however this time the

temperature is compared as a function of the distance from the radiosonde launch sites. The final calibration technique once more examines the radiosonde temperature to the in situ temperature once more however temperatures recorded near the tropopause are excluded due to the extreme temperature fluctuation near that region.

While standard deviations of the four sensors was nearly 2 K, the total measurement uncertainty was roughly 0.20 K. Uncertainties still remained between the START-08 and the Terrain-induced Rotor Experiment (T-REX) mission with the research temperatures showing a difference in bias between ~2-2.5 K. This difference in measured temperatures could be attributed to recovery factors and other research options that are not known for the T-REX missions.

All four techniques showed good data accuracy, and combining the data from the techniques we can expect that the temperature difference equates to 0.0 ± 0.2 K. In the 2005 WMO report, random radiosonde measurements errors were found to be <0.2 K during the night and <0.3 K during the daytime for the troposphere and stratospheric ice measurements. These findings suggest that the later measurements are similar to those of typical radiosonde errors. As the number of radiosonde data sets decreases so too does measurement accuracy (to roughly 0.3 K). These findings strongly suggest that the temperature probes on the aircraft are indeed accurate and can be used for accurate data measurements and assessment. All biases can be seen in Table 1 below, Table 2 shows biases across all four of the techniques on each sensor.

Table 1: Biases for Techniques on Temperature Measurements

Technique	Description	Bias
Technique 1	Compare in situ measurements to radiosondes	<0.21 K
Technique 2	Remove particular temperature thresholds (> 4 & 5 K) indicated a slight warm bias	$.07 \pm .11$ K
Technique 3	Slight cool bias by removing data within certain range	$-.09 \pm .23$ K
Technique 4	Removed radiosondes near tropopause, which is identified by significant temperature variation within a range	$-.17 \pm .20$K

Table 1: Four techniques used to determine temperature of flight borne thermometer using radiosondes

Table 2: Biases for Sensors on Temperature Probes

Sensors	Bias
Air Computer	$1.74 \pm .21$ K
Left Sensor	$.58 \pm .20$ K
1st right Sensor	$.43 \pm .20$ K
2nd right Sensor	$-.03 \pm .19$ K

Table 2: Temperature Biases for each aircraft based sensor

Trace gases, especially water vapor, will be used to proxy stratospheric and tropospheric air similar to Pan (2007). The water vapor observations were taken using a device called a Vertical Cavity Surface Emitting Laser hygrometer (VCSEL), which measures water vapor content in the atmosphere (Zondlo, Paige, Massick, and Silver 2010). The VCSEL uses a fiberized laser that passes near infrared light between gold coated mirrors to form the optical measurement cell. Measurements are sampled at a frequency of 1500 Hz, with high precision (<3%), and accuracy (5-10%). The accuracy of the sensor makes it well suited for a wide range of atmospheric conditions such as warm, moist boundary layer or cold, dry stratospheric air. Issues with the VCSEL during RF01 and RF02 prevented this data from being used during these flights.

Ozone is the other atmospheric constituent that will be heavily analyzed in this project (Proffitt and McLaughlin 1983). It was observed using a dual-beam UV-absorption ozone photometer (NOAA O_3), which consists of a mercury lamp, and two sample chambers that measure 254 – nm radiation transmitted through the chambers. The ozone absorption cross-

section at this wavelength is accurately known and can be easily assessed and calculated. Data was sampled at a rate of 1 Hz and the minimum detectable concentration of ozone is 0.6 ppbv.

Pressure was calculated using Honeywell sensors that were connected to the outside of the aircraft in a cross shape and attached to a radome. Honeywell pressure sensors are shown to be accurate to +/- 0.0005 PSI, and can collect pressure measurements at a rate of .05 Hz.[1] Honeywell sensors are also responsible for calculating wind speeds and magnitudes coupled with GPS calculated coordinates in the aircraft.

3.2. The <u>U</u>niversity of <u>W</u>isconsin – <u>M</u>adison <u>N</u>onhydrostatic <u>M</u>odeling <u>S</u>ystem (UW-NMS)

The UWNMS was first designed in 1992 as a quasi-compressible, nonhydrostatic model. The UWNMS is fully scalable (with proper microphysical adjustments to the grid parameters) making it useful for simulations ranging from operational forecasts, to dynamical eddy simulations smaller than 50 meters, to global scale cloud simulations. A summary of the dynamics and previous data are summarized in Table 3.

Table 3: UWNMS dynamics and data summary (Adams 2002)[1]

• Quasi-Compressible Nonhydrostatic Model (Tripoli, 1992)
• Variably Stepped Topography[2]
• Time – split compressible dynamics scheme employed, using a hybrid 2nd order leapfrog (dynamics) and Crowley (scalars) advection.
• Thermodynamics based on prediction of ice-liquid variable (Tripoli and Cotton, 1981)
• Pannegrossi and Ackerman cloud active radiation
• Surface layer based on Louis (1979) findings
• Microphysics based on Tripoli's (1991) alterations of Flatau *et al* (1989)
• 6th order vertical and 4th order horizontal numerical filters

3.2.1. Enstrophy conservation:

The UWNMS is unique over other nonhydrostatic models in that it includes enstrophy conservation and a computationally efficient, fully non-Boussinesq formulae. Enstrophy is one half of the square of vorticity and is an important contributor to the Navier-Stokes equations particularly for turbulence. Enstrophy can be proportional to the decrease of energy during a fluid flow in quasi-geostrophic scenarios. Enstrophy conservation has been shown to replicate

---

[1] Courtesy of Amanda Adams master's thesis which can be found at http://www.aos.wisc.edu/~amanda/adams_ms.pdf

[2] Variable step topography is unique to the UW-NMS in that it uses the lowest grid box and has a variable depth that matches surface elevation. The surface boxes are finite differenced implicitly to ensure stability. The step boundary conditions conserve vorticity and momentum, allowing the UW-NMS to properly assess subtle topography changes and having no severe slope restrictions; representing topography elevation changes as small as 1m (Amanda Adams thesis: 2002)

realistic energy spectra by preventing an "enstrophy cascade" that is preventing smaller errors

from enlarging over the course of a model run and also removing numerical aliasing (Tripoli

1992).

3.2.2. Governing Equations:

The quasi-compressible momentum forms of equations used in the model are given by

Equation 2:

$$\frac{du_i}{dt} = \frac{\partial u_i}{\partial t} + \frac{\partial m_j u_i}{\partial x_j} - u_i \frac{\partial m_j}{\partial x_j} \quad \textbf{(2)}$$

$$= \epsilon_{i,jk} u_j f_k - \frac{\frac{1}{\rho}\partial p}{\partial x_i} - \delta_{i3} g + F_i,$$

Where u_i represents Cartesian velocity components, x_i is the Cartesian distance, t is time, g is the

acceleration of gravity, p is pressure, f_k is the kth component of the earth's vorticity, δ_{ij} is

Kronecker delta, and F_i represents turbulent diffusion (Tripoli 1992).

Equation 3 (below) is the momentum form of equation 2 and is often used in three-

dimensional mesoscale and cloud-scale models and decouples the three Cartesian components of

motion into three simplified advective scalar equations. It is easily finite differenced in order to

predict the movement of a scalar in a prescribed flow field. Terrain fields can be applied to the

momentum form, causing them to resemble Cartesian form and retain momentum conservation

principles (Tripoli and Cotton 1982). Horizontal equations of motion can then be manipulated to

yield the enstrophy equation used in the model seen in equation three.

$$m_i = \rho u_i \text{ (3)}$$

$$\frac{\partial u_i}{\partial t} = +\epsilon_{i,jk} m_j \eta_k - \frac{\partial K}{\partial x_i} - \frac{1}{\rho}\left(\frac{\partial \rho}{\partial x_i}\right) - \delta_{i3} g + F_i, \text{ (4)}$$

The enstrophy equation used in the model combines all velocity components through vector principles. Instead of being scalar, the tendency is viewed as dynamic balances between inertial forces, pressure gradient forces, and gravitational forces (Tripoli, 1992). All rotational accelerations are grouped into a single vorticity term, and the remaining inertial acceleration is seen as a kinetic energy gradient in a similar form as a pressure gradient force.

3.2.3. Boundary Layer Turbulence:

The convective boundary layer represents the lower portion of the troposphere and is most directly impacted by the effect of incoming solar radiation to Earth's surface. It extends from the surface of the Earth to the capping inversion, a depth that can vary from meters to kilometers based on seasonality, meteorological conditions, radiation, and winds. Due to planetary boundary layer contact with the planet's surface, heating plays a significant role in the production of buoyancy. The absorption of radiation in this layer also heats air above it through convection. This convection generates eddies via rising air and wind shear, which then begin an overturning process.

The boundary layer can also be identified by a near-surface inversion. This inversion can be driven by a difference in dew point lapse rates (-0.2°C/100m) and temperature lapse rates (100°C/100m), which can suppress convection. The UWNMS uses a local diffusion scheme based on K-theory, which parameterizes subgrid-scale fluxes by making them proportional to the

local gradient of transported quantity. The name originates from the use of an eddy diffusivity

constant, noted as K. In the UWNMS eddy diffusivity is based on turbulent kinetic energy in the

UWNMS, which is different from many mesoscale models that use a set profile for K in the

boundary layer. The UWNMS local diffusion is a 1.5 level closure, which retains prognostic

equations for zero-order statistics like temperature and humidity for equations and variance for

the same variables (Adams 2002). Horizontal and vertical eddy diffusivities are set to the same

scale length based on vertical grid spacing. The total source for turbulent kinetic energy is based

on mechanical, buoyancy, divergence, and dissipation source terms, which are influenced by the

three-dimensional deformation computed from a predicted velocity field, a three-dimensional

velocity divergence, and the dissipation constant.

The convective boundary layer can often be dominated by large eddies capable of

transporting against a local gradient, which cannot be represented by K-theory. A correction term

was added to the turbulence diffusion equation in order to correct and account for this effect, in

an effort to capture the impact of large eddies to the total flux. This term only transports entropy

against the gradient in regions where the boundary layer is stable.

3.2.4. Initialization parameters:

The initialization files used consisted of ECMWF 2.5° ERA Interim/Land initialization

data. Topography and boundary conditions set for the model depend upon the specific dates of

the flight missions, with side boundaries being continuously updated. Time steps were set at 30 s

intervals, which would last over multiple days. The model data was split into subfiles ranging

from 20 to 4000 min covering the duration of each flight as well as time preceding and beyond

the flight. Grid points were set up in the x,y, and z directions, creating a three-dimensional

analysis space. 152 grid points were used in the x and y direction with 60 in the z direction. In

the x and y direction the grid spacing was set in 20 km spacing, with a vertical grid setup at 300

m. The model overall covered a domain of 3040 km by 3040 km in the x-y direction, and vertical

domain extending up to 15 km altitude. Radiation parameterizations were set (Table 3) and were

integrated into the system every 3600 s. The grids were positioned in the middle of the flight

coordinates in latitude and longitude, and were adjusted and moved as needed for individual

flights in variable direction to encompass not only the flight path but also convective mixing and

other synoptic scale events that influenced mixing.

4. Methods

Our primary objective is to use a combination of the UWNMS model data and START-08 data in an effort to analyze STE on both a synoptic and mesoscale. Flight paths must be analyzed and studied in an effort to study their proximity to jet cores. Flight RF04, RF06, and RF18 are selected primarily because of their proximity to jet cores coupled with the presence of mixed air throughout their respective flight paths. Jet cores are typically present in regions with large horizontal gradients in PV contrast.

After analyzing each flight, model runs of the highlighted samples will be investigated. The model runs are analyzed using VIS5D and are used to investigate trough events and the cyclone's overall structure. Using trajectories, the model can indicate the flow of air over time which will be used to investigate the process of STE. The western side of the trough is studied in an effort to study sinking stratospheric laminae. The sinking stratospheric laminae are predicted to form underfolds, by pushing tropospheric air up over the stratospheric air creating a stratospheric intrusion. On the eastern portion of the trough, convective activity pushes tropospheric air over top of stratospheric air, (Rowe and Hitchman 2015, 2016) where it is hypothesized to be pushed downstream by advecting air masses mixing with stratospheric air and creating a tropospheric intrusion. Thunderstorm outbreaks inject significant amounts of tropospheric air into the lower stratosphere. To analyze the updrafts and paths of air parcels during these events, the trajectory tool in VIS5D will be used. The trajectory tool highlights single air parcels during the model run. This will indicate where the air flows once it reaches the lower stratosphere allowing analysis of air motion in and around the jet streak, using a similar method to Homeyer *et al.* (2010).

5. START-08 Aircraft Flight Data – constituents and flights

The analysis presented in this chapter was designed to show constituents captured by the aircraft in the START-08 mission. These observations are used to display mixing, air masses, and jet cores during these flights. Every flight in the START-08 mission was analyzed and it was determined that three flights would be of particular interest due to their proximity to a vertically stretched dynamic tropopause and a jet core; RF04, RF06, and RF18. All three of these flights observe tropopause folds and fly in close proximity to jet cores and capture a plethora of mixed regions.

5.1. Flight RF04

Flight RF04 was the fourth flight of the START08 mission, and took place Monday, 28 April 2008, on a flight between Colorado and Ohio. The five day forecast indicated a strong trough pushing from the Hudson Bay across the northeastern United States, eventually pushing eastward into the mid-Atlantic. The trough is also visible in the 200 hPa chart, reaching as far south as OK and TX sandwiched by ridges on the east coast and the Rockies. A merged polar and subtropical jet is also visible at the 200 hPa level, as seen in figure 3, on the eastern portion of the trough reaching from southern Texas up to New York. Low tropopause heights were measured west of the trough and as far east as Illinois. As indicated by Figure 4 this trough represented the focus of this flight. Water vapor imagery displays a cyclone over Wisconsin with a large cirrus deck extending to the east coast and the Rockies and a dry slot moving northward from Texas into Kentucky.

The flight began at 1520 UTC and ended at 2216 UTC. Horizontal flights managed to capture separation between the dynamical and thermal tropopause. This case is suitable for

studying the downward moving stratospheric laminae on the western portion of the trough.

Figure 4 displays the trough and its location as well as the flight path throughout RF04. This

specific flight provides optimal data for studying STE by virtue of its proximity to the

aforementioned trough. Figure 5 indicates a region of particular interest as absolute vorticity

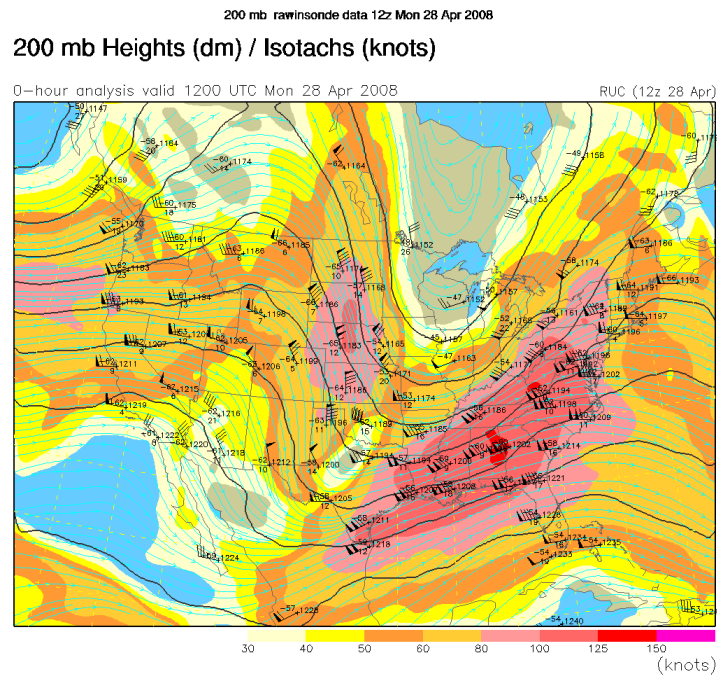gradients are high, indicating a region of probable STE.

Figure 3: 200 mb heights and isotachs and maximum wind speeds from 0 (white) to 150 knots
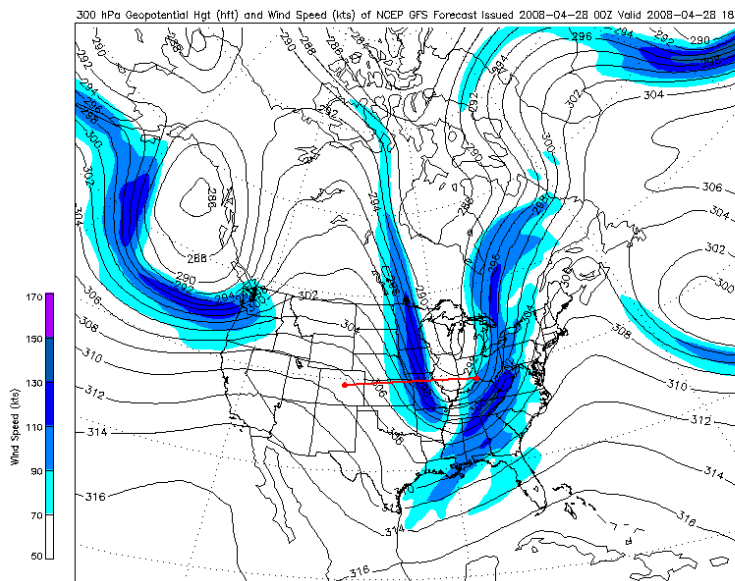
(red)

Figure 4. Flight RF04 300 hPa winds contoured from white (50 kts) to purple (170 kts) and the

flight path indicated in red on 04-28-2008 at 18Z
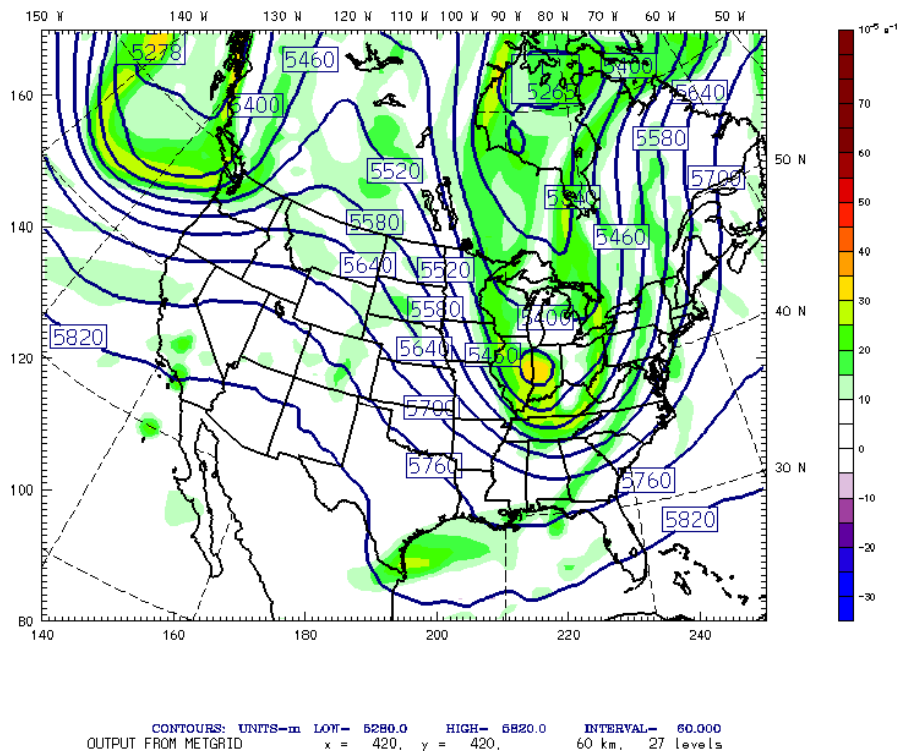
Figure 5: Absolute Vorticity measured from white (0 $10^{-5}m^{-1}$) to orange (40 $10^{-5}m^{-1}$) and contoured geopotential heights in meters

Figure 6 represents a summary of the flight mission as well as cross sections through the flight of PV, forecasted by the GFS. The top left panel displays a tilted tropopause via the yellow isosurface. The purple isosurface represents PV, and the blue isosurface represents a jet core. The portion of the jet core that borders the tropopause has a large horizontal PV gradient and represents a region of strong subsidence, which can be viewed below the jet core by the stratospheric intrusion of high PV air. The second panel represents a cross section of PV with the flight placed on top of it. The contours represent wind speeds in black, and potential vorticity in purple. The last two panels represent the flight path in both altitude and position.
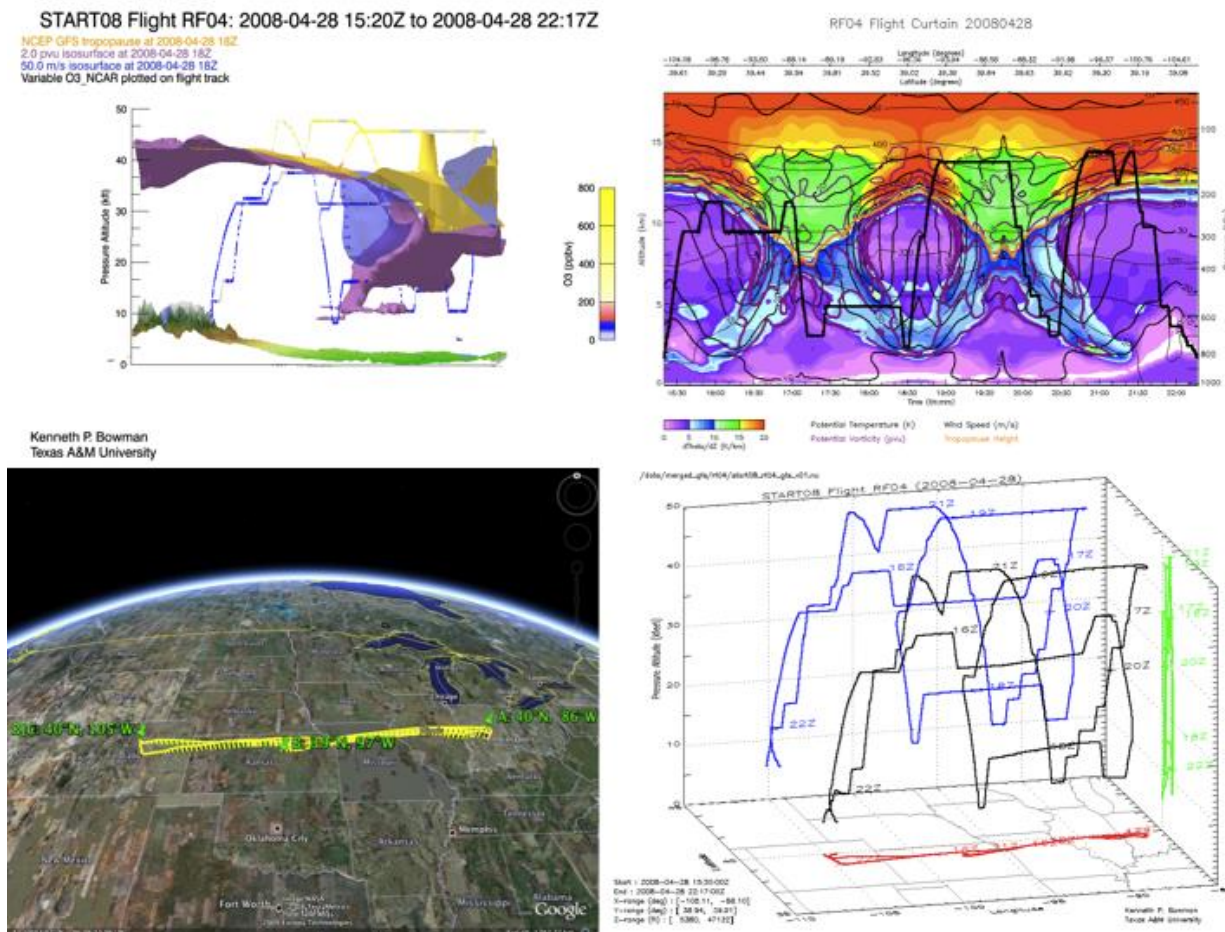
Figure 6. Flight curtain RF04 containing top left: 50.0 m/s wind isosurface (blue), and 2 PVU isosurface (purple), an ozone isosurface (yellow), the flight path (blue), and a tropopause indicator (yellow line); top right: contoured PV (purple to red), flight path (black), tropopause (orange line), potential temperature contours (black), potential vorticity contours (purple) and wind speed contours (black); bottom left: 3-dimensional view including latitude and longitude of the flight over Google Earth map; bottom right: flight path with corresponding times written above the portions of the flight.

The colored flight segments in Figure 7 were used as a primary area of focus because of their proximity to a predicted jet core. Jet cores are typically present near vertically stretched dynamic tropopauses as with high horizontal gradients of PV. In the highlighted segments, the

ascent from the dark green through the yellow portions, should contain some resemblance of a jet

core. Subsidence should be observable underneath of the jet core to indicate mixing. The

UWNMS will be used to study air masses surrounding the jet to understand the overall flow of

air at different altitudes in this region. Trajectories will be used through the UWNMS in order to

study the pathways of the air flow through the segments.
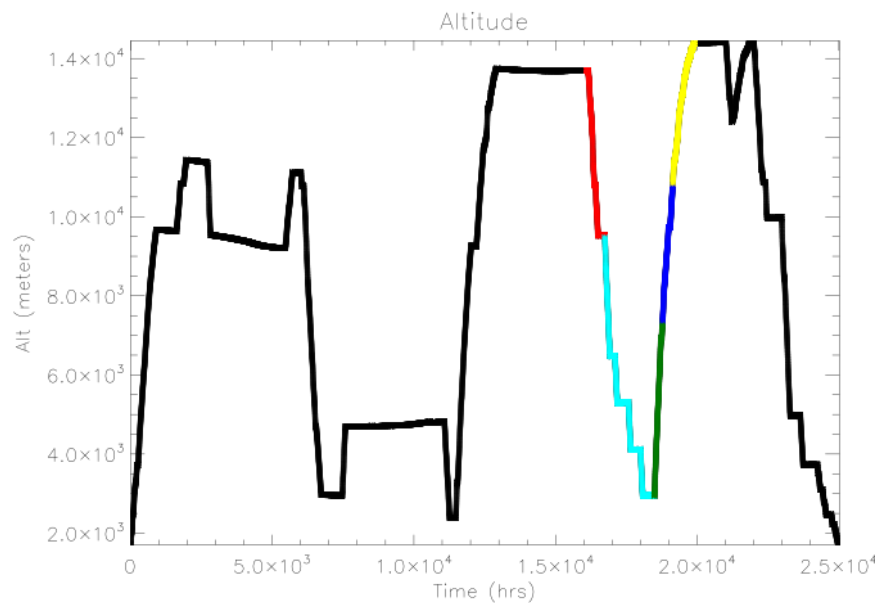
Figure 7: Flight RF04: Path in time – altitude with colored coded segments of focus following its

altitude (y axis in meters) versus time (x axis in seconds).

Figure 8 shows tracer-tracer plots on the left panels and PV right panel. The cyan

segment indicates the most mixing in the region, with high levels of both ozone and water vapor.

The green segment is also highly mixed, followed finally by the dark blue segment. It should be

noted that all three segments make up observations in the troposphere, whereas the stratospheric

segments (yellow and orange) contain little to no mixing. The segments fall along the western

portion of the trough; indicating sinking stratospheric air in the region and mixing occurring in

the troposphere. Also of note is the fact that, in spite of the blue and green segments leading into

and reaching the jet stream (as shown in Fig. 8), there appears to be significant mixing in the segment, which can be explained by Shapiro's (1980) study that turbulent mixing is common along jet cores providing a mechanism to create mixing within and around jet cores. The slight increase in PV in the blue segment followed quickly by a decrease in the blue segment and then a significant increase would seem to indicate at least some mixing occurring in that region and might indicate the presence of two separate air masses, with slightly more stratospheric air being indicated by higher PV values.

A)

B)

C)
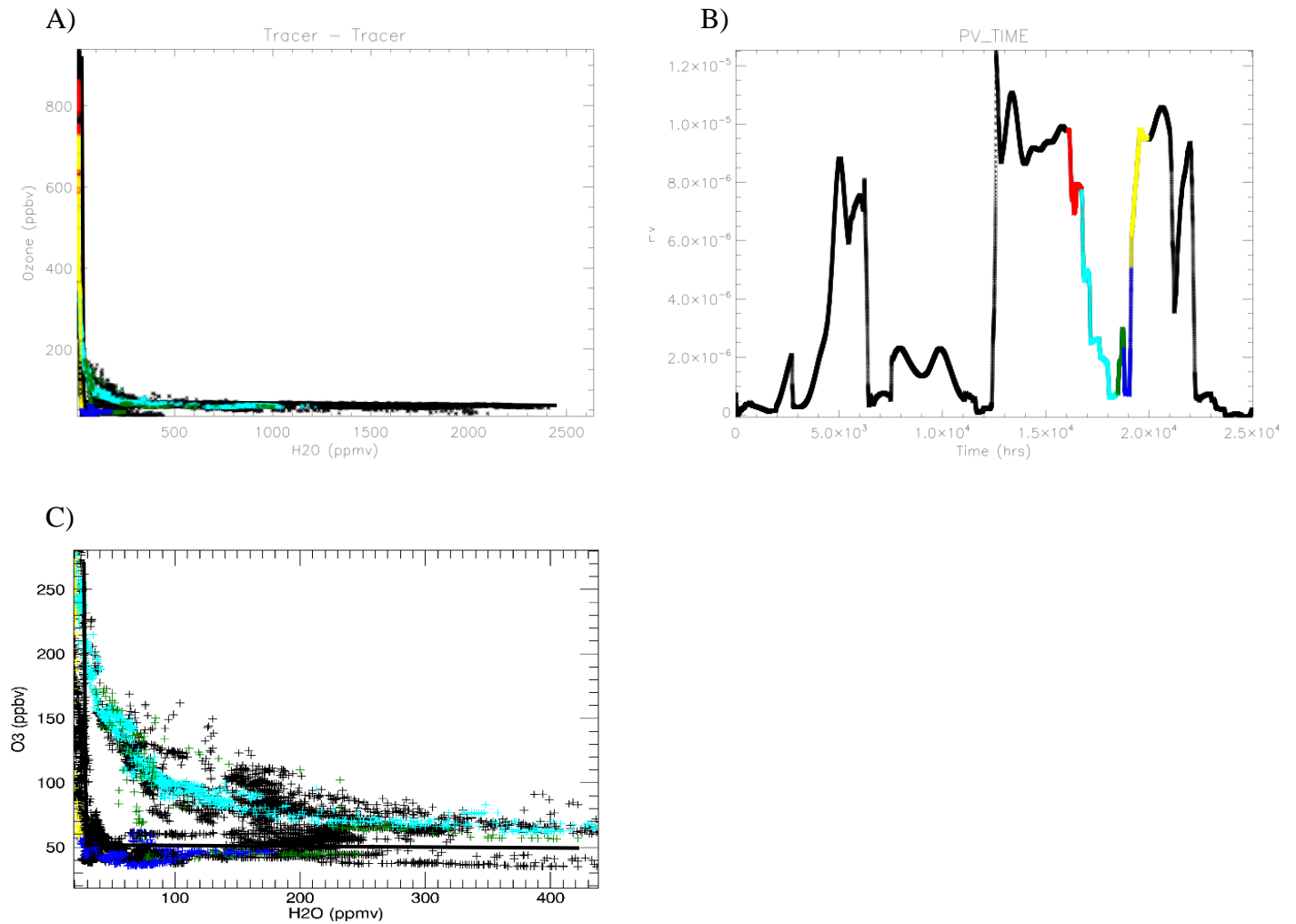
Figure 8: Flight RF04 tracer-tracer plot represented by A) with H_2O (ppmv) versus ozone (ppbv);

PV on y axis and time on x axis represented by B); PV in the GFS model versus flight time C)

zoomed-in tracer-tracer plot from A) for the range 0-300 ppbv ozone and 0-450 ppmv water

vapor. Black L shape is placed into the plot for typical transition from the upper troposphere to

the lower stratosphere

The winds within the segment seem to confirm the positioning of the jet with strong

winds approaching speeds of 60 ms^{-1} in the meridional direction, with some eastward

displacement as well. Figure 7 indicates the wind direction and speed with the left panel showing zonal winds and the right panel displaying meridional winds. Due to the positioning of the flight (never towards the base of the trough) it was not unexpected that zonal winds never reached speeds of ~120 knots as the strongest zonal winds are present at the base of the trough. However, towards the trough axis near jet streaks and jet cores, meridional winds will be much stronger than zonal winds. As expected, speed and directional shear are present in regions of mixing, and appears strongest around the jet core. Wind shear is necessary for a folding tropopause and mixing.

A)

B)

C)
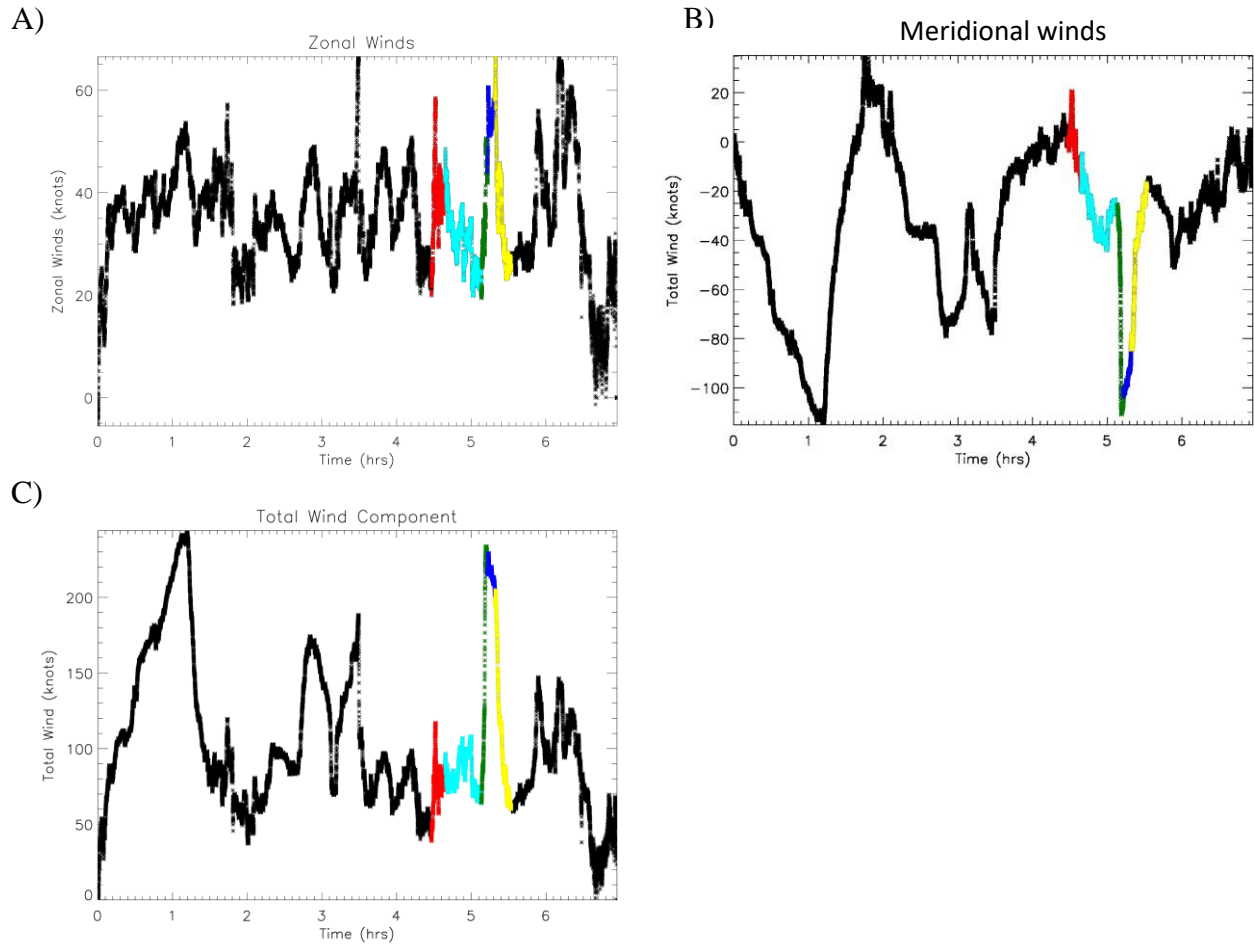
Figure 9: Zonal wind components represented by A) meridional wind components represented by B) winds (knots) and total wind components represented by C) during Flight RF04 over time (x axis in hours after takeoff); segments are correlated with Figure 7 color coded segments.

The dark blue and green segments appear to indicate at least some amount of mixing. Mixing becomes evident in Fig. 10 when all other data points are removed from the highlighted segments. With no real structure to the data, particularly in the L shaped transition, some mixing is occurring in this region. Both segments appear to capture multiple air masses, with both of them portraying two separate L shaped sections. Both sections require further analysis. Also of

note is the high density of air observations in the blue section with readings ~40 ppbv ozone and 50 ppmv water vapor. The double L shape of the plot indicates two separate air masses within the segment.
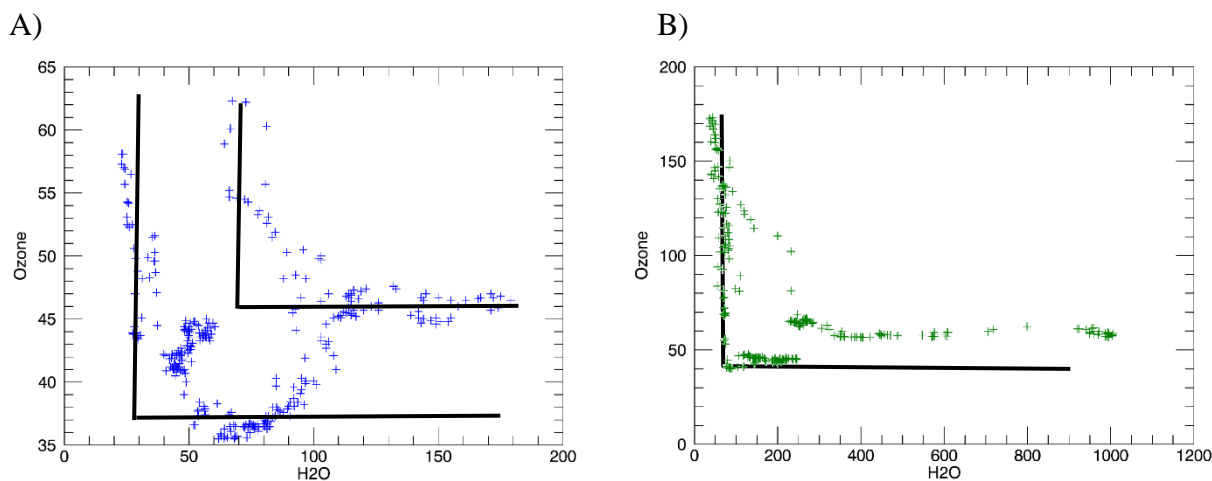
A)

B)

Figure 10: Water vapor versus ozone in RF04 in color-coded segments from figure 5 with figure A) representing ascent through a jet core and figure B) representing ascent underneath the jet core. L-shape for reference to typical upper troposphere to lower stratosphere transition

Figure 11 gives a better indicator of what is occurring within the jet streak itself. Only data points with winds greater than 85 knots are included from this flight. These winds are determined to be fast enough to be considered a jet streak, and the tracer-tracer plots give a good indicator of mixing that could be occurring within the jet streak itself. Given the "double L" shape, it appears the flight captures two separate instances of a jet streak, one is not particularly mixed with a clean transition through the tropopause and a dense group of points that are low in water vapor and ozone density. However the second shape is well mixed with high readings of both ozone and water vapor as well as a much less L shaped transition from the troposphere into

the stratosphere. Once more these observations can be explained by Shapiro's (1980) hypothesis

that turbulent mixing creates an outlet for mixing in the jet core itself. The turbulent mixing does

not appear to be the primary form of mixing within this flight mission however.
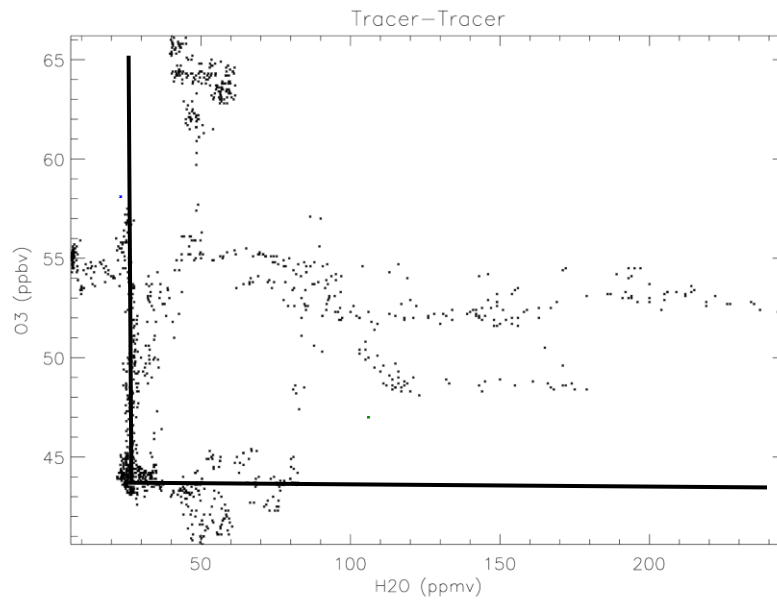

Figure 11: Water vapor (ppmv) on the x axis – ozone (ppbv) on the y axis of points with

meridional winds greater than 85 knots representing the jet streaks.

5.2. Flight RF06

Flight RF06 was the sixth flight on the START08 mission and occurred on 1 May 2008 from 19:52 UTC to 00:11 UTC of 2 May. The forecast from the GFS indicated a large region of possible tropopause folding along the western United States indicated in Figure 13 as indicated by a large horizontal PV gradient seen in the two top panels. A deep trough with high values of PV can be viewed in Figure 12 A) and B) in the Colorado region. The peak wind speed was measured to be at the base and along the western portion of the trough which is the region the flight took place in as seen in Figure 14. The 200 mb chart (Figure 12) indicates a circulation controlled by a trough in the west and ridge in the east. High levels of absolute vorticity are present in the Utah region, which also contains a very low tropopause affiliated with the low pressure system (Figure 15). Regions of high PV seen in Figure 16 along the western portion of the trough and through the base of the trough as well in Utah and Colorado. Cross sections along the jet using potential vorticity indicate a strongly vertical-tilted tropopause and thus a significant tropopause fold indicating strong potential for mixing, as seen in Figures 12 and 17
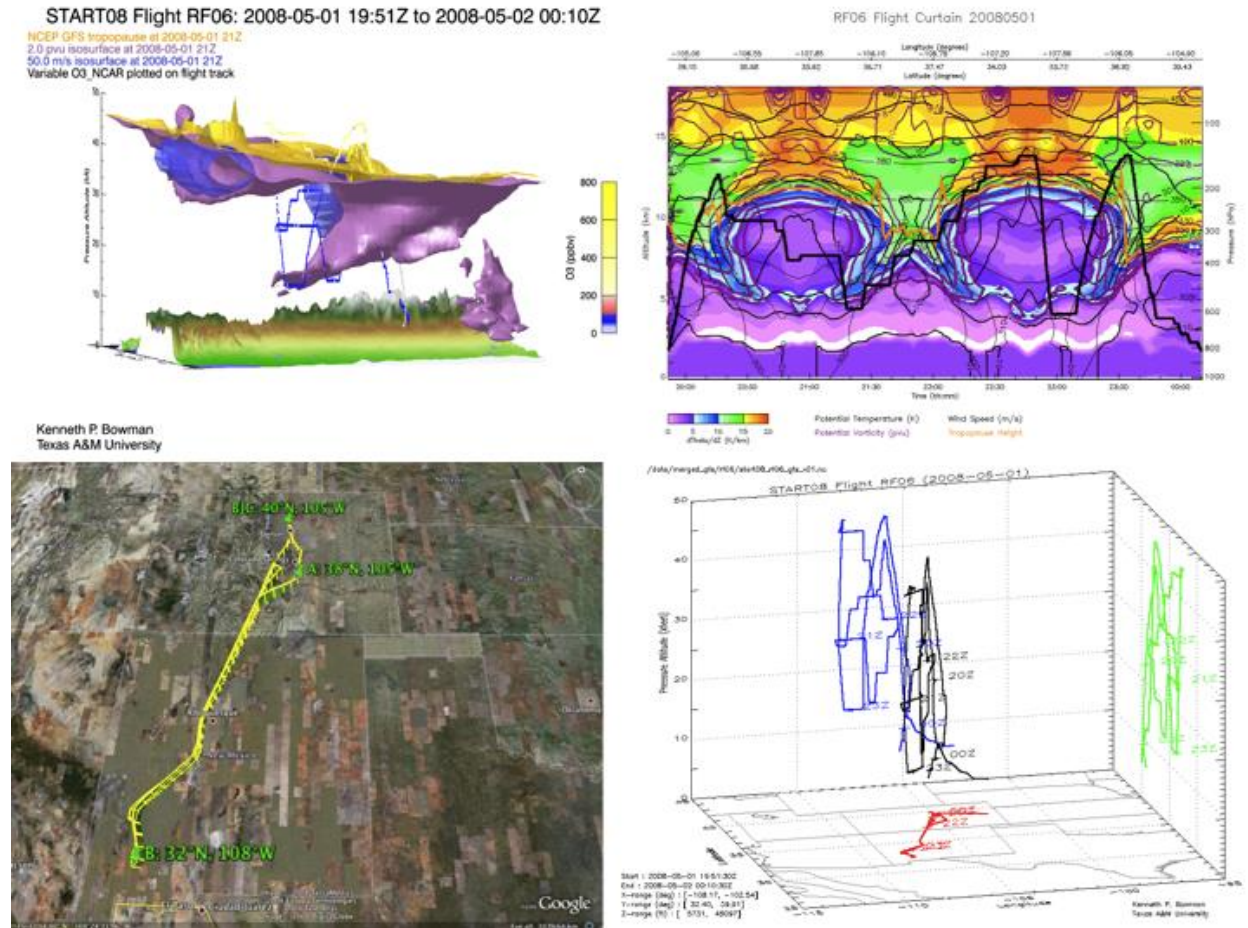
Figure 12: Flight curtain RF06 containing top left panel: 50.0 m/s wind isosurface (blue), and 2 pvu isosurface (purple), an ozone isosurface (yellow), the flight path (blue), and a tropopause indicator (yellow line); top right panel: contoured PV (purple to red), flight path (black), tropopause (orange line), potential temperature contours (black), potential vorticity contours (purple) and wind speed contours (black); bottom left panel: 3-dimensional view including latitude and longitude of the flight over Google Earth map; bottom right panel: flight path with corresponding times written above the portions of the flight.

A)
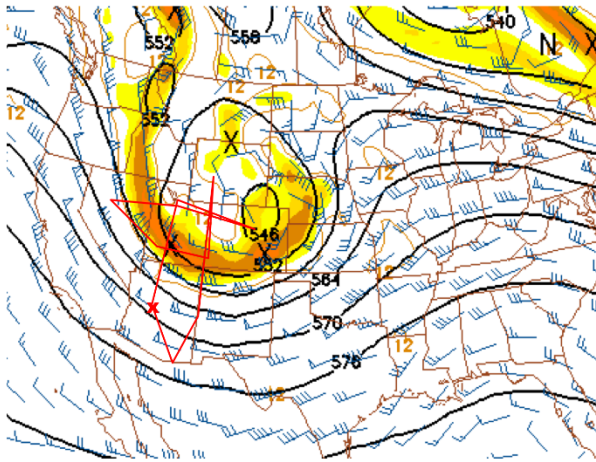
B)
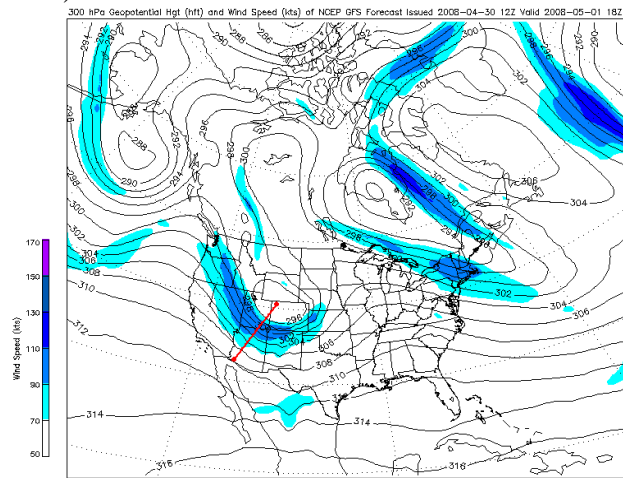
Figure 13: Panel A shows the flight path (red) absolute vorticity colored white (least) to dark orange (max) and wind barbs, with geopotential heights contoured on a 300 hPa map. Panel B shows 300 hPa winds from white (<50 kts) to dark blue (>170 kts) along the trough during RF06 with the focused region of the flight in red. Both panels represent data from the GFS valid for 05-01-2008 at 18Z
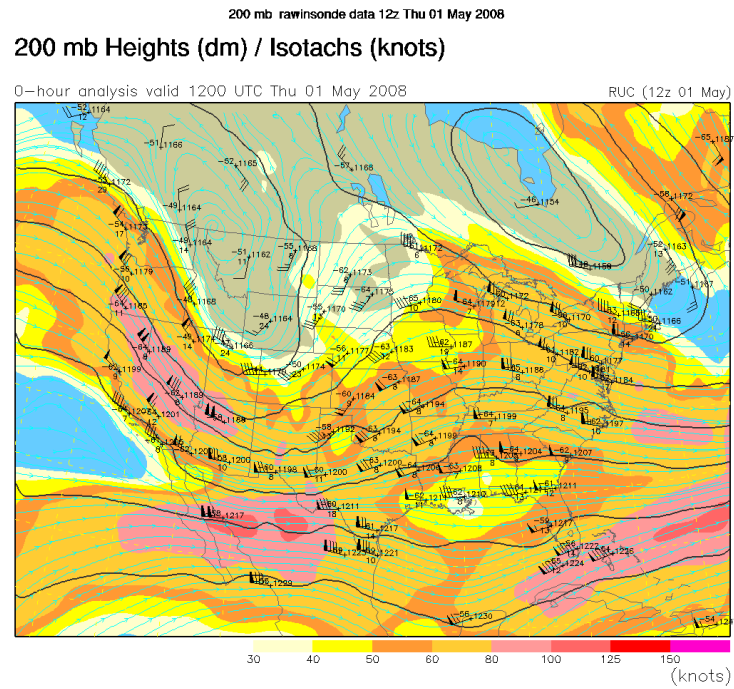
Figure 14: 200 hPa heights and isotachs and wind speeds from 0 (white) to 150 (pink) knots.
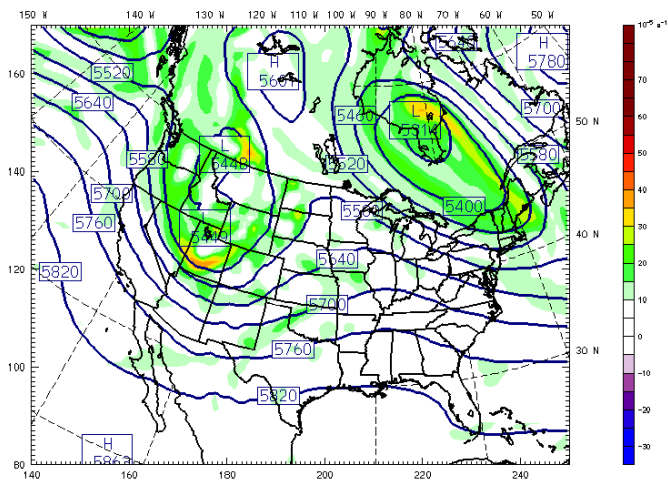
Figure 15: A) represents absolute vorticity from 0 (white) to 50 (orange) and geopotential heights contoured in meters at 500 hPa. B) Maximum wind speeds in m/s and tropopause heights from 5000 Pa (red) to 50000 Pa (blue).
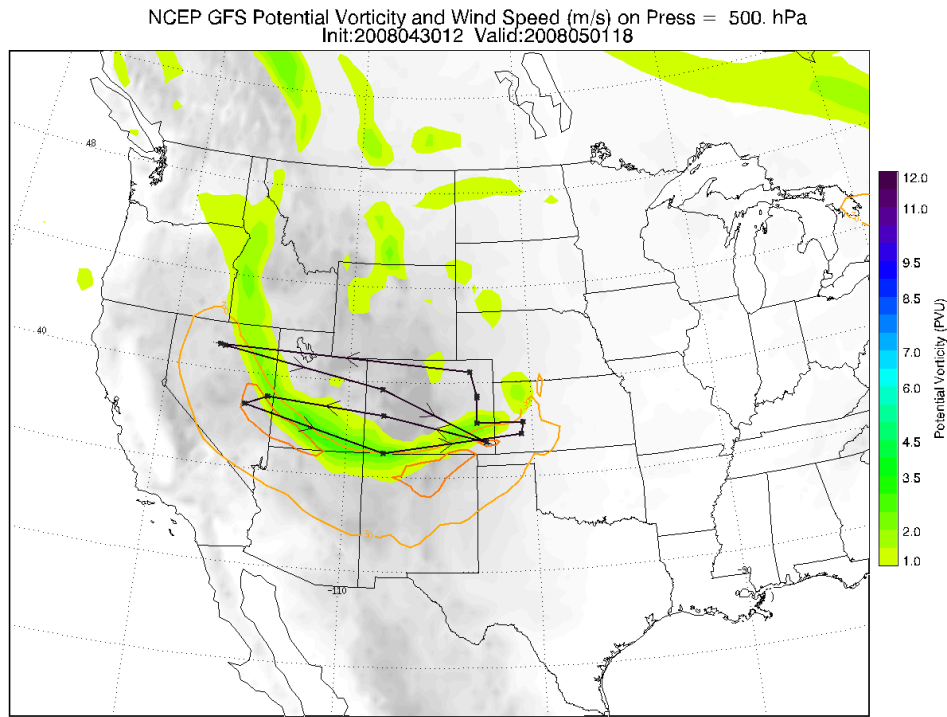
Figure 16: Potential vorticity at 500 hPa colored from 1 PVU (yellow) to 4.0 PVU (green) and predicted flightpath for RF06
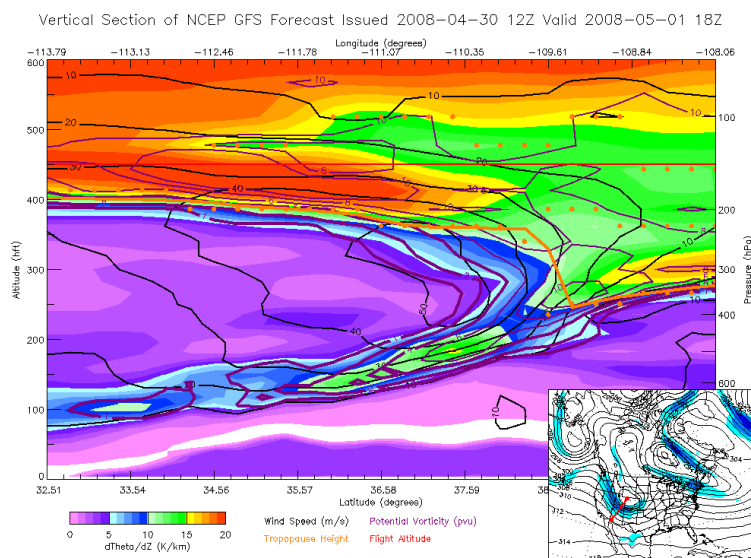
Figure 17: Flight RF06: GFS forecast output of potential vorticity contoured during a tropospheric intrusion and vertical tropopause (orange line)

Due to the proximity of the jet core and tropopause, RF06 was divided into two segments. This is due to the frequency and depth of tropopause folds, meaning a high fidelity of data needed to be captured. In Figure 18 the flight is split into two important regions of focus. The first group of segments analyzed in figure 18, labeled in the cyan and red colors, emphasize an ascent through a tropopause fold. The second highlighted group of segments focuses on a steady ascent through an expected jet. Another stratospheric laminae should be present on the western portion of the trough. This trough does not sink quite as deeply as RF04's but the flight track offers multiple opportunities to capture activity surrounding the jet core and activity surrounding a vertically stretched tropopause with a large potential temperature gradient in the second segment.

Each of the segments in Figure 18 was selected due to different PV values seen in Figure 12 all future plots in this flight analysis will be color coded to represent the same segment, i.e.

the red segment in Figure 18 represent the red segment in tracer-tracer plots. The cyan segment

is of interest due to the presence of a jet streak. Atmospheric constituents and concentrations will

be analyzed in this region. The blue to orange segments also represent a portion of the flight

where the aircraft flies in close proximity to a large horizontal potential temperature gradient

where a jet is forecasted to be present.
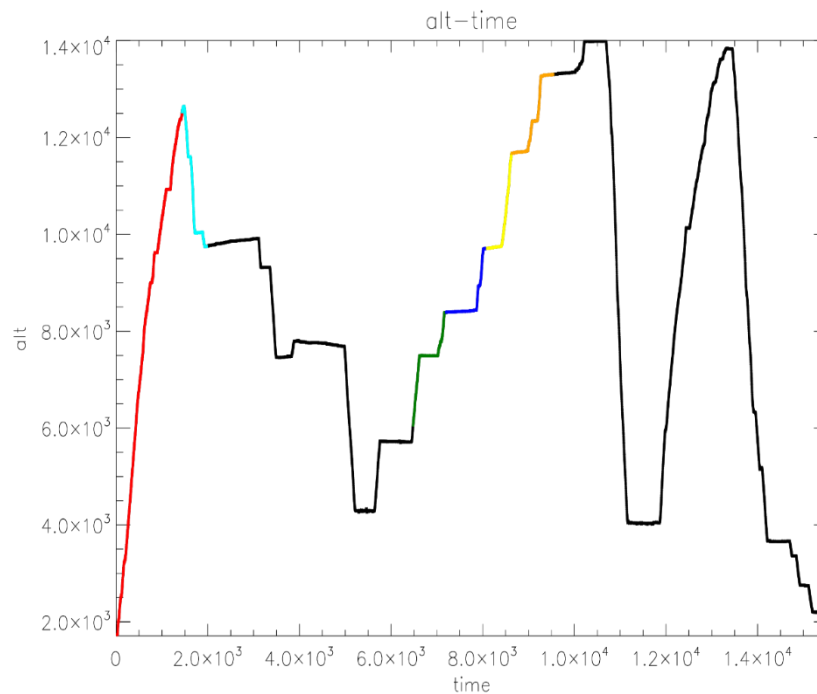
Figure 18: The flight profile of RF06 with color-coded segments in altitude (y axis in meters) vs

time (x axis in seconds).

Panel A) in Figure 19 represents the first ascent recorded by the aircraft. Despite

measurements taken in the upper troposphere, low values of water vapor are present. Typical

values of water vapor in the upper troposphere fall in the range of 50 to 100 ppmv while in this

segment values closer to 10 to 25 ppmv in water vapor concentration were measured. The cyan

region in Panel B) of Figure 19 shows a clear cross over in the tropopause via a large gap in observations from roughly 20 ppmv water vapor and high ozone air to roughly 30 ppmv water vapor and low ozone air. Due to the pronounced transition from the troposphere to the tropopause seen from 30 ppmv water vapor and 200 ppbv ozone to 20 ppmv water vapor and 400 ppbv ozone, there doesn't appear to be much mixing occuring in the cyan segment. Due to the lack of organization in the distribution of the data points in the red segment one can infer that mixing was occurring.

A)

B)
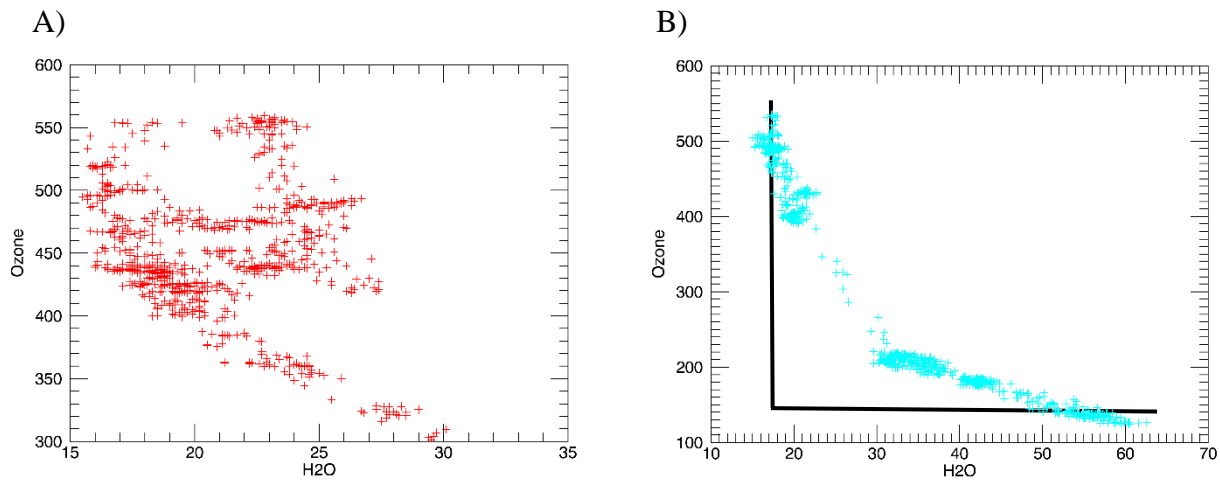
Figure 19: Tracer – tracer plots for RF06 with H_2O (ppmv) along the X axis and ozone (ppbv) along the Y axis of segments from Figure 12 with panel A) representing the aircrafts first ascent through the upper troposphere, and panel B) representing descent through the tropopause. Scales are not constant due to the presence of different trends present in the segments. L-shape for reference typical transition from upper troposphere to lower stratosphere

The complete set of measured water vapor and ozone data of RF06 is presented and illustrated in Figure 20. The green segment is the most well mixed segment of the flight, and represents the region of the flight below the jet in the upper troposphere. The yellow portion

represents the portion of the flight within the jet core itself and while it is less mixed than the green segment.
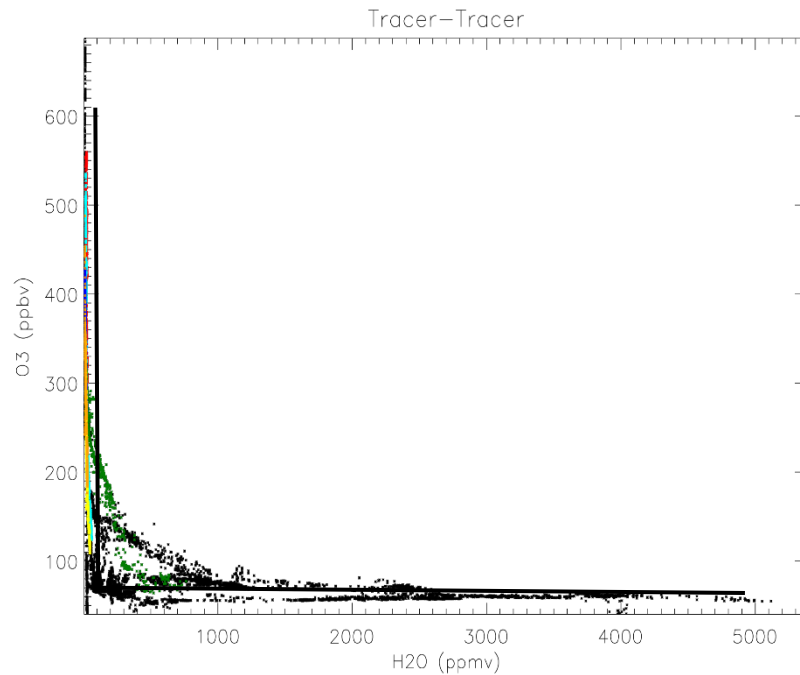
Figure 20: Tracer-tracer plot of H_2O on the x-axis (ppmv) and ozone on y-axis (ppbv) with colored segments defined by flight segments of interest in Fig.12. L shape placed in for reference to typical upper troposphere to lower stratosphere transition

Figure 21 represents each individual segment plotted in tracer-tracer form in an effort to remove the noise from other portions of the flight. As already mentioned, the green segment (Figure 21, Panel A) does appear to be the most well mixed portion of the flight with a very pronounced bend structure and with portions of the flight containing 200 ppmv water vapor and 200 ppbv ozone. The yellow segment (Figure 21, Panel C) does appear to indicate some mixing

due to its linear trend. Mixing is most prominent in the green region followed by the yellow region which signifies intense subsidence beneath the jet as high measurements of ozone are present. Turbulent mixing is providing the mechanism for mixed air in and around the jet core (Shapiro 1980), seen in the yellow segment. The orange segment (Figure 21, Panel D) represents the portion of the flight just above the jet core. The structure would seem to signify two separate air masses in the segment, one that lacks water vapor and is ozone rich thus being stratospheric in nature, and the other that appears less mixed due to its linear shape as water vapor decreases. In the case of RF06, stratospheric air is being pulled down into the troposphere more prominently than tropospheric air is being transported into the lower stratosphere.

A)

B)

C)

D)
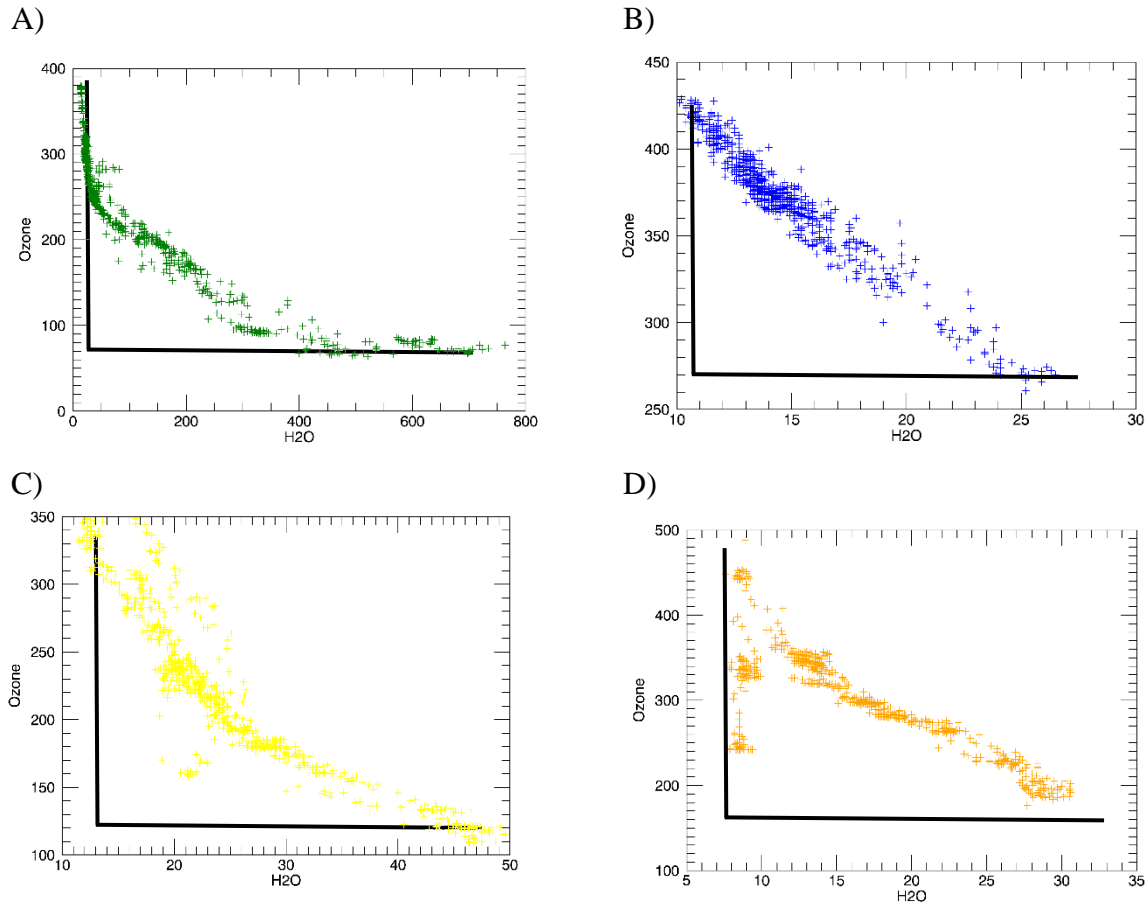
Figure 21: Tracer-tracer plots of RF06 with H2O (ppmv) along the X axis and ozone (ppbv) along the Y axis of previously highlighted segments from Figure 12. Note the different scales on the x axes. A) Represents the first climb towards the jet core and across a vertically stretched dynamic tropopause. B) Shows the ascent through a jet towards the jet core. C) Represents the mixing in the jet core itself. D) Represents air masses in the lower stratosphere above the jet. Note the different scales for each segment. L-shapes placed into plots for typical transition from upper troposphere to lower stratosphere

Potential vorticity is a common diagnostic used to identify stratospheric and upper tropospheric air masses. As seen in Figure 22, the green segment captures both stratospheric and

tropospheric air. This is shown by the large spike in PV values followed by two quick drop-offs, thus indicating two passes through the tropopause. Recalling Figure 12, this portion of the flight flies directly through the vertically stretched dynamic tropopause. In the orange segment, it was previously determined that the flight flew through a dynamic tropopause however the PVvalues appear to drop. This indicates the presence of tropospheric air or slightly mixed stratospheric air within the region. In the cyan segment another PV anomaly appears, despite the steady decrease in altitude there is a significant spike in PV near the dynamic tropopause indicating a large stratospheric air mass. Finally the transition from the latter portion of the dark blue segment and into the yellow segment shows yet another interesting anomaly. Despite a steady increase in altitude (as seen in Figure 18), PV values drop quickly indicating a tropospheric air mass surrounded by a large stratospheric air mass. Recall from Figure 18 that the yellow segment contained very little water vapor, which suggests that the air is stratospheric. This would appear to indicate mixing within the jet core due to tropospheric-like PV and stratospheric-like water vapor and ozone concentrations.
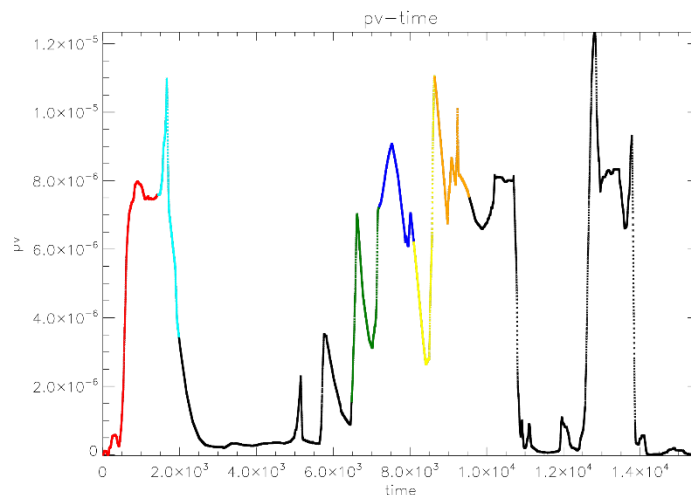
Figure 22: PV (x axis in PV units) from GFS analyses over time (y axis in seconds) with highlighted segments from Figure 12.

Figure 23 represents another tracer-tracer plot with a threshold for wind speeds above 75 knots. For flight RF06 only the zonal component reached wind speeds at this threshold, which is representative of a jet streak. Like RF04 there appears to be as many as three separate air masses and jet streaks captured during this flight. Once more there appears to be slight mixing which can be attributed to turbulent mixing around the jet core. Interestingly there appears to be a greater impact in overall mixing via turbulence in this case than in RF04 with higher values of both H_2O and ozone. The jet could also be along a sloped theta surface providing sloped isentropes which push the flow of air into the jet core itself. Further analysis is necessary.
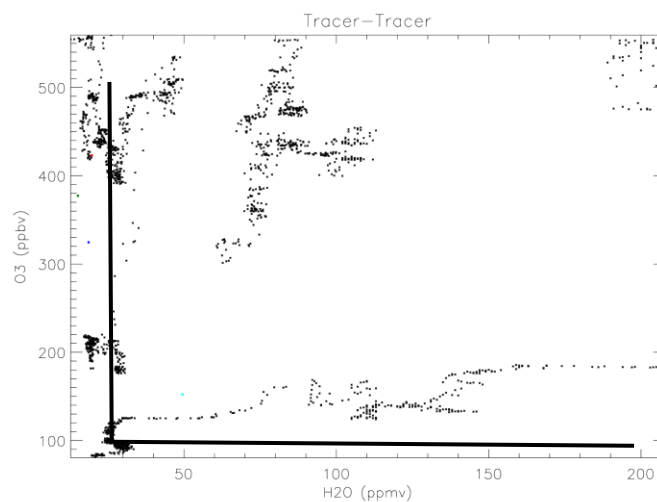
Figure 23: Water vapor (ppmv) on the x axis – ozone (ppbv) on the y axis of points with zonal winds greater than 85 knots representing the jet streaks. L shape placed in to reference typical transition from upper troposphere to the lower stratosphere

Wind shear is necessary to cause the tropopause to fold, and exchange of air masses to occur between the UTLS. Contrary to that, weaker winds are detected within the green segment

as shown in Figure 24, in spite of the significant mixed constituents and the changes in PV. There appears to be a significant relationship between wind shear and potential vorticity however, with sharp changes in direction and speed closely associated with rapid changes in potential vorticity. This can be seen in the cyan segment where a sharp zonal wind increase of ~50 knots (possibly indicating a jet core) and meridional wind change of approximately ~40 knots. Another region of sharp change in wind shear is the green to yellow transition. The blue segment shows a steady, steep climb in wind speed, which peaks in the yellow segment in the jet core. The orange segment also has wind shear present particularly in the meridional direction as well which can provide a source for STE which could lead to interaction between stratospheric and tropospheric air masses and ultimately changes in PV values. Wind speeds in this segment vary by as much as ~40 knots. As the orange segment passes into the lower stratosphere the meridional wind component decreases. There are also changes in the vertical component of the wind that correspond with the wind shear and quick PV changes. Total winds follow a very similar trend to the zonal component, indicating a zonal wind dominated system.
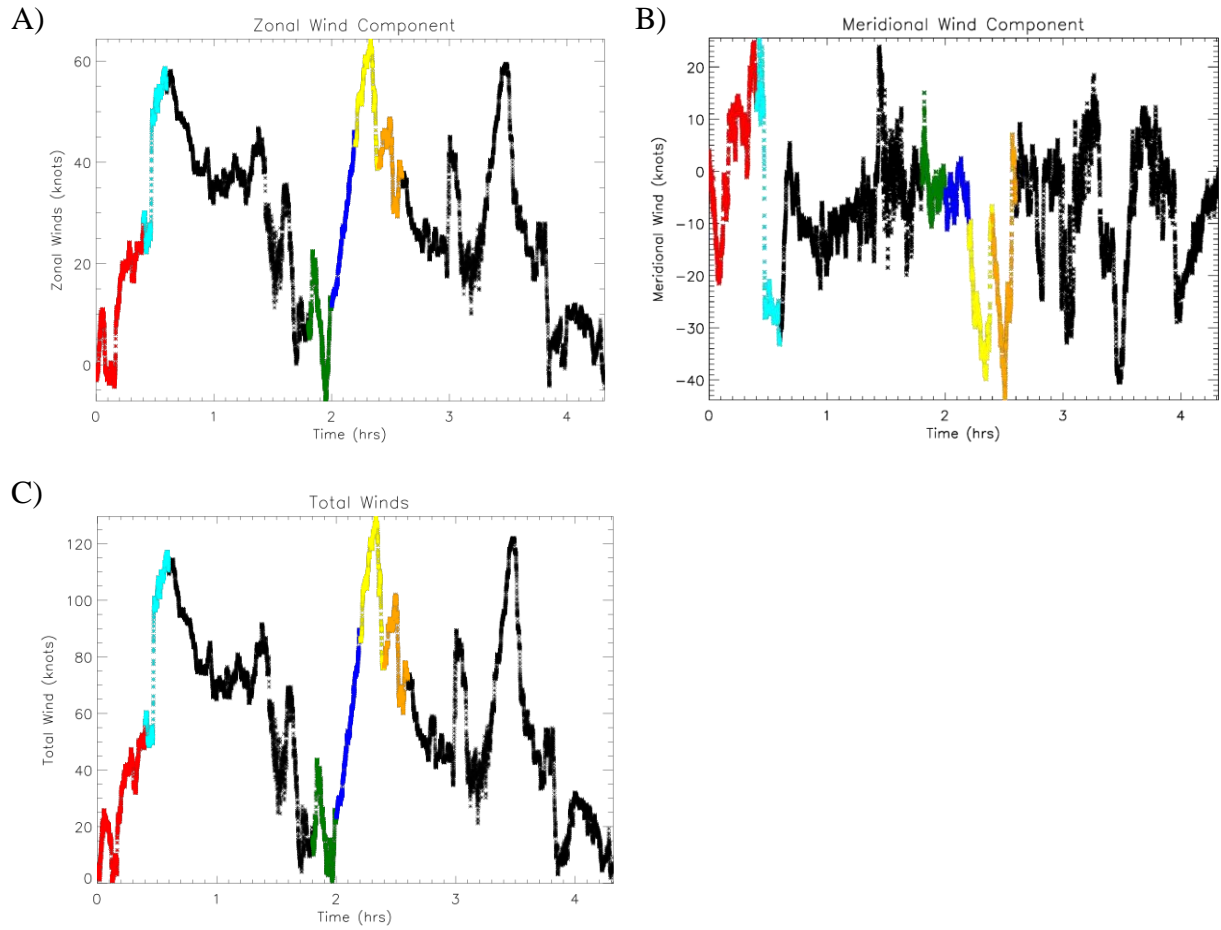
Figure 24: A) Zonal B) meridional components, and C) total wind components as a function of time in knots in RF06 with color-coded segments as in Figure 12. Note the different axis scales.

5.3. Flight RF18

The final mission in the START08 campaign, RF18, managed to include a flight through a jet streak twice through an ascent and descent. The mission took place on June 27th 2008 and the duration of the flight lasted much longer than the other flights as it was the last mission, and provided an opportunity to observe middle atmosphere phenomena. The first portion focused on a region near Montana and over the Canadian border where a large horizontal PV gradient is present. The 200 mb chart seen in figure 25 indicates a short wave trough over the Montana – Idaho region. The GFS indicates a strengthening polar jet in the region as seen in figure 26, with a low tropopause and an intensifying cyclone. High values of absolute vorticity seen in figure 27 are also present along the Montana and Idaho region, indicating a high likelihood of mixing.

The other portion of the mission explored a convective air mass in the Midwestern United States, specifically over South Dakota, Nebraska, and Iowa. There was a much larger convective region near Minnesota but was too distant for the flight. The area of focus is along a path from Sioux Falls, SD to Fort Dodge IA, which are perpendicular to anvil outflow. This perpendicular line was followed at three different levels: Above the cloud level, the tropopause level, and the anvil level (overshooting top). The first fly-through was too high due to a missed forecast by the GFS. The second fly-through was at the correct level. Figure 28 indicates a large horizontal PV gradient and some mixing around a prominent jet core.
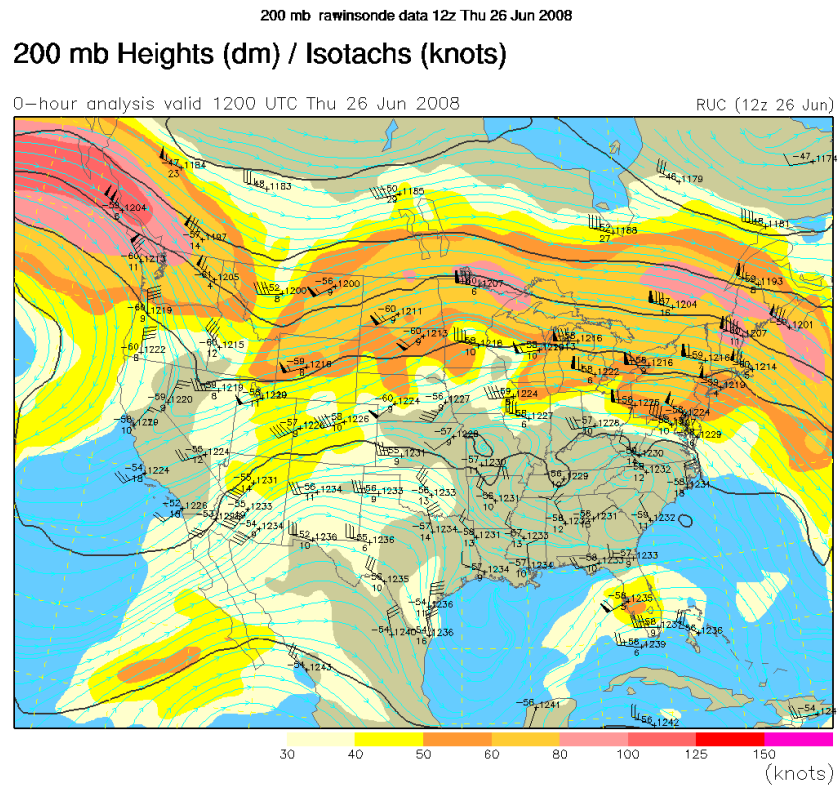
Figure 25: 200 mb heights contoured with isotachs and wind speeds from 0 (white) to 150 knots (pink)
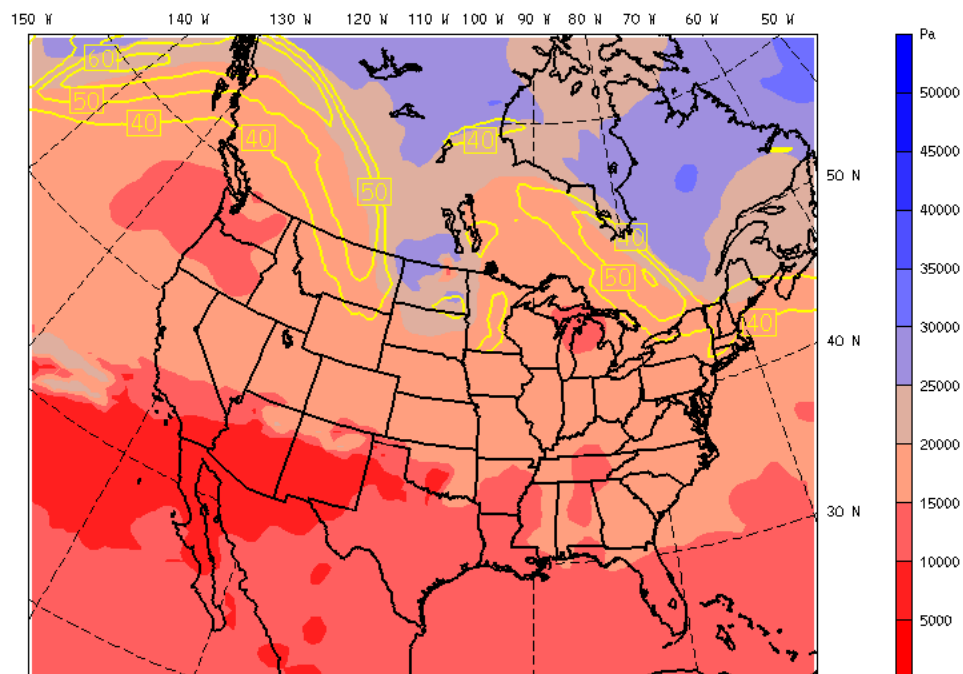
Figure 26: Maximum wind speeds in m/s in yellow contours, tropopause heights from 5000 Pascals (red) to 50000 Pascals (blue)
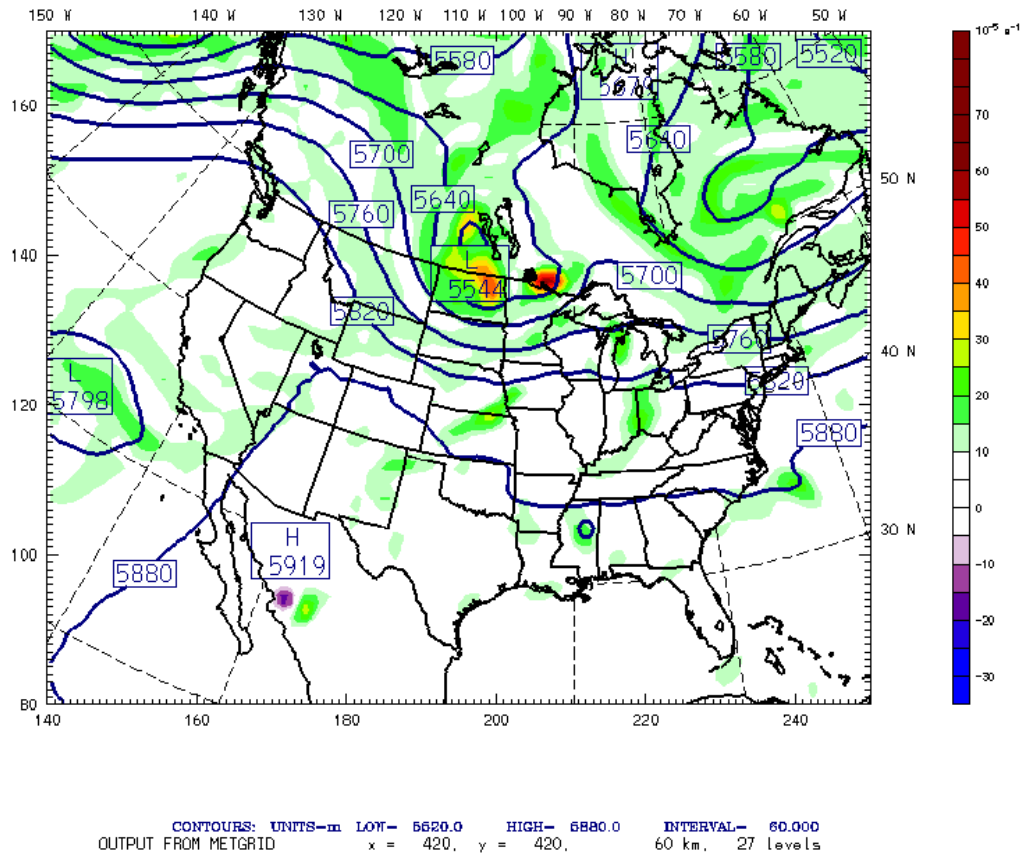
Figure 27: Absolute vorticity from 0 (white) to 50 (red) and geopotential heights contoured in meters at 500 hPa.
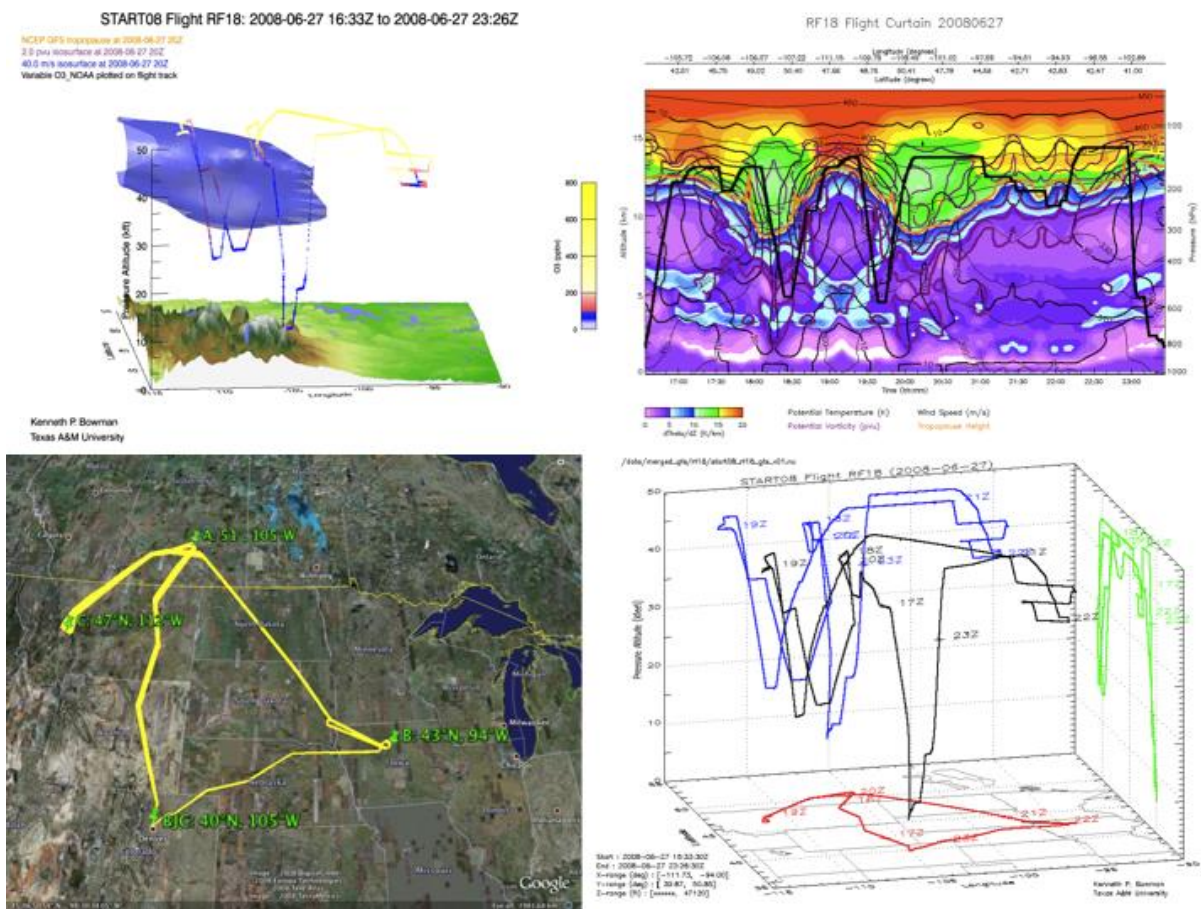
Figure 28: Flight curtain RF18 containing top left: 50.0 m/s wind isosurface (blue), and 2 pvu

isosurface (purple), an ozone isosurface (yellow), the flight path (blue), and a tropopause

indicator (yellow line); top right: contoured PV (purple to red), flight path (black), tropopause

(orange line), potential temperature contours (black), potential vorticity contours (purple) and

wind speed contours (black); bottom left: 3-dimensional view including latitude and longitude of

the flight over Google Earth map; bottom right: flight path with corresponding times written

above the portions of the flight.

There will be two highlighted segments on this mission because it was longer than the previous mission and the trough was short and curved. GFS forecasts indicated that the aircraft's flight path should take it directly through a jet streak on the back end of the trough. Measurements from this flight, therefore, should be able to provide data on the stratospheric lamina on the western portion of the trough, and convections contributions to overfolds on the eastern portion of the trough, through the thunderstorm outbreak. Figure 29 indicates 300 hPa winds showing the region of the jet streak that the flight would fly through and the trough in its entirety.
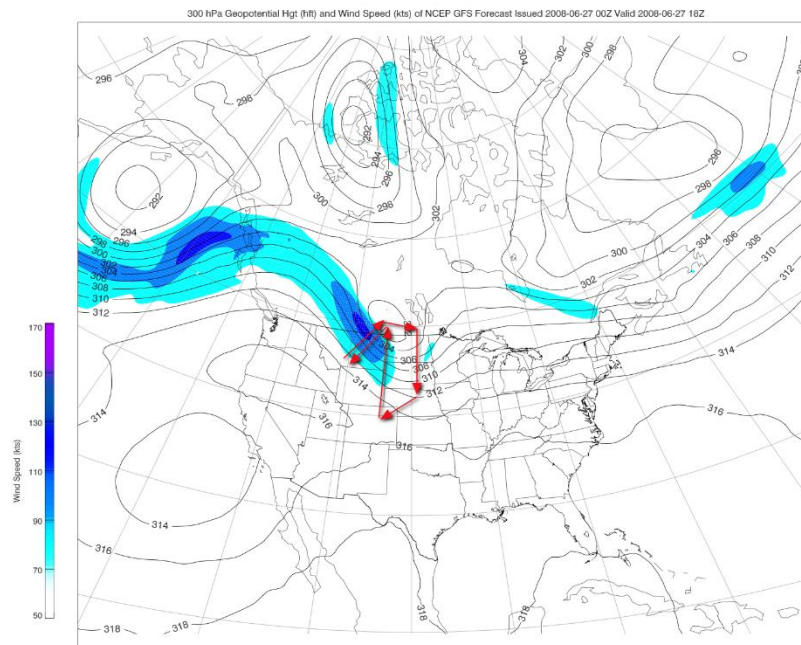
Figure 29: 300 hPa winds from minimum (white < 70 kts) to maximum (dark blue > 170 kts) and contoured geopotential height (black lines) in hectofeet, and flight path in red arrows.

Figure 30 indicates the positioning of the flight during the mission and the highlighted segments. These segments were selected and highlighted due to their proximity to a jet core and

a large horizontal PV gradient. PV, indicated in the second panel in Figure 28, insinuates segments of dark green and yellow should be of particular interest as they represent the aircraft's ascent and descent through the jet core. Prominent mixing is expected in portions of these segments, and heavy wind shear is as well. The UWNMS will be used to further investigate the lifespan of the air associated with this system particularly in or near the jets.

A)

B)
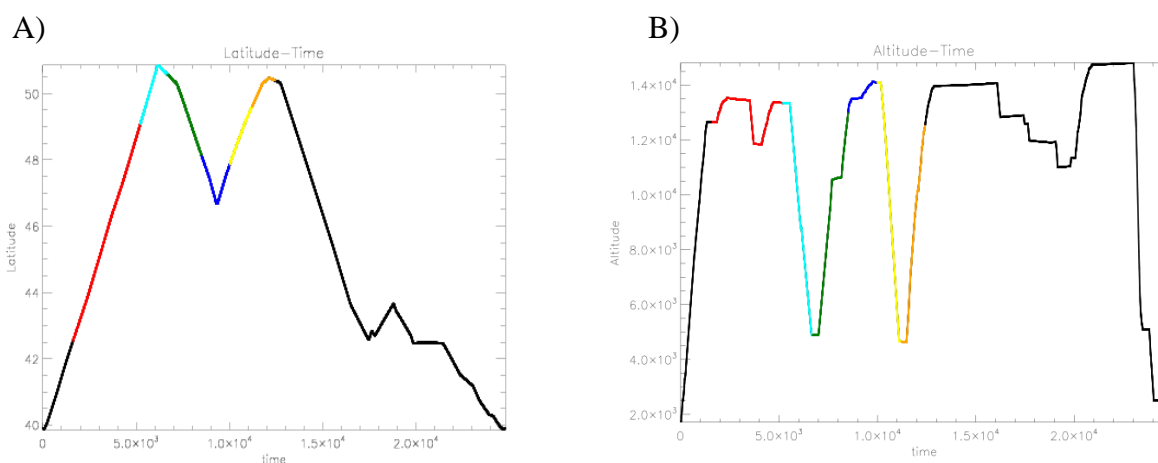
Figure 30: Panel A) represents latitude (y axis) – time (x axis in seconds after takeoff) with highlighted segments of focus. Panel B) represents altitude (y axis in meters) and time (x axis in seconds after takeoff) with highlighted color coded segments as defined by PV structures in Fig. 26.

The tracer-tracer plots in Figure 31 indicate considerable mixing in this system, in particular the dark green, cyan, and yellow segments. This is of interest as these segments come closest to the jet streaks, and indicate the most amount of mixing indicating significant subsidence. Mixing in the green segment is notable as wind speeds are the strongest in this segment, approaching speeds of a jet. The well-mixed air can be identified by the more linear

shape of the slope rather than the hard sloped "L-shape" commonly seen when transitioning from

the troposphere through the stratosphere using H_2O and O_3.

A)   B)
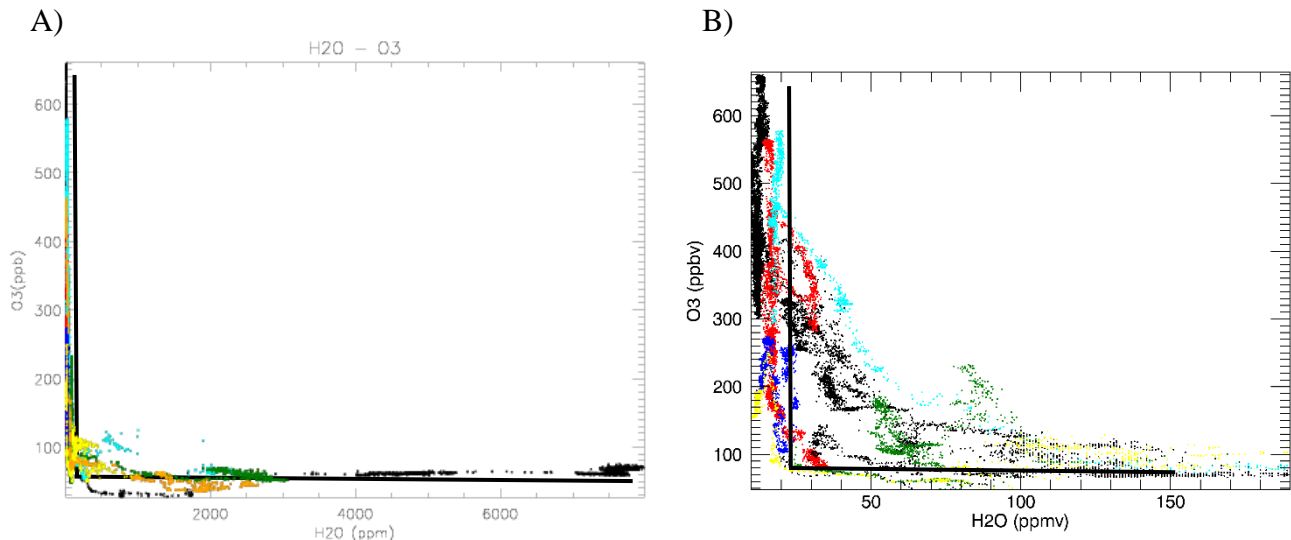
Figure 31: A) represents Tracer-tracer plots for Flight RF18 with color-coded segments from

Figure 28. Panel B) is zoomed in to a 0-700 ppbv ozone and 0-190 ppmb water vapor range. L

shape for reference for typical upper troposphere to lower stratosphere transition.

      The individual segments of the flight (Fig. 32) are shown separately in an effort to

remove noise. These individual tracer legs seem to indicate further that the cyan, green and

yellow segments are very well mixed moving through the tropopause. In all of these segments a

tropopause is observable with portions of the measured air masses being low in both ozone and

water vapor. However without mixing, the transition should be a hard-sloped L – shape and these

plots indicate some sort of mixing with observations breaking those transitions. The green and

cyan segments also appear to capture a separate air mass with a second dense portion of

observations that is water vapor rich but ozone depleted. Methane oxidation can create a slight increase in water vapor above the tropopause creating a C-shape in the chart. In the red segment, there appears to be two separate maxima as water vapor increases twice above the minima of the tropopause. This indicates two separate influencing air masses in the segment. In the lower stratosphere a slight increase in water vapor can be observed due to the oxidation of methane producing water vapor. In the red segment however there appears to be two maxima above the tropopause. The second C-shaped maxima that overlaps could be a second air mass within the area. The cyan segment depicts a slight amount of mixing as it descends through the tropopause and back into the water vapor rich troposphere. This is manifest by the slight increase in ozone concentration in the upper troposphere. The blue segment, once again contained no real organization, in spite of its stratospheric composition with varying amounts of water vapor in the segment. Oxidation could explain some of the increased water vapor in the lower stratosphere however due to the lack of a linear shape, some mixing is present. The yellow segment also comes within close proximity of a jet core, and once more displays regions of mixing with water vapor concentrations reaching 200 ppmv and ozone concentrations reaching 100 ppbv in the upper troposphere which could indicate subsidence or a circulation around the jet core, further analysis is required. There appears to be an overall lack of mixing in the orange segment, however the mixed region could be driven by turbulence between the UTLS in the jet core. Finally the orange segment suggests little to no mixing, containing the basic L shape one would expect as the aircraft flies through the troposphere into the stratosphere.
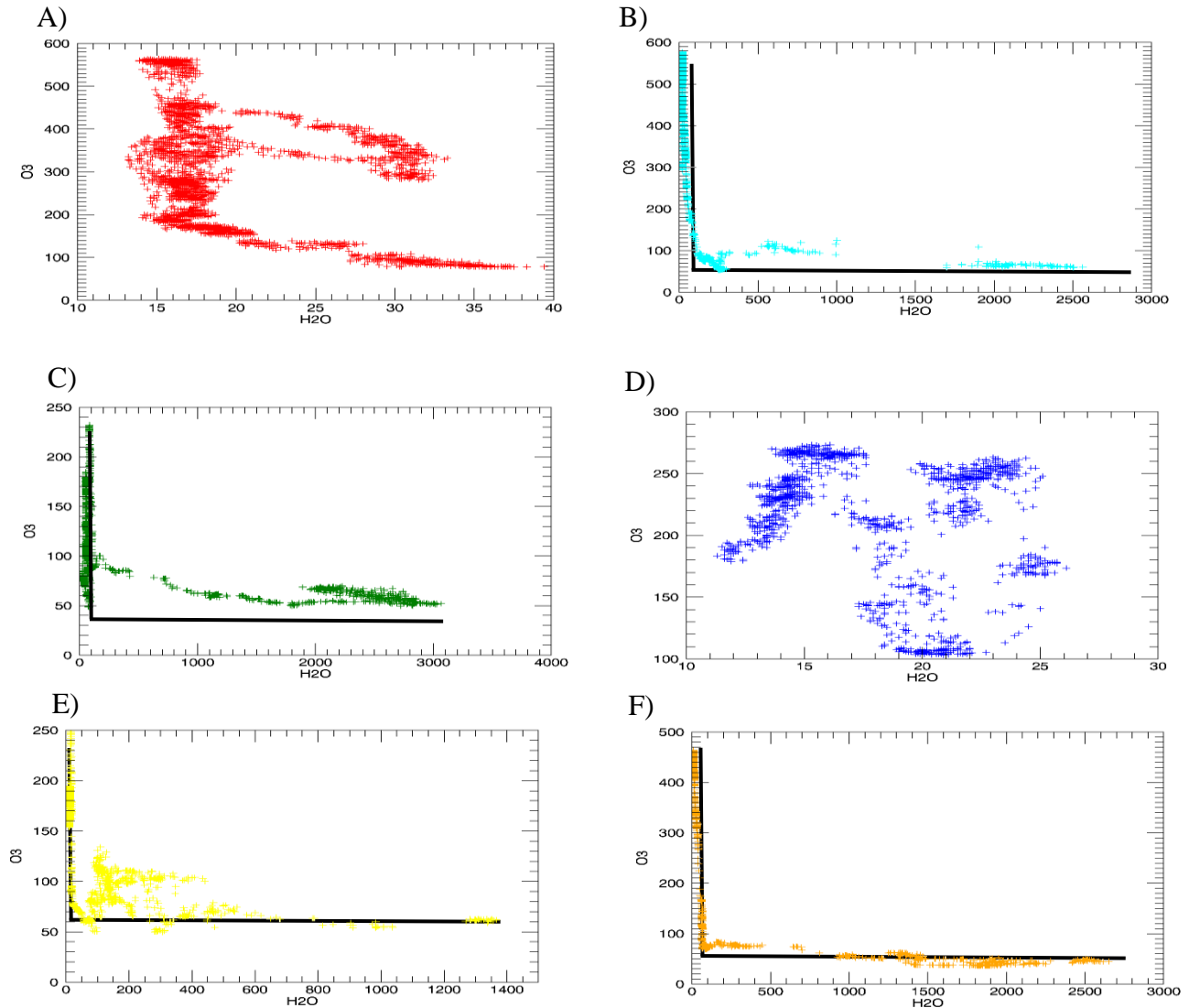
Figure 32 Tracer – Tracer plots of RF18: ozone on the y axis (ppbv) and water vapor (ppmv) on the x-axis, each of which correspond to the color-coded segments from Figure 20. Panel A) steady altitude in the lower stratosphere, panel B) descent through the tropopause, panel C) ascent through the upper troposphere through the a jet streak, panel D) the aircraft maintaining altitude in the lower stratosphere, panel E) descent through the jet core, panel F) ascent through the tropopause in the lower stratosphere. Scales on the axis are different in order to capture different phenomena in the segments. L shape for reference to typical upper troposphere to lower stratosphere transition

PV can also indicate the presence of interaction between stratospheric air and tropospheric air by showing rapid changes in values. Figure 33 shows the potential vorticity throughout the flight over time, with the color-coded segments. A large gradient of PV can indicate the tropopause, and coupled with large wind speeds an intrusion process around a jet core. The green segment becomes a portion of further interest. Despite the increase in altitude, very little increase in potential vorticity is observed. The blue segment, which immediately follows the green segment, also shows a significant increase in PV despite maintaining its altitude in the stratosphere indicating the presence of tropospheric air within the region. The green segment indicates a slight uptick in stratospheric air which could be the result of a significant amount of subsidence beneath the jet core indicating more tropospheric air. This is further supported by the high measurements of water vapor observed in the green segment. The sharp change in PV seen in the blue region indicates a large PV gradient, indicating a crossing over into the stratosphere above the jet core, this supports the tracer-tracer plot records, with a very dry ozone rich measurement. Figure 32 indicated higher than expected portions of ozone within the flight indicating prominent mixing occurring in or around the jet core and the rapid changes in values could indicate turbulent mixing within the core. The PV values of the yellow and orange segments are typical for an ascent into the stratosphere and descent into the troposphere. However, as shown in Figure 32, mixed portions were captured in the yellow segments, but no intrusions or mixing were visible in PV (Figure 33) indicating further turbulent mixing. The red segment also showed an interesting anomaly, where a slight decrease in altitude was met with a sharp decrease in PV followed by an increase in PV. This could indicate that the plane was hovering right along the tropopause or slight mixing involved in a transition layer.
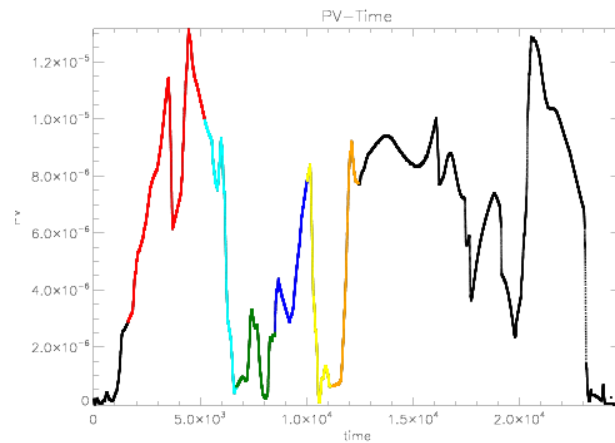
Figure 33: PV (y) – time on the x axis (seconds after takeoff) during flight RF18 using GFS analyses with color-coded segments from Figure 20.

Figure 34 is an indicator of all points in a tracer – tracer format of meridional winds that reach a threshold of 85 knots in RF18. There does not appear to be much organization in Figure 34 and a high concentration of points with low amounts of water vapor and ozone, indicating an unmixed region in the flight. Therefore, mixing did not occur in the jet stream in this mission and the flight. This is of note as the PV charts appeared to capture turbulent activity within and around the jet core itself as seen by the rapid changes in PV values. Turbulence does not appear to play a significant role in data captured in this flight.
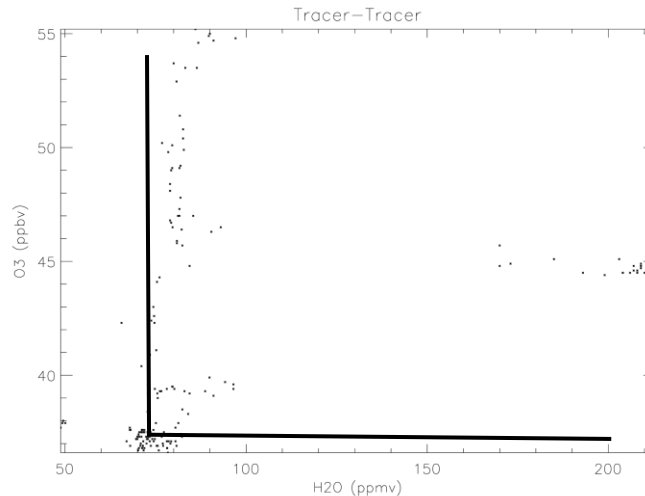
Figure 34: Water vapor (ppmv) on the x axis – ozone (ppbv) on the y axis of points with meridional winds greater than 85 knots representing the jet cores. L shape is placed for reference for typical upper troposphere to lower stratosphere transition

Figure 35 shows wind speeds in the highlighted segments. As expected through the system, in the green segment winds reach their top speeds throughout this flight in both the zonal and meridional direction, approaching 115 knots meridionally in the green segment, and a ~75 knots zonal component. Likewise the yellow segment showed significant amounts of wind speed, indicating that these are the two most likely segments for a jet streak to be present. Due to the high amounts of mixing observed in the previous plots and the heavy tropospheric presence mixing is occurring within this segment and around the jet streak itself. Wind speeds in the cyan to yellow segment increased by ~60 knots in the zonal direction and ~75 knots equatorward. Shear is crucial for overfolds and underfolds to form and for mixing. In all of the segments, speed shear is prominent. Once more the red segments shows a rather interesting decrease in wind speed along that slight decrease in altitude indicating possible mixing in this segment along

the dynamic tropopause. The magnitude of the two wind components indicates a very strong jet core in the red, green, and yellow regions which is interesting as the yellow and green regions show significant subsidence and tropospheric air, whereas the red portion of the flight is very stratospheric with high concentrations of ozone measured and lower amounts of water vapor.

A)

B)

C)
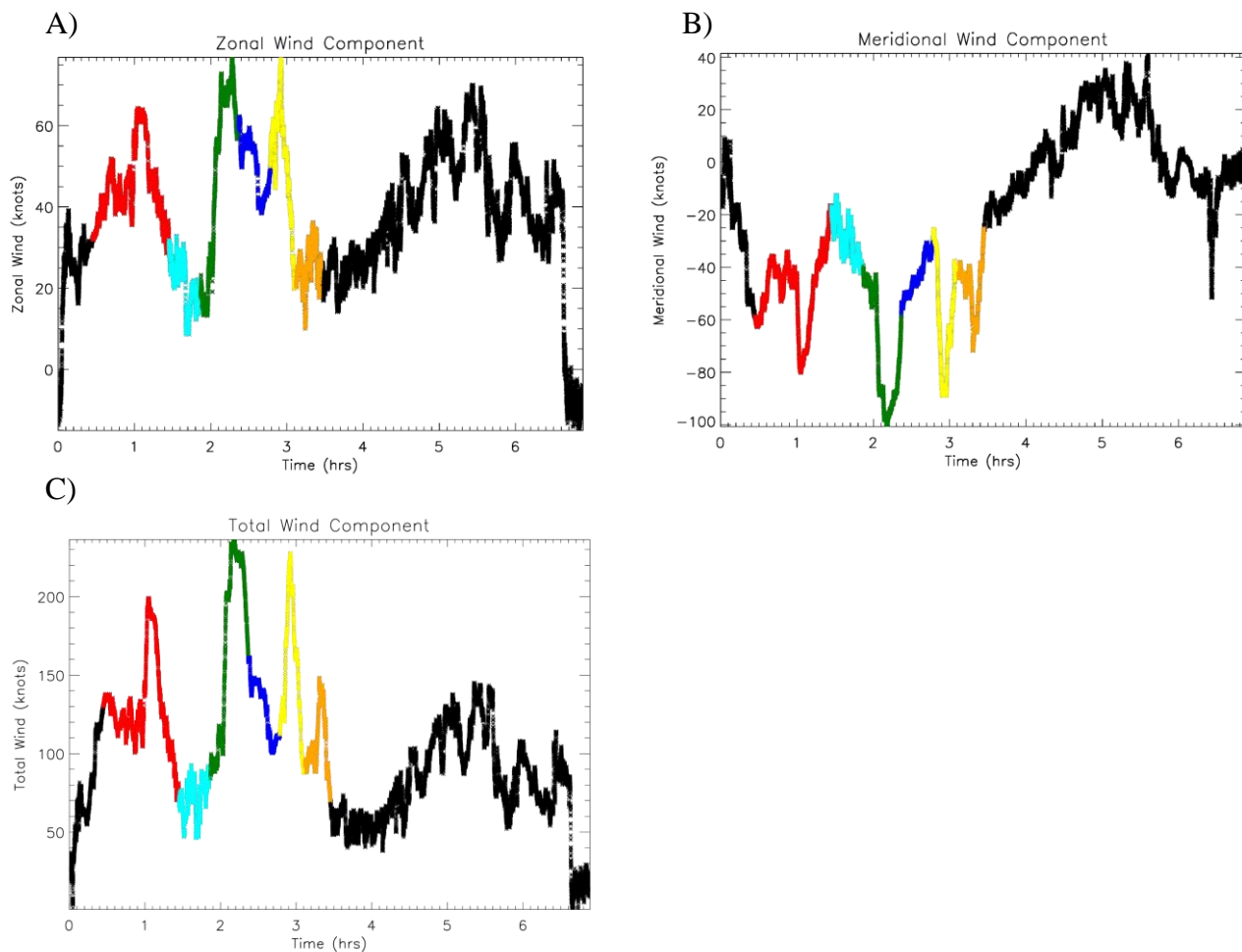
Figure 35: Aircraft-detected a) zonal, b) meridional, and c) zonal and meridional magnitude components (knots) as a function of time along the flight path for RF18.

6. UWNMS Simulations

This chapter describes simulations of the UWNMS model during the three flight missions discussed in chapter 5. Synoptic and mesoscale phenomena will be viewed using spliced together model cross sections through the VIS5D viewing software. Each of these model simulations will be compared to their respective START08 data in order to display the accuracy of the UWNMS constituents during these events. Flight paths have also been coded into the model as a separate tracer, allowing visualization of the flights positioning during synoptic scale events.

One of the primary indicators of stratospheric air used in our model runs is the use of a tracer that increases linearly from 0 at the surface to 1 at the top of the model, which is 15 km in these model runs called tracer3. This tracer can help identify tropospheric air that gets inserted into the lower stratosphere by intense convection as well as sinking stratospheric laminae in the troposphere.

6.1. Flight RF04

Flight RF04 flew across the Midwest states from Colorado to Illinois. The flight path is highlighted in Figure 36 by a red tracer. Figure 36 also indicates from a top down view tracer3. These values are contoured from blue (0 representing tropospheric air) to red (1 representing the top of the model, in this case 15 km stratospheric air). As indicated by the model the back end of the trough reaches down into Iowa and the front end of the trough reaches into West Virginia and Ohio. What becomes immediately evident is that high values of tracers at lower altitudes can be observed along the trough, particularly the western side. This higher volume of the tracer indicates subsidence as stratospheric air sinks to this altitude, indicating the presence of an upper level front. Streamlines and potential temperature contours indicate a sinking motion, and trajectories that track the motion of air parcels indicate the same conclusion: stratospheric air has a slow sinking motion on the western portion of troughs where slow persistent subsidence is expected to take place. The trough is surrounded on either side by high pressure systems along the east coast and the Rockies. This high tropospheric air can be attributed to rising air in the warm conveyor belt east of the trough.

To the west of the trough a deep ridge has developed indicated by the high-pressure system that forms in southwestern Texas. This ridge can be indicated using tracers as well as divergence aloft results in sinking stratospheric air in that same area. In Figure 36 the high pressure system can be recognized in the southwest corner by a high concentration of tracer values as convergence from the lower stratosphere sinks causing an increase in stratospheric air in the region.
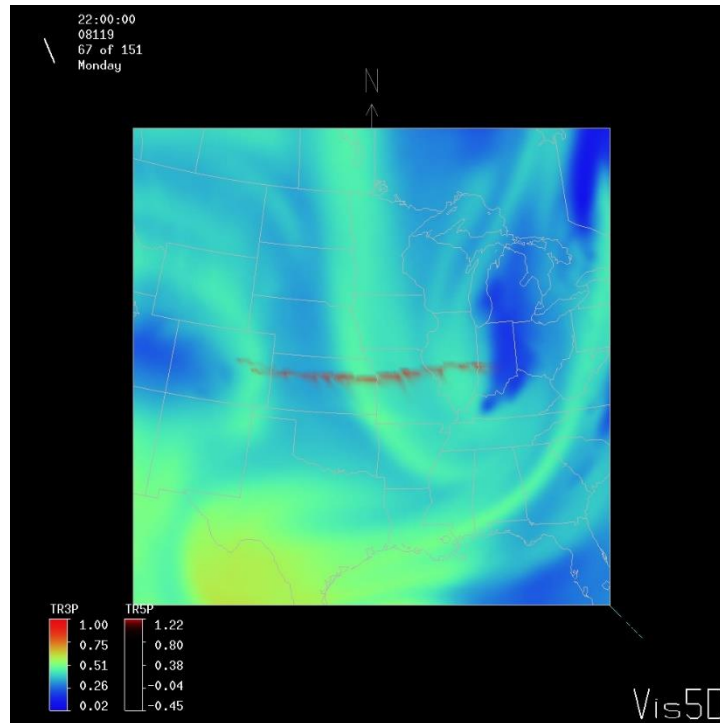
Figure 36: Flight path of RF04 in red over a horizontal slice of the tracer contoured from blue (tropospheric air with tracer value ~0) to red (stratospheric air with tracer value ~1) at a ~6km horizontal slice viewed from the top down.

Figure 37 represents another top down view of tracer3 but also contains the jet streaks flanked by the trough. The poleward component of the jet is indicated by a pink color with wind speeds reaching ~120 knots. The green segment represents a meridional wind component of the jet, with winds reaching ~120 knots. As the cyclone matures, the trough tilts notably negatively, indicating a matured cyclone and increased vertical wind shear as well as strong thermodynamic instability driven by differential advection. As the trough continues to tilt the poleward wind component appears to strengthen and organize at the expense of the meridional component.
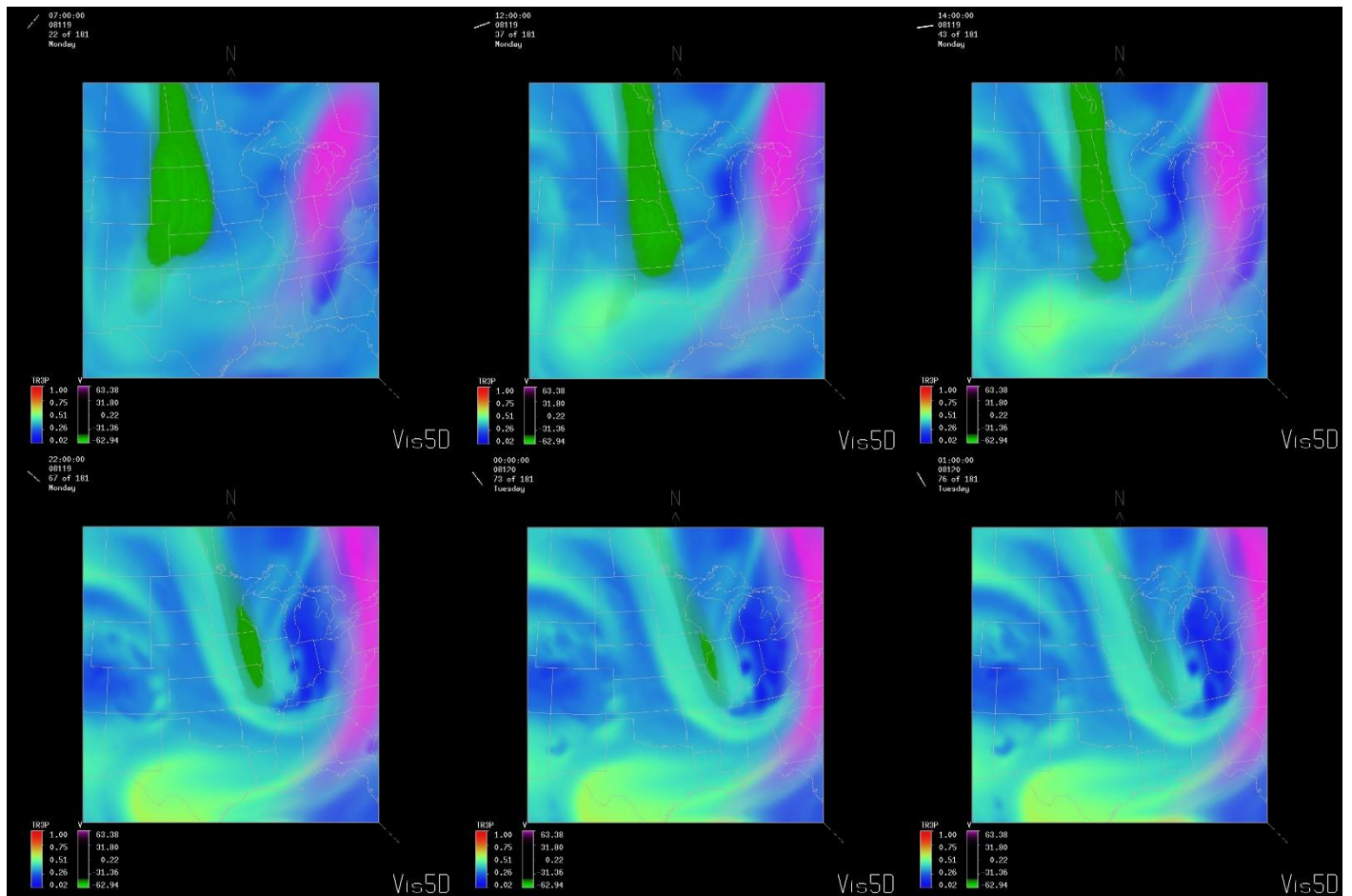
Figure 37: Northward winds (~120 knots) in pink, southward winds (~-120 knots) in green, tracer from blue (0 representing tropospheric air) to red (1 representing stratospheric air at 17.5 km) at an altitude ~6 km from a horizontal slice looking from the top down. Data was collected from 07:00 on 04/28/2008 to 01:00 on 04/29/2008

Figure 38 is a comparison of the model data and flight data for RF04 winds. The red represents the model, and the blue the flight. The plot on the left represents zonal winds, while the plot on the right represents meridional winds. The UWNMS accurately depicted winds, with

some inaccuracies are to be expected due to resolution. Quick changes and peaks in the winds

measured in the flight, that were not captured by the model can be explained by the difference in

rates of data collection; the model captures data once every 30 seconds, whereas the flight

captures the same wind data every second. The model also captures horizontal resolution at a

scale of ~20,000 meters creating lots of variability in wind motions associated with wind

phenomena at smaller scales that were not captured by the model but were by the aircraft. This is

much more pronounced in the vertical winds observed later. This can explain the more jagged

peaks in the flight data compared to that of the model. Panel C) represents the magnitude of both

wind components and gives a better estimation of the model's overall ability of capturing winds.

Once more the model accurately portrayed winds, particularly large anomalies like jet maxima

with small errors that can be defined as spatial resolution issues.

A)

Zonal Wind Component

B)

Meridional Wind Component

C)

Total Winds
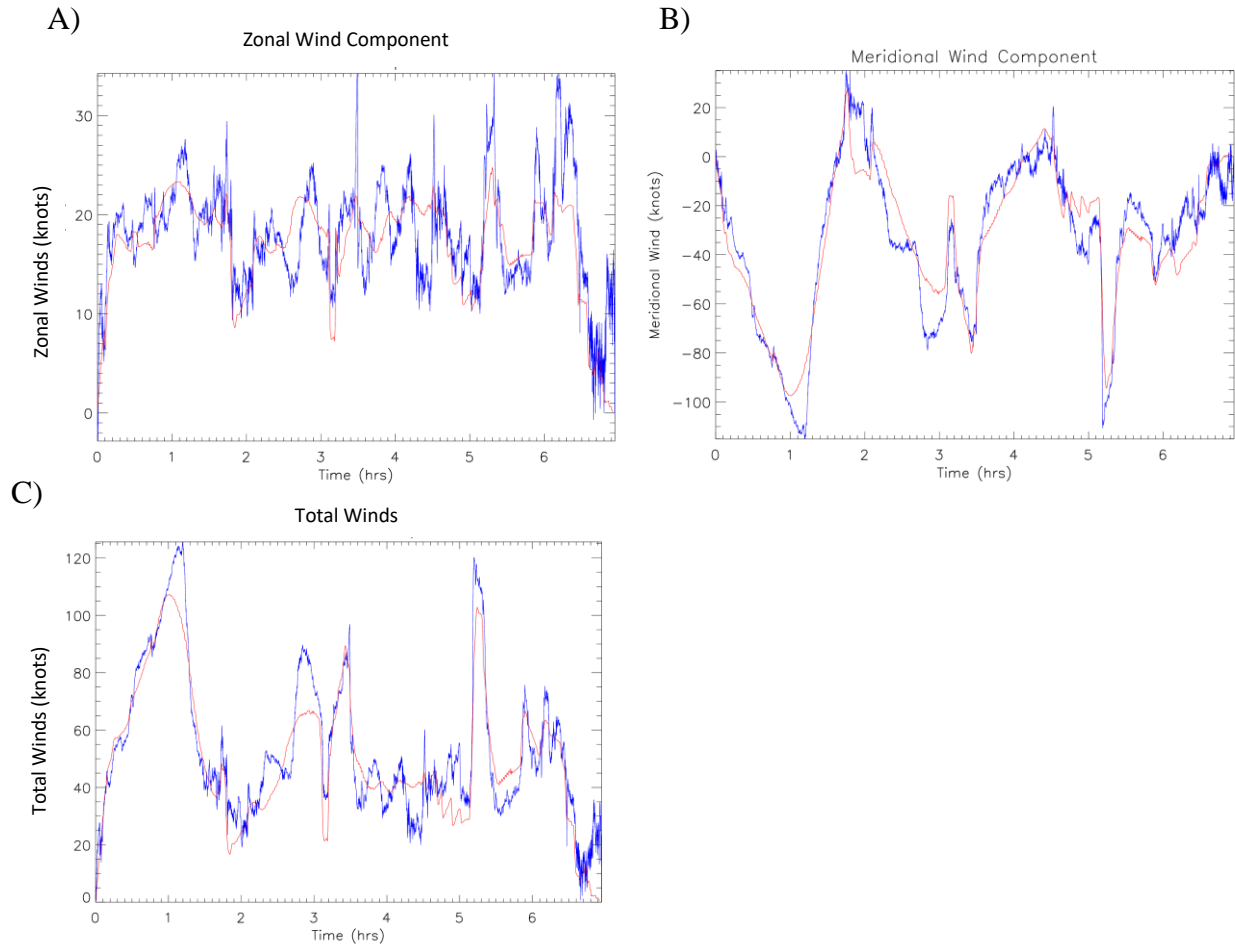
Figure 38: model (red) and flight (blue) data for zonal A) and meridional B) and the magnitude of the two components C). This comparison is done over time of the flight in hours

Figure 39 indicates more comparisons between the model and the flight. Panel A) represents Tracer3 in the model through a red color and potential temperature in blue color. Theta gradients modulate potential vorticity and the trends from tracer3 compare favorably. Panel B) compares the same tracer to PV. Potential vorticity and the tracer both had to be placed on the same scale in order to be compared. Trends from the model's tracer do appear to follow overall trends from PV. It was never the intent for values of tracer3 to compare to PV, thus the

close accuracy of the two constituents is not a concern. Originally the importance of the tracer was to compare it to stratospheric trends, and in that aspect, the tracer compares favorably to PV, which has already been shown to represent stratospheric air.

A)

B)
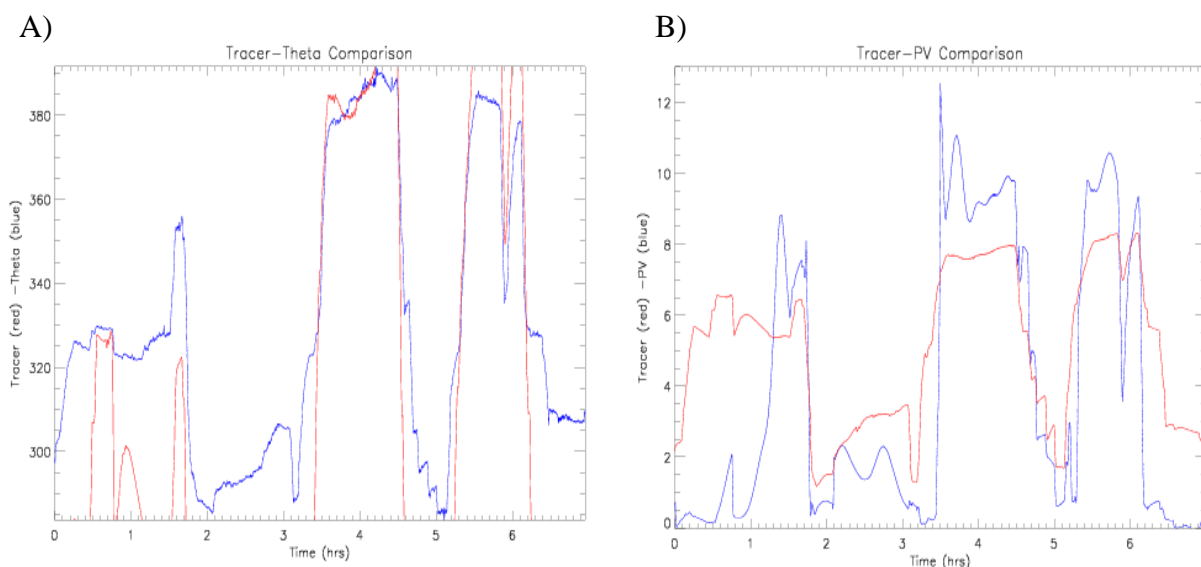
Figure 39: Potential temperature (blue) tracer (red) comparison observed over time in panel A) and potential vorticity (blue) compared to tracer (red) over time in panel B) for RF04

Unfortunately the UWNMS struggled to capture vertical winds (comparisons can be seen in Figure 53) and an alternative to indicating sinking air was found due to spatial resolution issues. Due to the UWNMS' scale in this study many small scale dynamical processes could not be calculated. Results below show that air parcel trajectories in southward or northward moving air follow streamlines and potential temperature contours. Streamlines represent flow in a constant direction. The trajectories placed in the system follow the same downward-sloped path that the streamlines and potential temperature contours both represent into the troposphere indicating sinking air. The air typically follows sloped theta surfaces and which provides a vertical component to the motion of the air typically associated with upper level frontogenesis.

Due to the lack of accuracy in the downward winds, is assumed to be a scaling issue with the

model; potential temperature and streamline contours served as our sinking mechanism, as seen

in Figure 40. Figures of the downward winds will be discussed with Figure 53.
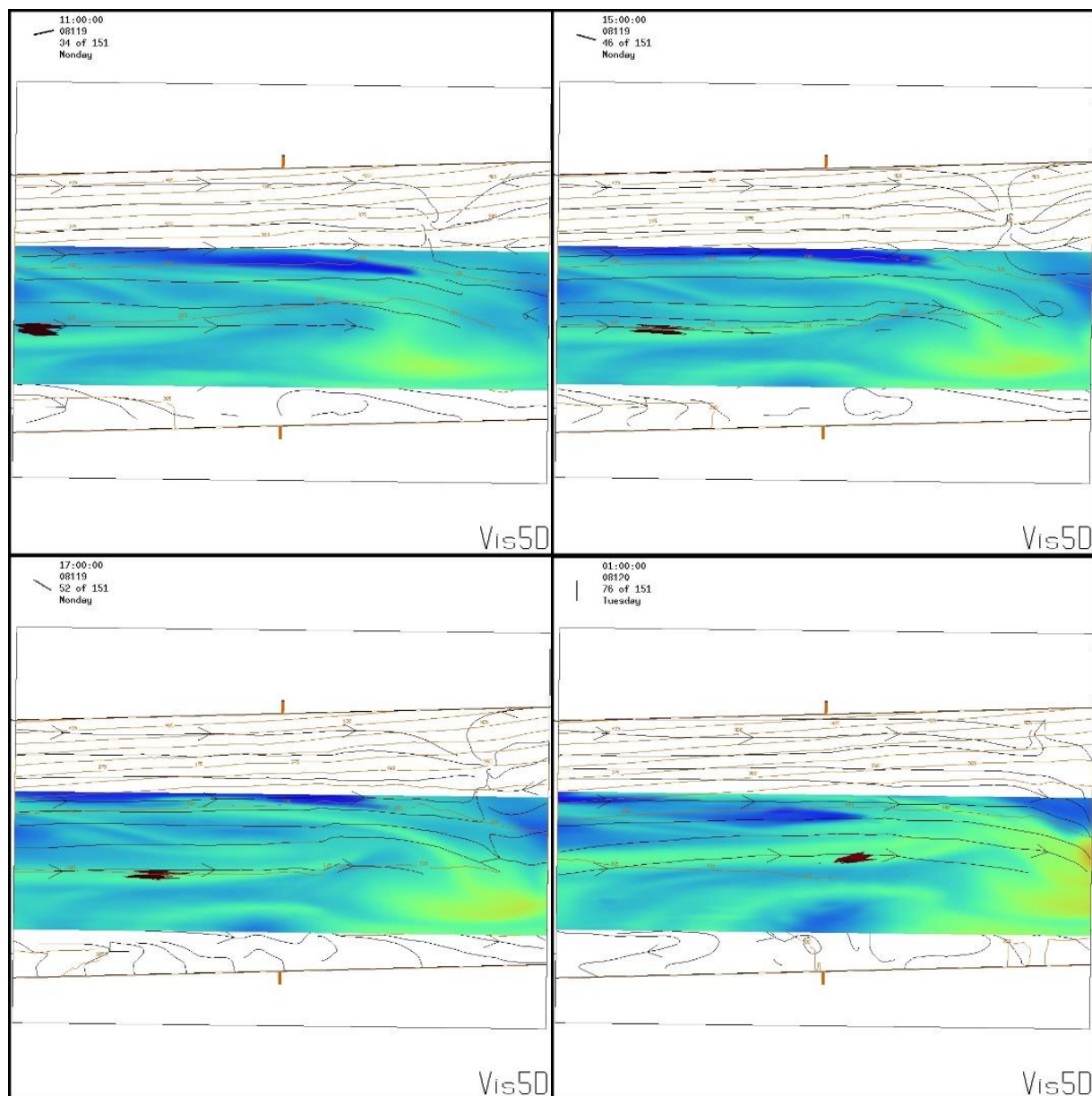
Figure 40: Trajectories (dark red) on a horizontal plane in RF04 with a vertical slice of potential temperature contours (in black) and streamlines (in orange) sliced on top of an oblique colored tracer plane from 0 (blue tropospheric air) to 1 (red stratospheric air) to determine the direction of flow

6.2. Flight RF06

Flight RF06 is another flight that showed frequent mixing. The model runs indicated a similar significant sinking stratospheric laminae sinking along the western portion of the trough. This stratospheric lamina indicates significant subsidence affiliated with upper level troughs, which undercuts the tropospheric air creating an intrusion. The flight flew right through one of these stratospheric laminae, and can be observed in figure 41. As the trough moved and the cyclone intensified, zonal winds seemed to intensify and the stratospheric air is pulled eastward. Of interest in this particular case, the stratospheric lamina is cleaved into two wedges by convective updrafts. One of the wedges precedes the line of convection, differing from that of flight RF04. The other wedge forms behind the line of convection, bracketing this region of convection between regions of low stratospheric air. The high concentration of stratospheric air behind the thunderstorms is consistent with what was observed in RF04. These lamina appear to be present before the thunderstorm outbreak, but tracer3 density increases which appears to be a byproduct of displacement of stratospheric air due to significant convection.
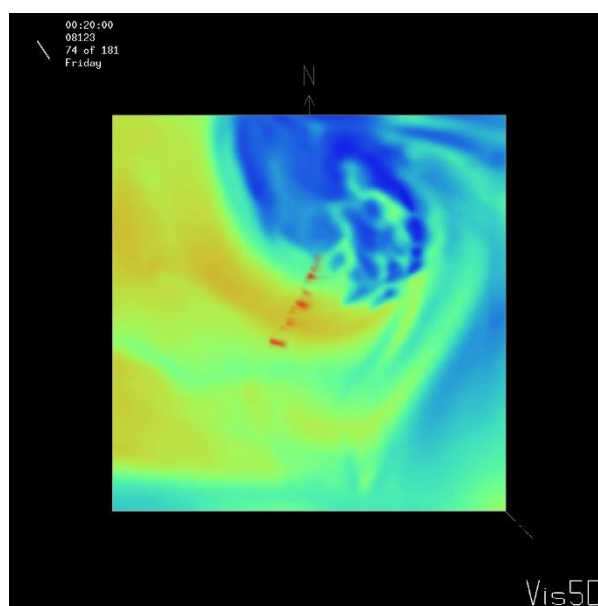
Figure 41: Flight RF06 flight path (red) over horizontal slice of the tracer contoured 0 to 1 (blue to red) at approximately 6 km.

RF06, much like RF04 is dominated by a northerly jet streak early in the life cycle of the trough. The green portion of the flight represents the northerly winds measured at velocities of ~120 knots. The pink portions of the flight indicate southerly winds measured at velocities of ~120 knots. Winds at these speeds indicate jet streaks and jet cores. There is no indication of any organized southerly jet until convection begins to develop and intensify. At the top of the convection, divergence aloft appears to lead to intensification of winds in the region, developing a jet streak and eventually organizing on the western portion of convection. Figure 42 suggests that as the cyclone intensifies, the northward component of the jet organizes and strengthens in concert with convective development.
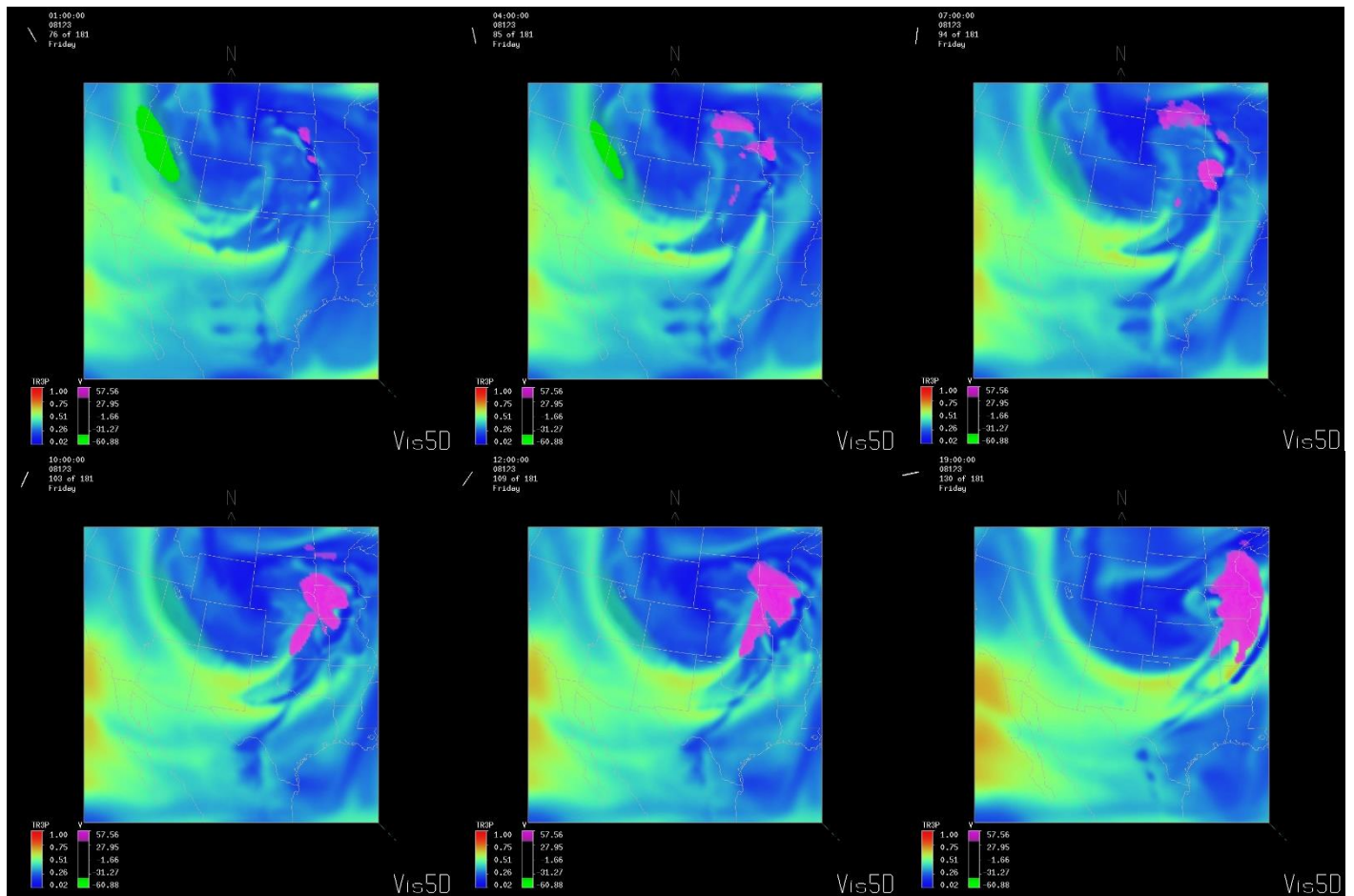
Figure 42: Flight RF06 horizontal slice of tracer at 6 km colored 0 to 1 (blue – 0 km to red – 17.5

km) and wind speeds greater than (less than) 120 knots in pink (green). Data was collected from

01:00 UTC to 19:00 UTC on 05/02/2008

Figure 43 represents the comparison of the model in red and the flight in blue. Wind

speeds and direction during RF06 are an important variable to measure. While the model

captures zonal winds (left) nearly perfectly, it struggled to capture the meridional winds as

accurately. However, there is a great deal of accuracy on overall trends. It must be noted that

observations for the model were collected every thirty seconds, whereas the flight collected data

every second, which would explain the immediate and swift changes in values in the flight data that the model may not capture accurately. Spatial issues may result in the missed measurements particularly in the meridional component. Due to the small magnitude of those winds, small microscale dynamic mechanisms that weren't capable of being captured by the model could influence the winds slightly which due to the scale of the plot may be magnified more. A better comparison of the accuracy of the model is the total wind component seen in panel C) which indicates the model captured wind magnitudes to a great detail of accuracy.

A)

B)

C)
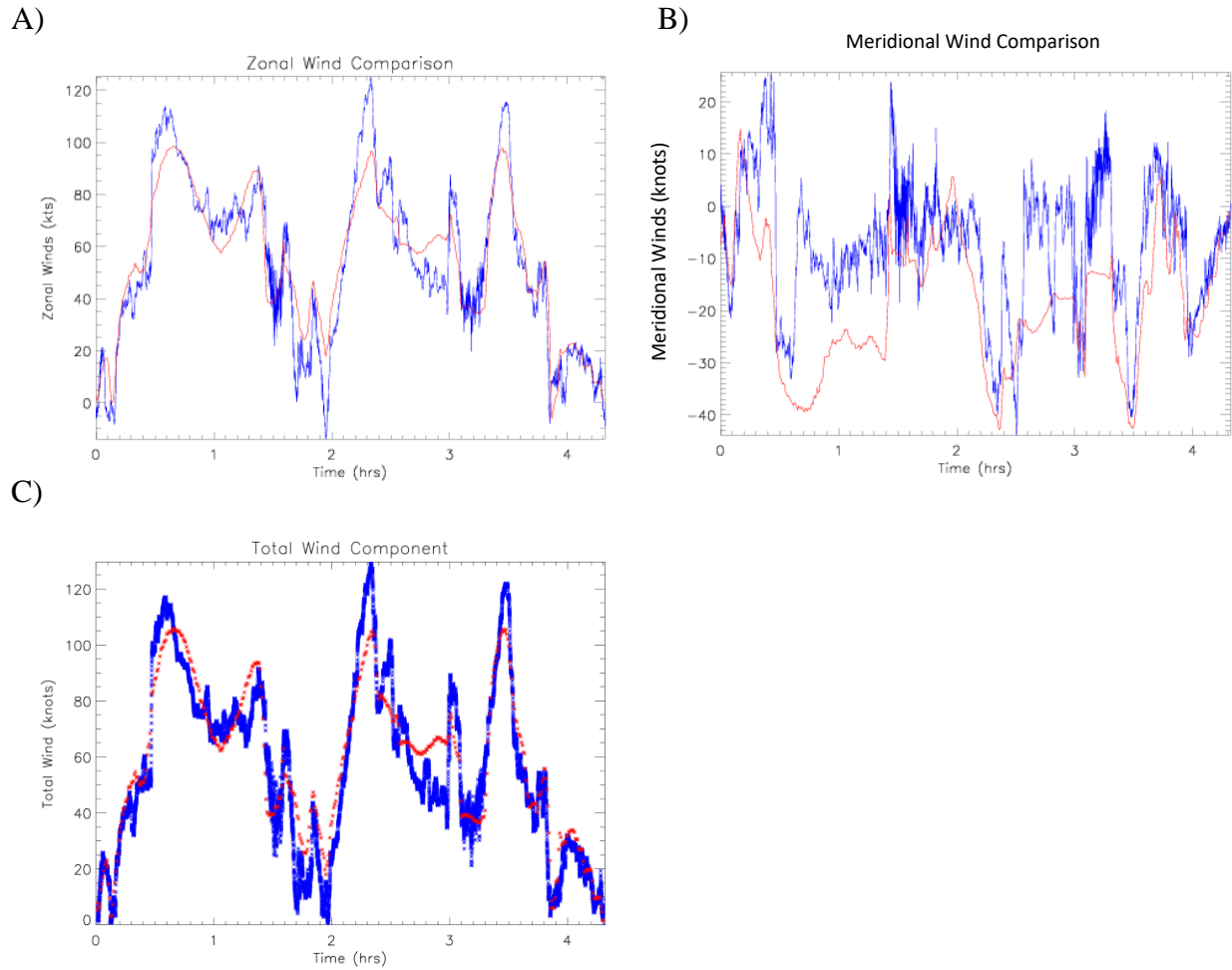
Figure 43: Model (red) and flight (blue) comparison of zonal A) and meridional B) winds in knots over time for RF06.

The model will also be compared to important constituents. Tracer3, which is set to 0 at the bottom of the troposphere and 1 at the top of the model, was compared to potential temperature in panel A) and PV in panel B) in figure 44. The tracer captures potential temperature values and trends accurately when placed on the same scale as potential temperature. Potential temperature gradients are a crucial factor for measuring sinking and rising air. PV, when placed on the same scale as the tracer, was captured accurately. While values were not

exact and precise, tracer3 does appear to capture gradients accurately, with large changes accurately depicting tight PV gradients.

A)

B)
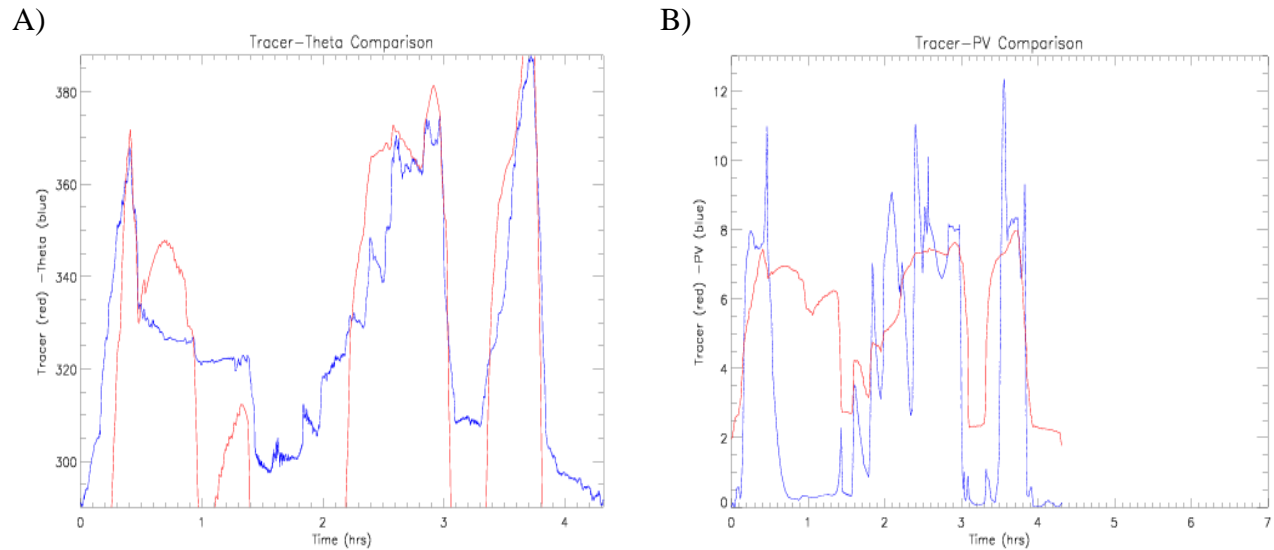
Figure 44: Potential temperature (blue) tracer (red) comparison observed over time in panel A) and potential vorticity (blue) compared to tracer (red) over time in panel B) for RF06

Flight RF06 was analyzed using potential temperature and streamline contours in an effort to capture sinking air trends. This process can be viewed in figure 45, which shows an oblique view of tracer3 on a 6 km plane. Trajectories were placed in the model plane to study the motion of air along the western portion of the trough. Air followed potential temperature contours and streamlines, sinking slowly along the jet streak indicating sinking stratospheric air. This process is very slow – trajectories sink at approximately 1km/10hrs though a distinct sinking phenomenon between the western portion of the trough and the meridional jet core.
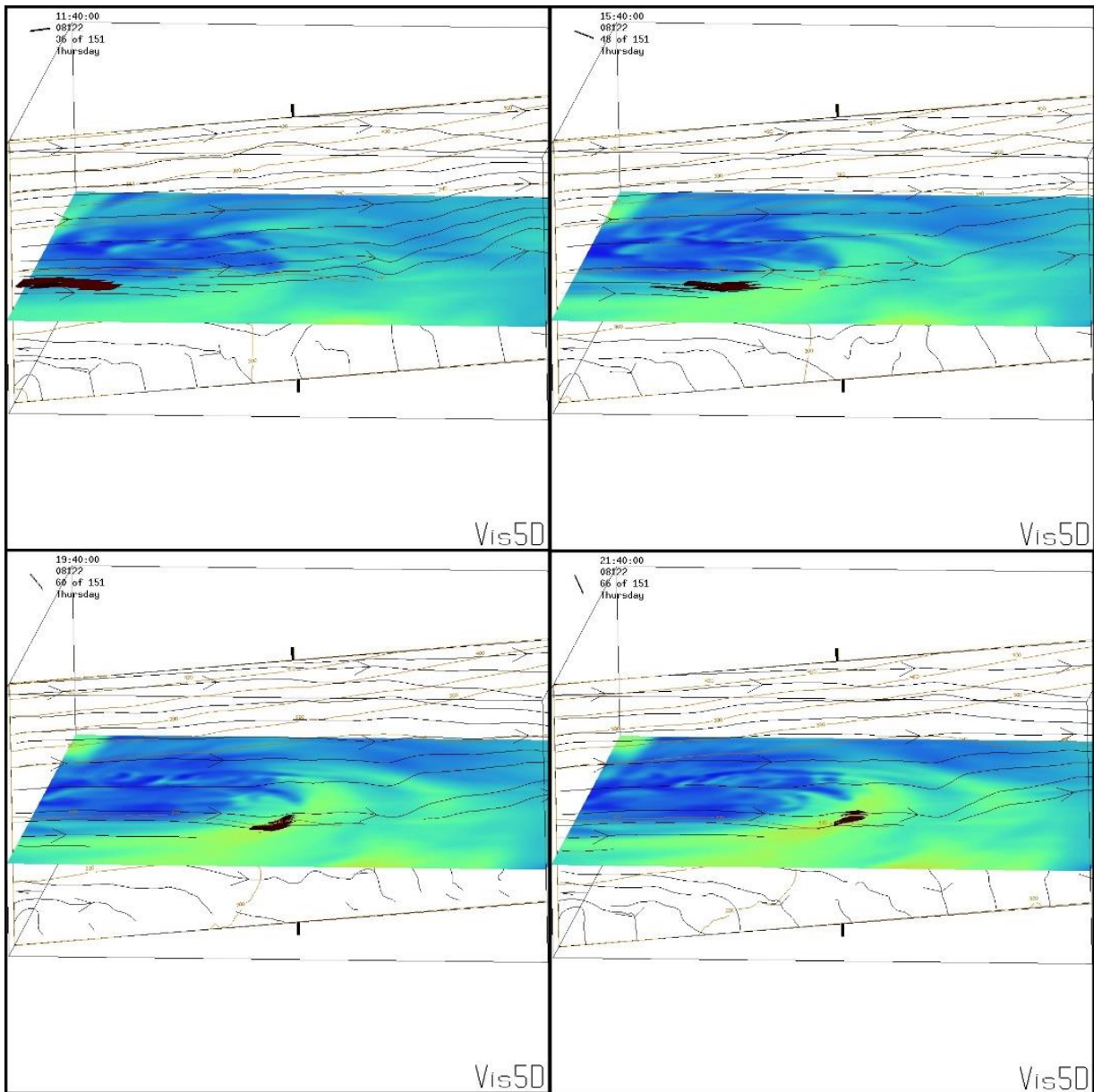
Figure 45: Trajectories (dark red) on a horizontal plane in RF06 with a vertical slice of potential temperature contours sliced on top of an oblique contoured tracer plane from 0 (blue tropospheric air) to 1 (red stratospheric air).

Flight RF06 also presented an opportunity to observe air around the jet during convection. As the trough intensified, a line of convection formed on the east side of the jet. As the convection begins to intensify, the air became destabilized and a jet streak became more organized in the poleward direction. For this portion trajectories were placed inside the thunderstorm's updraft in an effort to understand where they go before, during, and after the thunderstorm. The trajectories are labeled in Fig. 46 by light green ribbons, and blue to red color bar is associated with tracer3 and the pink region represents a ~105 knots jet streak moving poleward. The low tracer values in the lower stratosphere indicate a thunderstorm updraft. The trajectories follow the updraft into the lower stratosphere before dispersing and diverging downstream from the jet. It would appear that the trajectories follow the jet streak (the pink region represents regions of wind speeds ~55 105 knots) downstream, suggesting that tropospheric air can be advected downstream by winds and further creating an overfold of tropospheric air over stratospheric air.
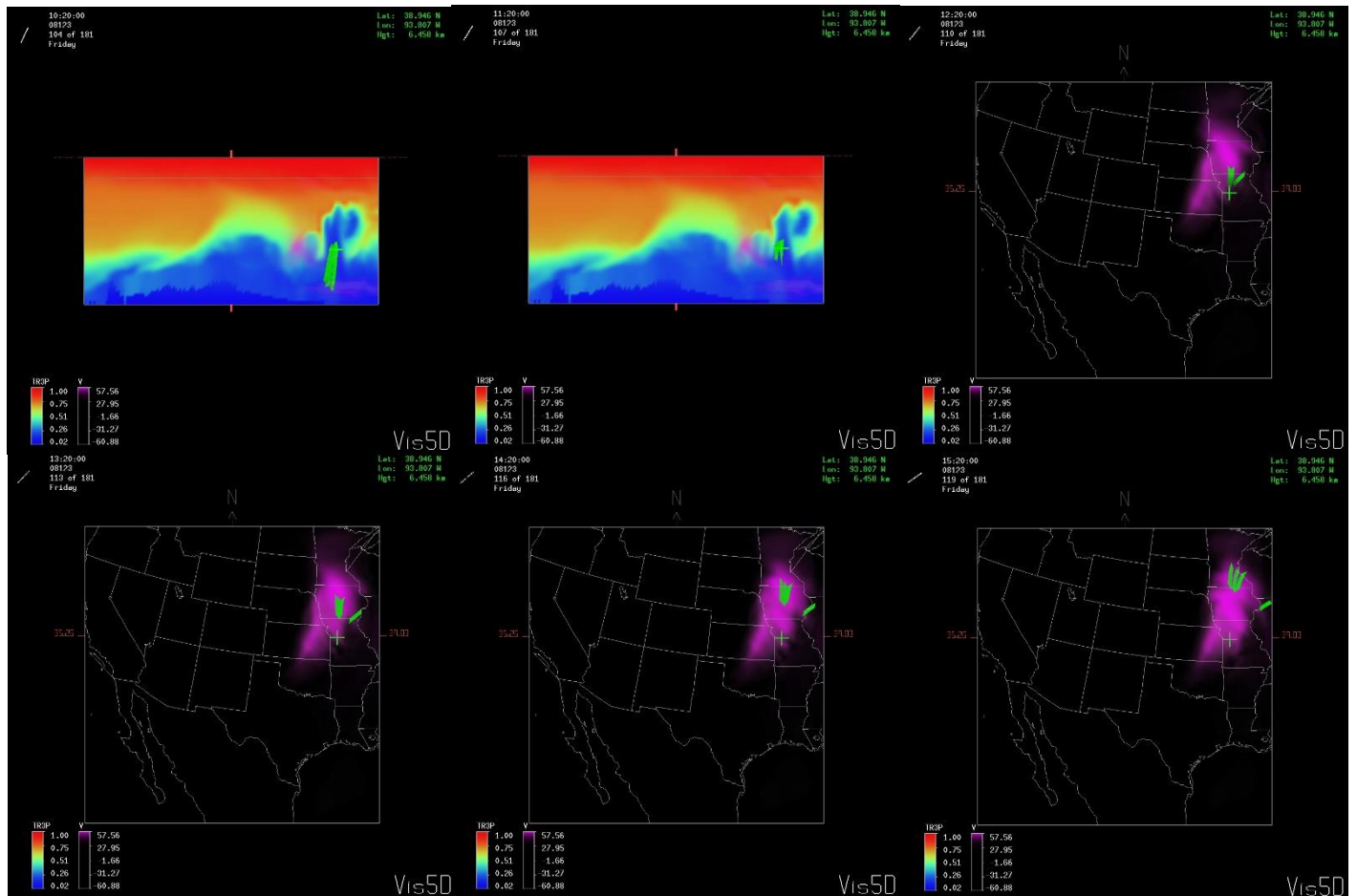
Figure 46: The first two panels represent thunderstorm view from the south with pink representing northward winds (~120 knots) the green represents trajectories of sampled air parcels and the vertical slice is of the tracer indicating a strong updraft into the lower stratosphere due to the insertion of tropospheric air, the last 4 panels represent a top down view of the same region in an effort to visualize the paths of the trajectories beyond the convection. This is a vertical slice taken from the south looking inward towards convective activity. Data was collected from 10:20 to 15:20 UTC 2 May 2008

6.3. Flight RF18

Flight RF18 contains another example of sinking stratospheric laminae. As was the case in RF04 and RF16, RF18 represents a strong trough with a meridional jet streak component. Subsidence is present along the western portion of the trough providing a sinking mechanism for the present stratospheric lamina. This sinking stratospheric air can be seen as low as 5 to 6 kilometers (Fig 47).

At the center of the trough a portion of higher tropospheric air can be affiliated with surface convergence associated with the cyclone. Unfortunately the flight flew before the lamina could completely form and organize and descend far enough south as seen in Fig. 47. The flight samples the atmosphere in front of the stratospheric lamina as well as a good portion of the future trough location, which will provide precursor measurements for the lamina. Figure 48 indicates the presence of both northerly and southerly jets. The green region represents northerly winds ~120 knots. The pink region in Fig. 48, represents southerly jet component, that seems to increase in strength and organization as the convection in Minnesota develops as well, which can be identified by a line of high tropospheric tracer3 values east of the northward jet component.
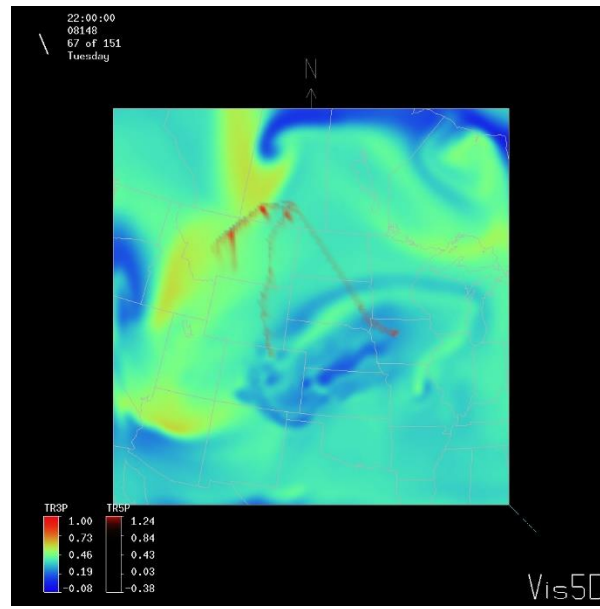
Figure 47: RF18 Flight path (red) on top of tracer3 0 (blue) to 1 (red) at ~6 km altitude in the

UWNMS at ~6 km on 06/27/2008 at 22:00 UTC
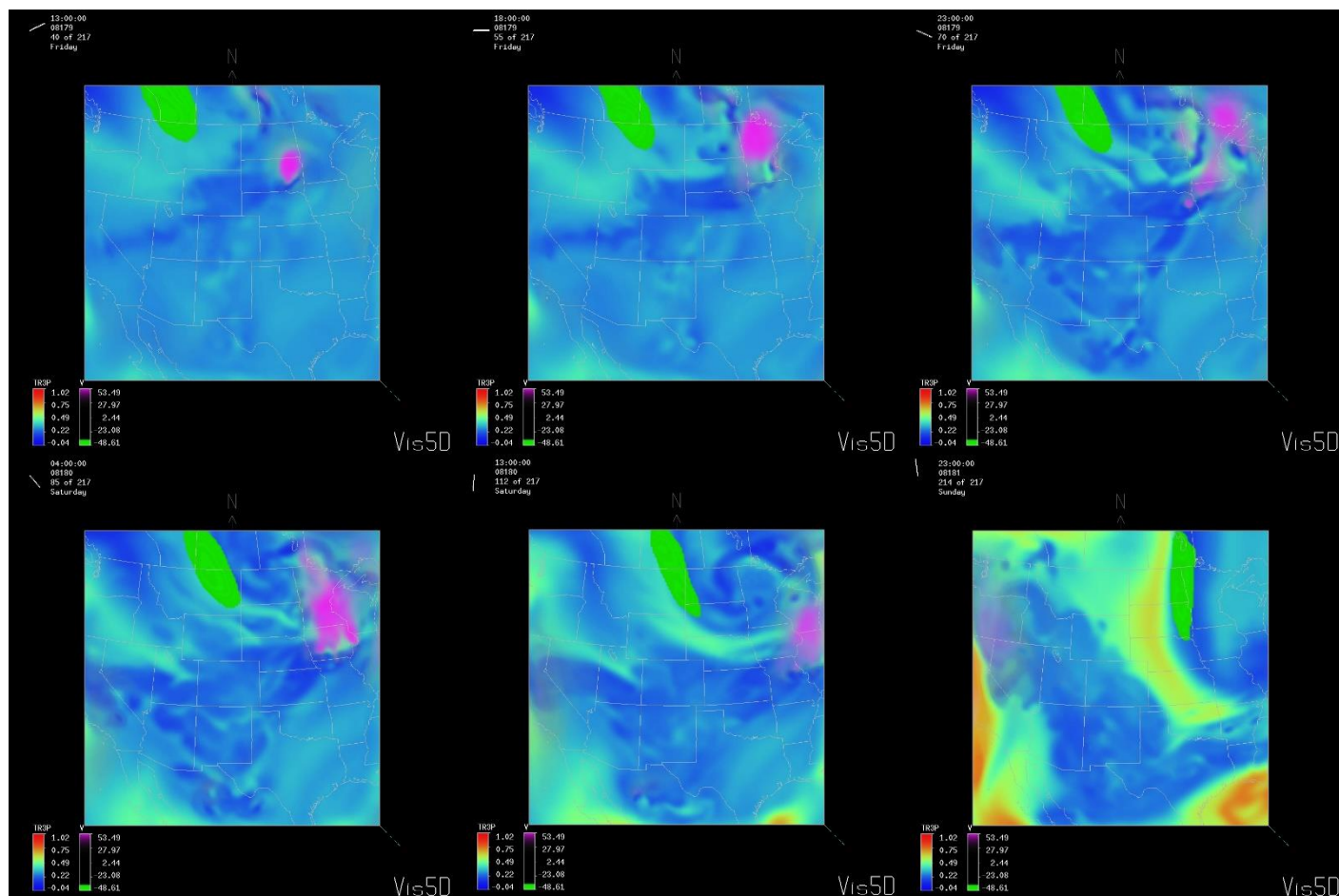
Figure 48: Flight RF18 tracer contoured 0 to 1 (blue to red) at 6 km and wind speeds greater than (less than) 120 knots in pink (green). Data was gathered from 13:00 UTC on 06/27/2008 to 23:00 on 06/28/2008

The zonal and meridional wind components were compared to the flight using the model. The model did an admirable job capturing wind components in both the zonal and meridional direction as seen in Figure 49. Error and uncertainty can be attributed to spatial resolution as the model. The model's 20 km grid spacing means that some small scale dynamic processes that could increase or decrease wind speeds may not be accounted for. The inaccuracies in the first

three hours of the flight in the zonal direction are troubling, however the model accurately

depicted both fly troughs of the meridional jet at ~2 hours and ~3 hours respectively. When

compared to the total wind speeds however outside of the first hour which can be attributed to a

spatial resolution issue, the model performs admirably particularly collecting the jet streaks

around the 2nd and 3rd hours of the flight.

A)

B)

C)
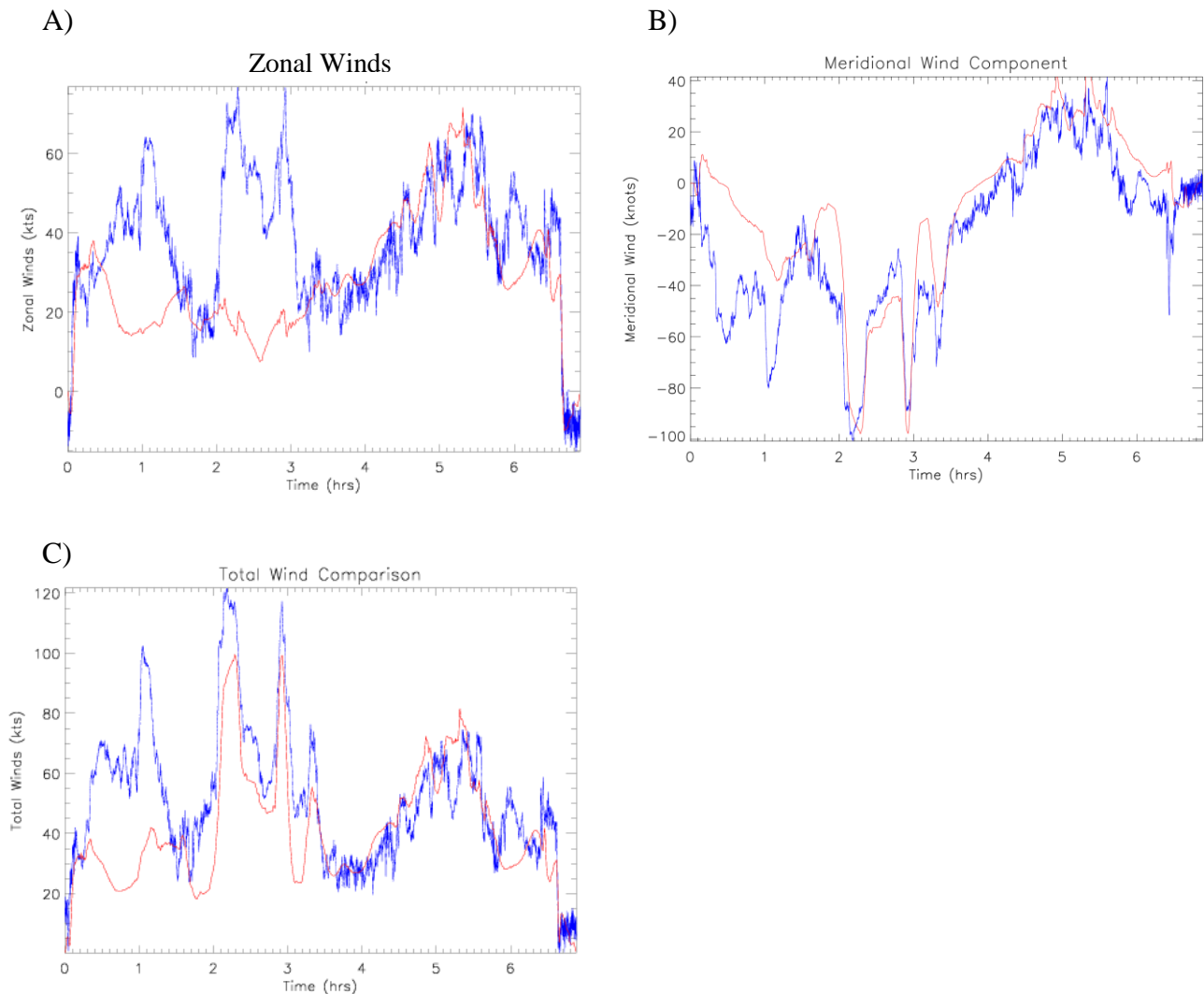
Figure 49: Winds in the zonal A) and meridional B) directions over time (hours after takeoff),

comparing with both the model (red) and the START-08 flight (blue).

RF18 had its tracer3 value compared to potential vorticity and potential temperature as well. The tracer did an accurate job capturing trends for both values displayed by the GFS in relation to the RF18 mission (Figure 50). The potential temperature gradients, which strongly influence potential vorticity, are capture accurately by the tracer when placed on the same scale. While the values weren't as accurate comparing potential vorticity and the tracer, it captured trends once again, indicating that the tracer3 gradients can be found in similar times and locations as PV gradients and in doing so accurately portray intrusions.

A)

B)
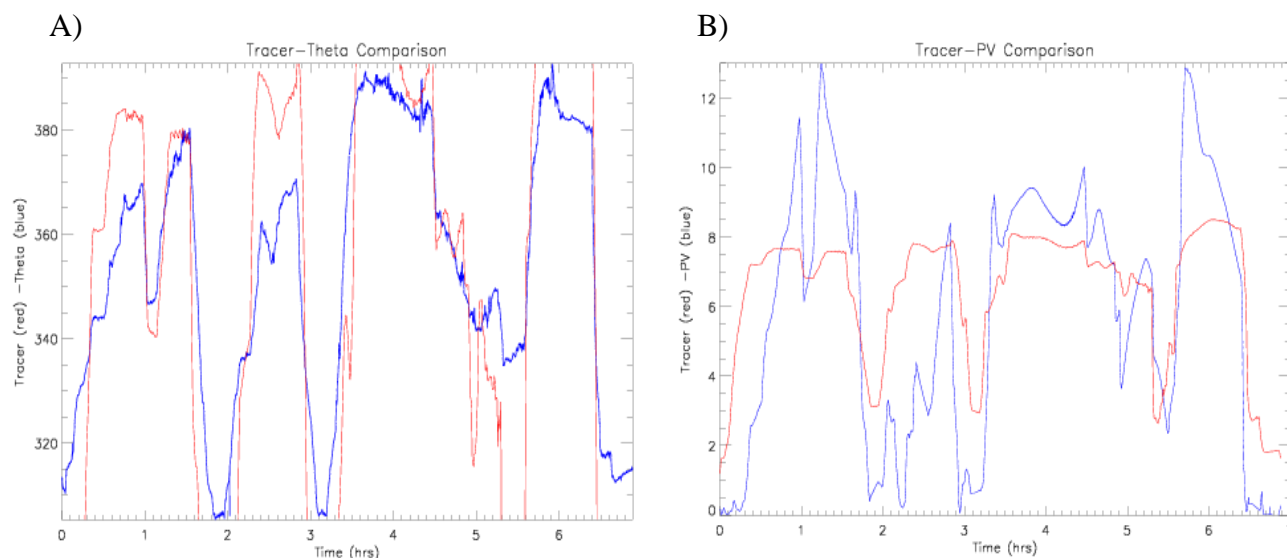
Figure 50: Potential temperature (blue) tracer (red) comparison observed over time in panel A) and potential vorticity (blue) compared to tracer (red) over time in panel B) for RF18

With the presence of a strong meridional jet streak, high concentrations of the tracer, and a trough it was necessary to analyze the air for a subsidence and sinking stratospheric air. Figure 51 represents an oblique view of tracer3 at approximately 6 km, with contours of potential temperature and the streamlines vertically through the stratospheric lamina. Trajectories were

placed in the lamina and by analyzing the motion of the air, it became evident that once again the air was sinking slowly on the western portion of the trough at a rate of ~1km/10 hrs. The air moves equatorward with a slight downward motion before reaching the end of the trough and moving eastward. The vertical motion becomes nonexistent when the trajectories reach the base of the trough and begin traveling east. This process indicates that an upper level is front, as slow persistent subsidence provides the sinking motion seen with the lamina. These sloped theta surfaces that the air flows along could also provide the sinking mechanism necessary to provide mixing in the jet core.
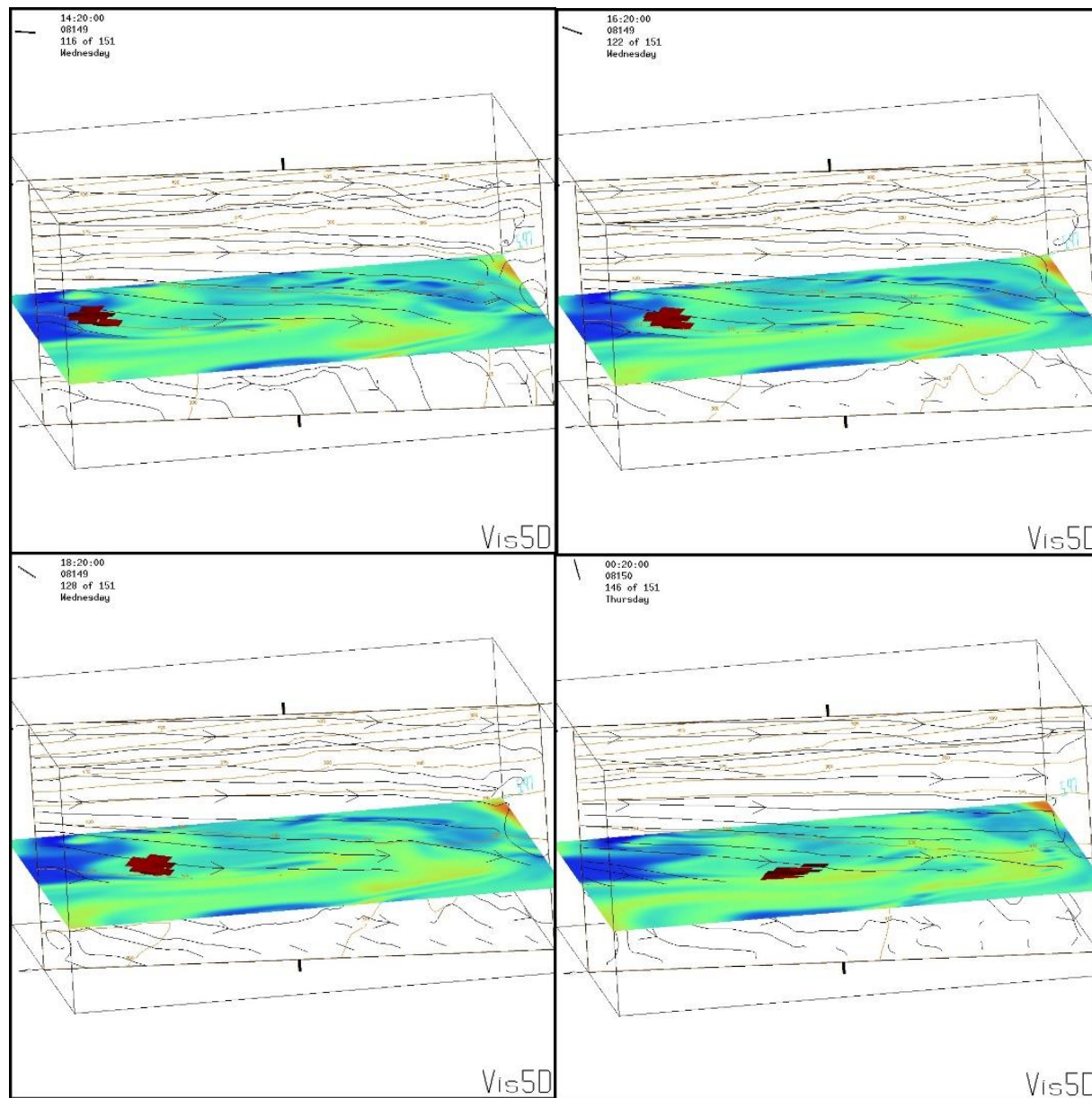
Figure 51: Trajectories (dark red) on a horizontal plane in RF18 with a vertical slice of potential temperature contours sliced on top of an oblique colored tracer plane from 0 (blue tropospheric air at 0 km) to 1 (red stratospheric air at 17.5 km).

Flight RF18 provided another opportunity to observe convective activity near the jet streak. Trajectories were placed within the convective activity to anticipate their origin and motion downstream. The initial 2 panels of Figure 52 represent a view from the south where the

trajectories can be observed flowing up the convective motion. The next 4 panels represent views from the north where the jet core is visible and the trajectories have flown beyond the vertical slice. The ribbons follow the jet streak poleward flowing over top of stratospheric air, creating a tropospheric intrusion into the lower stratosphere and providing more evidence for mixing.
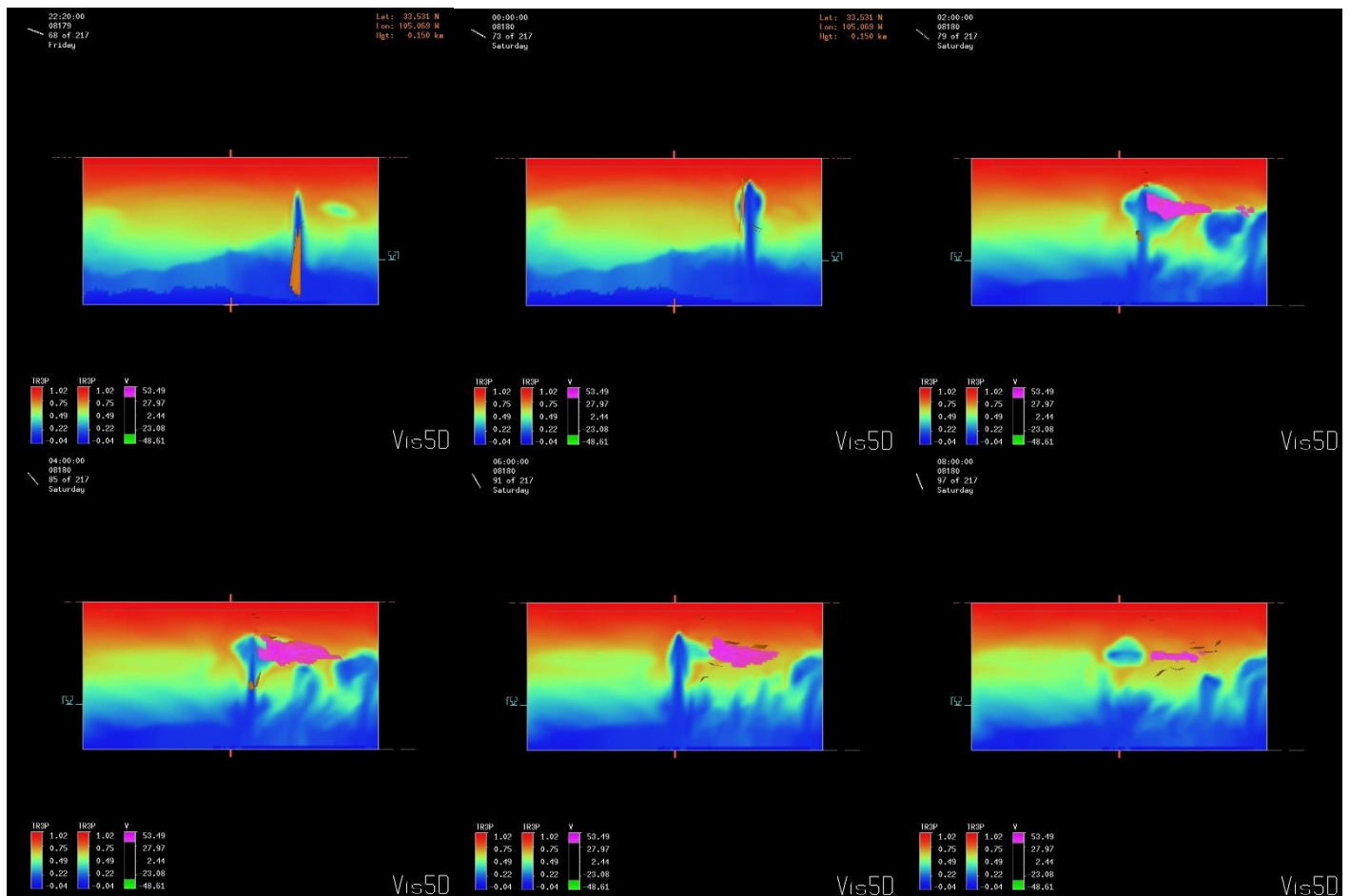
Figure 52: Flight RF18 convective view from the east and (first 2 figures) and the then the west (last 4 figures) the pink regions represent winds ~100 knots northward; the tracer runs from 0 (blue tropospheric air at the surface) to 1 (red stratospheric air at 17.5 km) trajectories are orange ribbons. Data was collected on day 06/27/2008 to 06/28/2008 from 22:20 UTC to 8:00 UTC

Lifting and sinking mechanisms had to be approached differently due to the models inability to accurately portray vertical winds due to its resolution and grid spacing. Comparisons with the START-08 aircraft in figure 53 indicates that vertical winds using the UWNMS are variable and cannot be trusted in this study to accurately portray vertical motion. A typical strong updraft is usually not much greater than 20 knots and many microphysical dynamics and properties can significantly alter data and observations. At 20 km grid spacing none of the smaller scale dynamical phenomena can be properly modeled, such as gravity waves and turbulence. However, the model does not adequately represent w associated with synoptic scale flow, as shown by descent along potential temperature contours and stream functions.
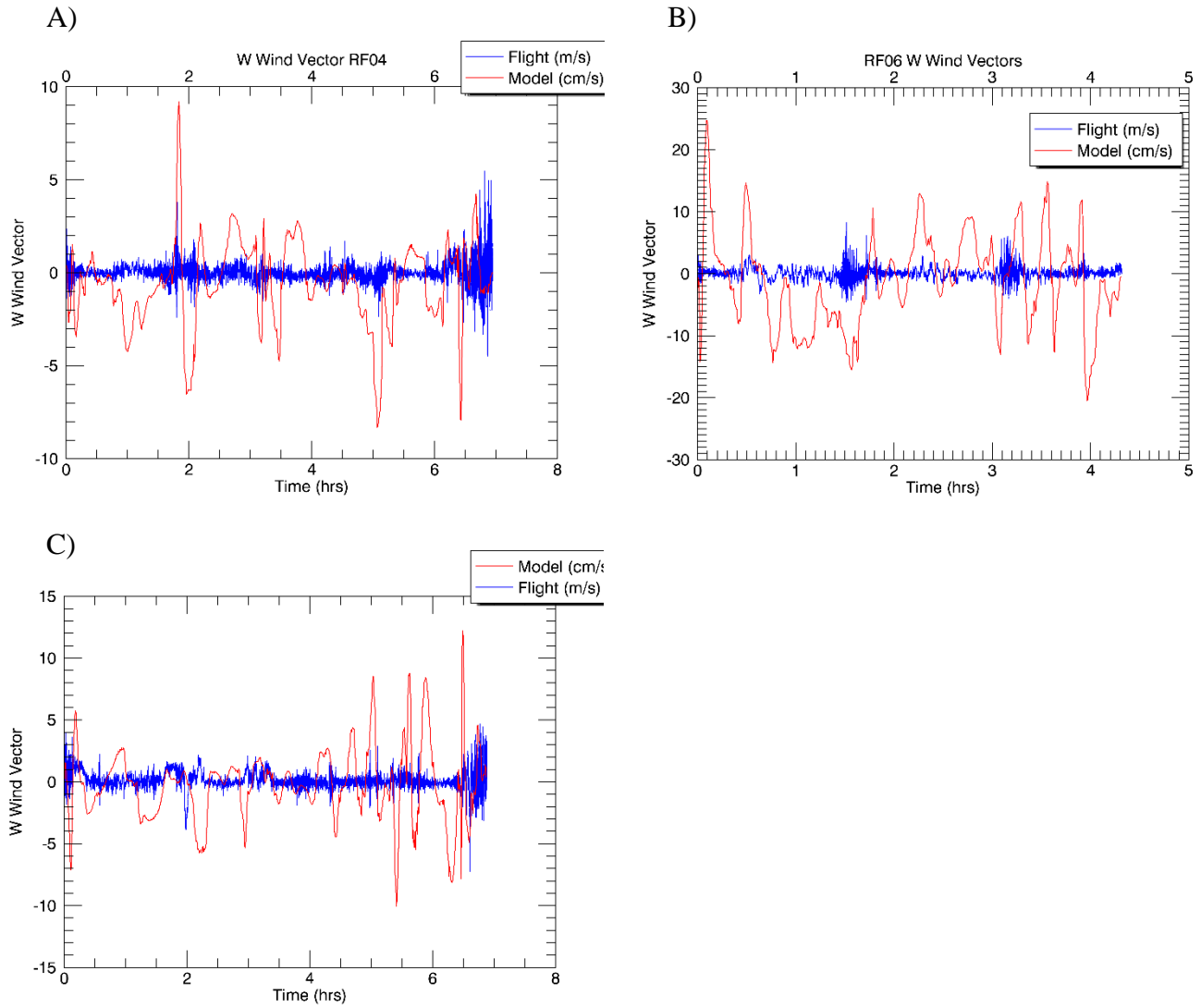
Figure 53: RF04 represented A), RF06 represented by B), and RF18 represented by C) and their

W wind components; for both the model (red in cm/s) and flight (blue m/s) over time.

7. **Conclusions**

7.1. Accuracy of Tracers in the UWNMS

The UWNMS displayed successful results for stratospheric tropospheric exchange events. Values showed accurate data within the resolution desired when compared with flight data with every variable except for vertical motion where the scale of the model struggled to capture small scale processes that contribute to vertical winds. While there were some discrepancies in data analysis, the major trends within the model followed the flight data quite well. The tracer used in a majority of these experiments also appeared to represent PV and stratospheric air quite well showing a useful alternative to showing horizontal PV gradients. Data analysis showed that stratospheric air was correctly labeled and registered using a basic tracer that equates to 1 at the top of the stratosphere and 0 at the bottom of the troposphere. The tracer then breaks down with altitude, leaving higher values in the stratosphere and lower values in the troposphere. The UWNMS variable, tracer3, accurately captured trends of potential vorticity, thus indicating that stratospheric air, tropospheric air, and the dynamic tropopause are accurately portrayed via this variable.

7.2. Synoptic scale mixing:

Synoptic scale mixing occurs over elongated upper-level troughs. STE occurs in the midlatitudes along synoptic scale troughs via two separate mechanisms. On the eastern portion of the trough, convective activity pushes tropospheric air into the lower stratosphere where winds carry the air downstream to be mixed into the stratosphere on a large scale along surface level fronts. Large amounts of stratospheric air subside slowly on the western side of the trough, which is driven by a strong southward jet and an upper level front. Theta contours as well as trajectories have shown a slow but steady decrease in altitude, suggesting that the stratospheric

air has a slight downward trajectory suggesting the presence of upper level fronts. This further indicates that these stratospheric lamina work as a mixing mechanism as well as a possibility to create underfolds as the stratospheric air undercuts the tropospheric air. Tracers and ozone observations indicate that significant subsidence in the western portion of the trough provides the primary mixing mechanism on the western portion of the trough. The overall effect of turbulent mixing needs further analysis as well, with mixed results in the three different flights.

7.3. Mesoscale mixing

Mesoscale exchange events were also viewed using VIS5D, allowing us to study the intrusions of tropospheric air during convective events. It was determined that convection injects a significant amount tropospheric air into the middle atmosphere continuously via the updraft. This air is pumped into the stratosphere via convective events where it is carried downstream by strong poleward jet streaks. This appears to provide significant mixing in small mesoscale events. Winds carried downstream create localized double tropopause events, supporting the idea of convection playing a role in STE. Multiple convection cases were observed, from cold fronts, to gravity waves, and all produced similar results. It would appear that convection in general dominates local exchange events. Interestingly, convection appeared to increase and excite troughs analyzed as well. As convection became prominent and mature, the winds along the jet flowing northward seemed to increase. This phenomenon appears to agree with the findings in Hitchman and Rowe (2016), which showed that inertial instability can force poleward wind maxima.

7.4. Tracer's Ability to Identify and Use As Stratospheric Constituents

The tracer is useful for showing the movement and dispersion of stratospheric and tropospheric air in the atmosphere. These can be used, on large synoptic scale events, to measure movements of air. However one must be careful to not take them for their exact values, as there are many discrepancies between using an actual constituent like ozone or water vapor in the place of the tracer. That being said tracer3 provides an accurate constituent for measuring trends in atmospheric events.

8. Future Work

The total impact of convections influence on STE needs further study. The rapid injection of tropospheric air in the lower stratosphere appears to be correlated with frontal activity in the lower troposphere. The injection of tropospheric air in the lower stratosphere appears to be much more rapid on the eastern portion of the trough than the steady subsidence present on the western portion of the trough. Convections overall contribution to STE needs to be analyzed further on both a small and large scale.

The total contributions to STE from mid-latitude phenomena requires further analysis. Chemical compositions of the mixed air must be studied further to understand the amount of water vapor sent into the lower stratosphere and the amount of ozone mixed into the upper stratosphere. There is still a large amount of uncertainty (8-44%) in the amount of ozone inserted into the troposphere from STE events (IPCC 4th assessment). The high uncertainty impacts estimations of water vapor amounts in the lower stratosphere and ozone concentrations in the upper troposphere. Turbulent mixing in and around the jet needs to be further analyzed in an effort to understand different driving forces between the different flights. In flight RF06 for instance, turbulence appeared to play a significant role in mixing, however flights RF04 and RF18 indicated little effect from turbulent mixing around jet level winds. The overall impact of turbulent mixing during STE events requires further analysis

Follow-up analysis using other models would be necessary in an effort to draw similar conclusions. We currently are unable to determine how much this result depends on the UW-NMS in its current configuration. At higher resolutions in the horizontal and vertical windows, vertical wind vectors and flow could be influenced.

A higher resolution run of the UWNMS may provide better data for the vertical wind components. Due to the interest in vertical motion for both mixing mechanisms discussed in this paper, proper analysis of vertical winds are necessary in order to determine what impact they may have on these sinking phenomena. Other models may provide better vertical data as well.

References

Andrews, D. G., J. R. Holton, and C. B. Leovy, 1987: *Middle atmosphere dynamics.* Academic Press, xi, 489 pages pp.

Bosart, L. F., 1970: mid-tropospheric frontogenesis. *Quart. J. Roy. Meteorol. Soc.*, **96,** 442-471.

Bowman, K. P., L. L. Pan, T. Campos, and R. Gao, 2007: Observations of fine-scale transport structure in the upper troposphere from the High-performance Instrumented Airborne Platform for Environmental Research. *J. Geophys. Res.-Atmospheres*, **112**.

Buker, M. L., Hitchman, M. H,m Tripoli, G. J., Pierce, R. B., Browell, E. V., Avery, M. A., 2005, Resolution dependence of cross-tropopause ozone transport over east Asia: *J. Geophys. Res. –Atmospheres*, **110**

Bush, A. B. G., and W. R. Peltier, 1994: tropopause folds and synoptic-scale baroclinic wave life-cycles. *J. Atmos. Sci.*, **51,** 1581-1604.

Chapman, S., 1930: XXXV On ozone and atmoic oxygen in the upper atmosphere. *The London, Edinburg, and Dubblin Philosophical Magazine and Journal of Science.*

Danielsen, E. F., 1968: stratospheric-tropospheric exchange based on radioactivity ozone and potential vorticity. *J. Atmos. Sci.*, **25,** 502-+.

Davis, C. A., 1992: piecewise potential vorticity inversion. *J. Atmos. Sci.*, **49,** 1397-1411.

Davis, C. A., and K. A. Emanuel, 1991: potential vorticity diagnostics of cyclogenesis. *Mon. Wea. Rev.*, **119,** 1929-1953.

Davis, C. A., M. T. Stoelinga, and Y. H. Kuo, 1993: the integrated effect of condensation in numerical simulations of extratropical cyclogenesis. *Mon. Wea. Rev.*, **121,** 2309-2330.

Dobson, G. M. B., 1973a: The Laminated Structure of the Ozone in the Atmosphere. *Quart. J. Roy. Meteor. Soc.*, 599 - 607.
1973b: LAMINATED STRUCTURE OF OZONE IN ATMOSPHERE. *Quart. J. Roy. Meteor. Soc.*, **99,** 599-607.

Eliassen, A., 1962: On the vertical circulation in frontal zones. Geofysiske publikasjoner.,
1990: *TRANSVERSE CIRCULATIONS IN FRONTAL ZONES.* 155-165 pp.

Eliassen, A., and S. O. C. Amer Meteorol, 1988: transverse circulations in frontal zones. *Palmen Memorial Symposium on Extratropical Cyclones***,** 182-185.

Fahey, D. W., *et. al.*, 1996: In situ observations of NOy, O-3, and the NOy/O-3 ratio in the lower stratosphere. *Geophys. Res. Letts.*, **23,** 1653-1656.

Fischer, H., *et. al.*, 2000: Tracer correlations in the northern high latitude lowermost stratosphere: Influence of cross-tropopause mass exchange. *Geophys. Res. Letts.*, **27,** 97-100.

Fischer, J., and M. Visbeck, 1993: deep velocity profiling with self-contained adcps. *Journal of Atmospheric and Oceanic Technology*, **10,** 764-773.

Forster, P. M. D., and K. P. Shine, 1997: Radiative forcing and temperature trends from stratospheric ozone changes. *J. Geophys. Res.-Atmospheres*, **102,** 10841-10855.

Hakim, G. J., D. Keyser, and L. F. Bosart, 1996: The Ohio valley wave-merger cyclogenesis event of 25-26 January 1978 .2. Diagnosis using quasigeostrophic potential vorticity inversion. *Mon. Wea. Rev.*, **124,** 2176-2205.

Harvey, V. L., R. B. Pierce, M. H. Hitchman, C. E. Randall, and T. D. Fairlie, 2004: On the distribution of ozone in stratospheric anticyclones. *J. Geophys. Res.-Atmospheres*, **109**.

Hegglin, M. I., and T. G. Shepherd, 2007: O-3-N2O correlations from the Atmospheric Chemistry Experiment: Revisiting a diagnostic of transport and chemistry in the stratosphere. *J. Geophys. Res.-Atmospheres*, **112**.

Hines, K. M., and C. R. Mechoso, 1991: frontogenesis processes in the middle and upper troposphere. *Mon. Wea. Rev.*, **119,** 1225-1241.

Hitchman, M. H., and A. S. Huesmann, 2009: Seasonal Influence of the Quasi-Biennial Oscillation on Stratospheric Jets and Rossby Wave Breaking. *J. Atmos. Sci.*, **66,** 935-946.

Hitchman, M. H., M. L. Buker, G. J. Tripoli, E. V. Browell, W. B. Grant, T. J. McGee, and J. F. Burris, 2003: Nonorographic generation of Arctic polar stratospheric clouds during December 1999. *J. Geophys. Res.-Atmospheres*, **108**.

Hitchman, M. H., M. L. Buker, G. J. Tripoli, R. B. Pierce, J. A. Al-Saadi, E. V. Browell, and M. A. Avery, 2004: A modeling study of an East Asian convective complex during March 2001. *J. Geophys. Res.-Atmospheres*, **109**.

Hitchman, M. H., M. L. Buker, and G. J. Tripoli, 1999: Influence of synoptic waves on column ozone during Arctic summer 1997. *J. Geophys. Res.-Atmospheres*, **104,** 26547-26563.

Hoinka, K. P., 1997: The tropopause: discovery, definition and demarcation. *Meteorologische Zeitschrift*, **6,** 281-303.

102

Holton, J. R., 1995a: Stratosphere - Troposphere exchange. Reviews of Geophysics, 403-439. 1995b: *Stratosphere - troposphere exchange reviews of geophysics.* **33.** Reviews of Geophysics.

Homeyer, C. R., K. P. Bowman, and L. L. Pan, 2010: Extratropical tropopause transition layer characteristics from high-resolution sounding data. *J. Geophys. Res.-Atmospheres*, **115**.

Homeyer, C. R., K. P. Bowman, L. L. Pan, E. L. Atlas, R. S. Gao, and T. L. Campos, 2011: Dynamical and chemical characteristics of tropospheric intrusions observed during START08. *J. Geophys. Res.-Atmospheres*, **116**.

Hoor, P., H. Fischer, L. Lange, J. Lelieveld, and D. Brunner, 2002: Seasonal variations of a mixing layer in the lowermost stratosphere as identified by the CO-O-3 correlation from in situ measurements. *J. Geophys. Res.-Atmospheres*, **107**.

Hoor, P., C. Gurk, D. Brunner, M. I. Hegglin, H. Wernli, and H. Fischer, 2004: Seasonality and extent of extratropical TST derived from in-situ CO measurements during SPURT. *Atmospheric Chemistry and Physics*, **4,** 1427-1442.

Hoskins, B. J., 1971: atmospheric frontogenesis models - some solutions. *Quart. J. Roy. Meteor. Soc.*, **97,** 139-&.

Hoskins, B. J., 1972: non-boussinesq effects and further development in a model of upper tropospheric frontogenesis. *Quart. J. Roy. Meteor. Soc.*, **98,** 532-&.

Hoskins, B. J., 1982: the mathematical-theory of frontogenesis. *Annual Review of Fluid Mechanics*, **14,** 131-151.

Hoskins, B. J., M. E. McIntyre, and A. W. Robertson, 1985: on the use and significance of isentropic potential vorticity maps. *Quart. J. Roy. Meteor. Soc.*, **111,** 877-946.

Keim, E. R., and Coauthors, 1997: Measurements of the NOy - N2O correlation in the lower stratosphere: Latitudinal and seasonal changes and model comparisons. *J. Geophys. Res.-Atmospheres*, **102,** 13193-13212.

Keyser, D., B. D. Schmidt, and D. G. Duffy, 1989: a technique for representing 3-dimensional vertical circulations in baroclinic disturbances. *Mon. Wea. Rev.*, **117,** 2463-2494.

Konopka, P., and L. L. Pan, 2012: On the mixing-driven formation of the Extratropical Transition Layer (ExTL). *J. Geophys. Res.-Atmospheres*, **117**.

Lackmann, G., 2011: Midlatitude Synoptic Meteorology, Dynamics, Analysis and Forecasting. American Meteorological Society.

Lackmann, G. M., D. Keyser, and L. F. Bosart, 1997: A characteristic life cycle of upper-

tropospheric cyclogenetic precursors during the experiment on rapidly intensifying cyclones over the Atlantic (ERICA). *Mon. Wea. Rev.*, **125,** 2729-2758.

Lamarque, J. F., and P. G. Hess, 1994: cross-tropopause mass-exchange and potential vorticity budget in a simulated tropopause folding. *J. Atmos. Sci.*, **51,** 2246-2269.

Loughe, A. F., C. C. Lai, and D. Keyser, 1995: a technique for diagnosing 3-dimensional ageostrophic circulations in baroclinic disturbances on limited-area domains. *Mon. Wea. Rev.*, **123,** 1476-1504.

Louis, J. F., 1979: Parametric model of vertical eddy fluxes in the atmosphere. *Boundary-Layer Meteorology*, **17,** 187-202.

Marcy, T. P., and Coauthors, 2004: Quantifying stratospheric ozone in the upper troposphere with in situ measurements of HCl. *Science*, **304,** 261-265.

McIntyre, M. E., and T. N. Palmer, 1983: Breaking planetary-waves in the stratosphere. *Nature*, **305,** 593-600.

McPeters, R. D., 1985: Response of ozone to the solar proton events during solar cycle 21: a theoretical interpretation. J. Geophys. Res.: Atmospheres.

Mudrick, S. E., 1974: Numerical study of frontogenesis. *J. Atmos. Sci.*, **31,** 869-892.

Murphy, D. M., and Coauthors, 1993: reactive nitrogen and its correlation with ozone in the lower stratosphere and upper troposphere. *J. Geophys. Res.-Atmospheres*, **98,** 8751-8773.

Nielsen Gammon, J. W., and R. J. Lefevre, 1996: Piecewise tendency diagnosis of dynamical processes governing the development of an upper-tropospheric mobile trough. *J. Atmos. Sci.*, **53,** 3120-3142.

Pan, L. L., P. Konopka, and E. V. Browell, 2006: Observations and model simulations of mixing near the extratropical tropopause. *J. Geophys. Res.-Atmospheres*, **111**.

Pan, L. L., W. J. Randel, B. L. Gary, M. J. Mahoney, and E. J. Hintsa, 2004: Definitions and sharpness of the extratropical tropopause: A trace gas perspective. *J. Geophys. Res.-Atmospheres*, **109**.

Pan, L. L., J. C. Wei, D. E. Kinnison, R. R. Garcia, D. J. Wuebbles, and G. P. Brasseur, 2007: A set of diagnostics for evaluating chemistry-climate models in the extratropical tropopause region. *J. Geophys. Res.-Atmospheres*, **112**.

Pan, L. L., and Coauthors, 2009: Tropospheric intrusions associated with the secondary tropopause. *J. Geophys. Res.-Atmospheres*, **114**.

Pan, L. L., 2014: Thunderstorms enhance tropospheric ozone by wrapping and shedding stratospheric air. *Geophys. Res. Letts.*, **41,** 7785-7790.

Plumb, R. A., 2007: Tracer interrelationships in the stratosphere. *Reviews of Geophysics*, **45**.

Postel, G. A., and M. H. Hitchman, 2001: A case study of Rossby wave breaking along the subtropical tropopause. *Mon. Wea. Rev.*, **129,** 2555-2569.

Raatz, W. E., R. C. Schnell, M. A. Shapiro, S. J. Oltmans, and B. A. Bodhaine, 1985: intrusions of stratospheric air into alaska troposphere, march 1983. *Atmospheric Environment*, **19,** 2153-2158.

Ravishankara, A. R., 2012: Water Vapor in the Lower Stratosphere. *Science*, **337,** 809-810.

Reed, R. J., 1953: an investigation of the development of a mid-tropospheric frontal zone and its associated vorticity field. F. Sanders, Ed., *J. Meteor.*, 338 - 349.

Reed, R. J., 1955: a study of a characteristic tpye of upper-level frontogenesis. *J. Meteor.*, 226-237.

Rotunno, R., W. C. Skamarock, and C. Snyder, 1994: an analysis of frontogenesis in numerical simulations of baroclinic waves. *J. Atmos. Sci.*, **51,** 3373-3398.

Rowe, S. M., and M. H. Hitchman, 2016: On the Relationship between Inertial Instability, Poleward Momentum Surges, and Jet Intensifications near Midlatitude Cyclones. *J. Atmos. Sci.*, **73,** 2299-2315.

Sawyer, J. S., 1956: The vertical circulation at meteorological fronts and its relation to frontogenesis. *Proceedings of the royal society of a mathematical physical and engineering sciences*.

Schneider, T., 2004: The tropopause and the thermal stratification in the extratropics of a dry atmosphere. *J. Atmos. Sci.*, **61,** 1317-1340.

Shapiro, M. A., 1970: On the Applicability of the Geostrophic Approximation to Upper-Level Frontal-Scale Motions. *J. Atmos. Sci.,* **27,** 408-420.

Shapiro, M. A., 1980: Turbulent mixing within tropopause folds as a mechanism for the exchange of chemical constituents between the stratosphere and troposphere. *J. Atmos. Sci.,* **37,** 994-1004.

Singh, H. B., and Coauthors, 1997: Trace chemical measurements from the northern midlatitude lowermost stratosphere in early spring: Distributions, correlations, and fate. *Geophys. Res. Letts.*, **24,** 127-130.

Smith, E. A., A. Mugnai, H. J. Cooper, G. J. Tripoli, and X. W. Xiang, 1992: foundations for statistical physical precipitation retrieval from passive microwave satellite measurements .1. Brightness-temperature properties of a time-dependent cloud-radiation model. *J. App. Meteor.*, **31,** 506-531.

Staley, D. O., 1960: evaluation of potential-vorticity changes near the tropopause and the related vertitcal motions, vertical advection of vortpcity, and transfer of radioactive debris from stratosphere to troposphere. *J. Meteor.*, 591-620.

Stephens, G. L., S. C. Tsay, P. W. Stackhouse, and P. J. Flatau, 1990: the relevance of the microphysical and radiative properties of cirrus clouds to climate and climatic feedback. *J. Atmos. Sci.*, **47,** 1742-1753.

Stohl, A., 2003: A backward modeling study of intercontinental pollution transport using aircraft measurements. *J. Geophys. Res.-Atmospheres*, **108**.

Sutcliffe, R., 1947: A contribution to the problem of development. Wiley & Sons, Ltd.

Trenberth, K. E., 1978: interpretation of diagnostic quasi-geostrophic omega equation. *Mon. Wea. Rev.*, **106,** 131-137.

Tripoli, G. J., 1992a: a nonhydrostatic mesoscale model designed to simulate scale interaction. *Mon. Wea. Rev.*, **120,** 1342-1359.

Tripoli, G. F., 1992b: an explicit 3-dimensional nonhydrostatic numerical-simulation of a tropical cyclone. *Meteorology and Atmospheric Physics*, **49,** 229-254.

Tripoli, G. J., and W. R. Cotton, 1981: the use of ice-liquid water potential temperature as a thermodynamic variable in deep atmospheric models. *Mon. Wea. Rev.*, **109,** 1094-1102.

Uccellini, L. W., 1984: comparative diagnostic case-study of east coast secondary cyclogenesis under weak versus strong synoptic-scale forcing - comment. *Mon. Wea. Rev.*, **112,** 2540-2541.

Uccellini, L. W., R. A. Petersen, K. F. Brill, P. J. Kocin, and J. J. Tuccillo, 1987: synergistic interactions between an upper-level jet streak and diabatic processes that influence the development of a low-level jet and a secondary coastal cyclone. *Mon. Wea. Rev.*, **115,** 2227-2261.

Wandishin, M. S., S. L. Mullen, D. J. Stensrud, and H. E. Brooks, 2001: Evaluation of a short-range multimodel ensemble system. *Mon. Wea. Rev.*, **129,** 729-747.

Wang, P. H., J. Fishman, V. L. Harvey, and M. H. Hitchman, 2006: Southern tropical upper tropospheric zonal ozone wave-1 from SAGE II observations (1985-2002). *J. Geophys. Res.*, **111**.

Weinheimer, A. J., J. G. Walega, B. A. Ridley, G. W. Sachse, B. E. Anderson, and J. E. Collins, 1993: stratospheric noy measurements on the nasa dc-8 during aase-ii. *Geophys. Res. Letts.*, **20,** 2563-2566.

Whitaker, J. S., L. W. Uccellini, and K. F. Brill, 1988: a model-based diagnostic study of the rapid development phase of the president's day cyclone. *Mon. Wea. Rev.*, **116,** 2337-2365.

Wirth, V., 2003: Static stability in the extratropical tropopause region. *J. Atmos. Sci.*, **60,** 1395-1409.